HIGH PERFORMANCE HYDROGEN EVOLUTION ELECTROCATALYST IN ALKALINE MEDIA

A thesis submitted for the degree of

Doctor of Philosophy

at

The City University
London

by

Maurice Chuen Mo MAN

This work was carried out under the supervision of Dr. A. C. C. Tseung and supported by the European Economic Commission, Contract No. 161-76-11 EH UK.

To my mother and father .....

ACKNOWLEDGEMENTS

I wish to acknowledge the assistance and encouragement given to me by my supervisor, Dr. A. C. C. Tseung. I would also like to express my grateful thanks to my student colleagues in the Electrochemical Research Group for many helpful discussions.

Thanks are also due to the X-ray Crystallography Group of the Physics Department for their guidance and the loan of their equipment, to [redacted] for performing D.T.A. analysis, and to [redacted] for typing this manuscript.

M. C. M. Man
Department of Chemistry
The City University
St. John Street
London EC1V 4PB

April 1978

ABSTRACT

The energy crisis of the seventies has triggered off tremendous interest towards the research and development of alternative energy sources for the future. The use of hydrogen as the ultimate secondary fuel in the future would be economically feasible if the advancement in water electrolysis technology by using off-peak energy derived from either nuclear or solar power, approaches 100% energy efficiency. The present investigation is directed towards this goal, in the line of searching for new, inexpensive electrocatalysts, and looking at the suitability of the teflon-bonded porous electrode structure, being used for the hydrogen evolution reaction in alkaline media.

Evaluation of nickel sulphide materials lead to the synthesizing and examination of cobalt-nickel-sulphur compounds from cobalt-nickel oxide of composition $NiCo_2O_4$. The kinetics of the sulphiding process were investigated. By studying the preparation parameters carefully, cobalt-nickel-sulphur compounds prepared were best represented by the empirical formula of $NiCo_2O_xS_y + S_z$, where $x + y \leqslant 4$, and $y >> z \geqslant 0$. The best iR corrected electrochemical activity for the hydrogen evolution reaction was 1 A/cm^2, at a potential of -170 mV vs D.H.E., in 5N KOH, at 70°C. The percentage of sulphur content in the cobalt-nickel-sulphur compounds play a major role in the determination of hydrogen evolution activity. The ability of cobalt-nickel-sulphur compounds to function efficiently as hydrogen cathode electrocatalysts, may be attributed to the defect structure of the catalysts, which show anion deficiency and thus

create electrons at the conduction band to facilitate the hydrogen evolution process. Powder crystallographic measurements of all cobalt-nickel-sulphur compounds in this work showed predominantly spinel-type crystal structure, but with distortions as a result of mixed phases contamination.

The teflon-bonded porous electrode structure was found to be more active for the hydrogen evolution reaction as compared to the 'dipping' porous electrode structure. The disintegration of the 'dipping' porous electrodes was sometimes observed either before or during the hydrogen evolution process. This may be attributed to the hydrogen embrittlement of the electrode supports during the sulphiding process.

Finally, the electrode kinetic parameters for the hydrogen evolution reaction were determined at temperatures of, 25^{o}C, 40^{o}C and 70^{o}C on cobalt-nickel-sulphur compound and a slow electrochemical desorption step is therefore suggested.

CONTENTS

Page

CHAPTER ONE:

Emerging Hydrogen Economy

1. Introduction 1

2. Hydrogen Production by Water Electrolysis 2

2.1. Main Causes for Efficiency Losses in Water Electrolysis 6

2.1.1. Activation Polarisation 7
2.1.2. Ohmic Polarisation 7
2.1.3. Concentration Polarisation 7

2.2. Areas of Research to Improve Energy Efficiency of Water Electrolysis Approaching 100% 8

3. Present Work 10

CHAPTER TWO:

Hydrogen Cathode Electrocatalyst

1. General Survey on the Hydrogen Evolution Reaction (h.e.r.) 12

2. Literature Survey on Ni-S System 15

3. Evaluation of Nickel Sulphide as Potential Cathode Electrocatalyst in Alkaline Media 17

3.1. Materials Used in Half-Cell Electrochemical Testing 17

3.1.1. The Electrolyte 17
3.1.2. Electrocatalysts and Their Sources 18
3.1.3. The Gases 18
3.1.4. Fabrication of Teflon-Bonded Porous Electrode 18
3.1.5. The Half-Cell Design 19
3.1.6. The Reference Electrode System 19

3.2. Half-Cell Electrochemical Testing 21

3.2.1. Steady State Polarisation Techniques .. . 21

Page

3.2.2. Potentiodynamic Polarisation Technique 21
3.2.3. Potentiostatic and Galvanostatic Stability Tests 24
3.2.4. The Correction of Ohmic Overvoltage (iR drop) 24

3.3. Electrocatalyst Characterisation 27

3.3.1. Aggregate Size Measurements 27
3.3.2. X-ray Powder Diffraction 27
3.3.3. Atomic Absorption Spectroscopy 27

4. Results 28

4.1. X-ray Analysis 28

4.2. Aggregate Size Measurements 32

4.3. Atomic Absorption Analysis 32

4.4. Half-Cell Electrochemical Results 32

5. Discussion 38

CHAPTER THREE:

Electrocatalytic Hydrogen Evolution With Cobalt-Nickel Sulphide

1. Introduction 41

2. Preparation of Sulphocobalties, $NiCo_2S_4$ 42

3. Electrocatalyst Characterisation 44

3.1. Electrical Conductivity Measurements 44

3.2. X-ray Powder Diffraction 46

4. Half-Cell Electrochemical Testing 46

5. Results 48

5.1. X-ray Analysis 48

5.2. Electrical Conductivity Measurements 51

5.3. Half-Cell Electrochemical Results 51

6. Discussion 55

Page

CHAPTER FOUR:

The Influence of Preparation Parameters on the Electro-Catalytic Activity of Cobalt-Nickel Sulphide

1. Introduction 61

2. Preparation of Cobalt-Nickel Sulphides 62

3. Electrocatalyst Characterisation 63

   3.1. Analysis of Cobalt-Nickel Sulphides 63

   3.2. X-ray Powder Diffraction 66

4. Half-Cell Electrochemical Testing 66

5. Investigation of the Thermal Behaviour of Freeze-Dried Cobalt-Nickel Oxide and Some of its Sulphided Products . .. 66

   5.1. Apparatus 66

   5.2. Materials 68

   5.3. Procedure 68

6. Results 70

   6.1. X-ray Analysis 70

   6.2. Analytical Results 70

   6.3. Half-Cell Electrochemical Results 80

   6.4. DTA Analysis 80

7. Discussion 93

CHAPTER FIVE:

The Application of Cobalt-Nickel Sulphide Electrocatalysts in Different Porous Electrode Structures for the Hydrogen Evolution Reaction in Alkaline Media

1. Introduction 100

2. Preparation of the Electrocatalyst and Electrodes 103

   2.1. Dipping Porous Electrode 104

Page

2.2. Teflon-Bonded Porous Electrode 104

3. Half-Cell Electrochemical Testing 105

3.1. Rotating Disc Electrode (R.D.E.) 105

3.2. Potentiostatic Pulse and Galvanostatic Pulse Technique 106

3.2.1. Experimental: Potentiostatic Pulse Technique 107

3.3. Double Layer Charging 111

3.3.1. Experimental: Double Layer Charging Technique 111

4. Electrocatalyst Characterisation 113

4.1. X-ray Powder Diffraction 113

5. Results 113

5.1. X-ray Analysis 113

5.2. Half-Cell Electrochemical Results 114

6. Discussion 119

CHAPTER SIX:

Kinetic Parameters for Hydrogen Evolution Reaction of Cobalt-Nickel Sulphide in the Dipping Porous Electrode Structure

1. Introduction 133

2. Possible Mechanisms 133

3. Basic Electrode Kinetics 135

4. Half-Cell Electrochemical Testing 138

4.1. Experimental 140

5. Results 141

6. Discussion 149

Page

CHAPTER SEVEN:

Conclusions and Recommendation for Further Work

1. Conclusions and Summary 161

2. Recommendations for Further Work 167

References

----------oOo----------

LIST OF TABLES

		Page
1.1.	Hydrogen production process - worldwide	1
2.1.	X-ray powder data for different nickel sulphides	29
2.2.	A.S.T.M. d-spacings for some related nickel compounds	30
2.3.	Average aggregate diameter (μ) for various nickel sulphides and freeze dried cobalt-nickel oxide	33
2.4.	Atomic absorption analysis of NiS (Technical Grade)	39
3.1.	X-ray powder data for different cobalt-nickel oxides	49
3.2.	X-ray powder data for different cobalt-nickel sulphides	50
3.3.	Electrical resistivity for cobalt nickel oxides and their corresponding sulphides	52
4.1.	X-ray powder data for the freeze dried cobalt-nickel oxide and its sulphided products	71
4.2.	X-ray powder data for the thermal decomposed cobalt-nickel oxide and its sulphided products	72
4.3.	Edax analytical concentration count for freeze dried and thermal decomposed cobalt-nickel oxides and their sulphided products	74
4.4.	Chemical analysis of different cobalt-nickel sulphides	79
4.5.	The thermal decomposition of cobalt-nickel oxides in air and in nitrogen	84
4.6.	The thermal decomposition of cobalt-nickel sulphides in nitrogen and in air	86
4.7.	The thermal decomposition of cobalt-nickel sulphides (the later stages of the decomposition in air)	88
4.8.	The thermal decomposition of cobalt-nickel sulphides (the later stages of the decomposition in nitrogen)	89
5.1.	X-ray powder data for cobalt-nickel sulphide prepared from thermal decomposed cobalt-nickel oxide and cobalt-nickel sulphide removed from a freshly prepared dipping porous electrode	115

		Page
5.2.	X-ray powder data for cobalt-nickel sulphides removed from dipping porous electrodes, which have been used in the h.e.r. at 400 mA, 500 mA in 5N KOH for 5 hours at 25°C	116
5.3.	X-ray powder data for cobalt-nickel oxide removed from a freshly prepared dipping porous electrode and thermal decomposed cobalt-nickel oxide	117
5.4.	The effectiveness factors for dipping porous electrode structure and teflon-bonded porous electrode structure at different potentials and temperatures	127
6.1.	Theoretical forecast kinetic parameters for the most probable mechanisms of the hydrogen evolution reaction	139
6.2.	Kinetic parameters for the hydrogen evolution reaction on cobalt-nickel sulphide dipping porous electrode in 5N KOH solution	150
6.3.	Arrhenius activation energies at different overpotentials in KOH solutions of pH 14.32, 14.0 and 13.06	155
6.4.	Reaction orders at different temperatures and potentials	157

LIST OF FIGURES

		Page
2.1.	Half-cell design	20
2.2.	Circuit for potentiostatic polarisation	22
2.3.	Circuit for galvanostatic polarisation	23
2.4.	Interrupter circuit	25
2.5.	Voltage and current decay curves in interrupter measurements	26
2.6.	Voltage/current curves for different nickel sulphides in teflon-bonded porous electrode structures	35
2.7.	Current/time curves for different nickel sulphides in teflon-bonded porous electrode structures	36
2.8.	Performance of various nickel sulphides in teflon-bonded porous electrode structures as a function of time	37
3.1.	Voltage/current curves for cobalt-nickel sulphide A and platinum black in teflon-bonded porous electrode structures	53
3.2.	Performance of cobalt-nickel sulphide A and platinum black in teflon-bonded porous electrode structures as a function of time	54
3.3.	Voltage/current curves for different cobalt-nickel sulphides in teflon-bonded porous electrode structures	56
3.4.	Voltage/current curves for cobalt-nickel sulphide D in teflon-bonded porous electrode structure	57
3.5.	Freeze drying apparatus	45
3.6.	Apparatus for the measurement of electrical conductivity on powder sample	47
4.1.	Apparatus for the determination of sulphide content in insoluble metallic sulphides	65
4.2.	A typical Edax analytical concentration count for cobalt, nickel and sulphur	75
4.3.	Electron micrographs of sulphided products prepared from freeze dried cobalt-nickel oxide	76

		Page
4.4.	Electron micrographs of thermal decomposed cobalt-nickel oxide and its sulphided products	77
4.5.	Kinetic curves of sulphiding freeze dried cobalt-nickel oxide	78
4.6.	Kinetic curves of sulphiding NiO and Co_3O_4	94
4.7.	Voltage/current curves for various cobalt-nickel sulphides in teflon-bonded porous electrode structures at 70°C	81
4.8.	The plot of performance vs catalyst loading for different cobalt-nickel sulphides in teflon bonded porous electrode structures	82
4.9.	Apparatus for sulphiding of cobalt-nickel oxide	97
4.10.	The effect of the atmosphere on the thermal decomposition on cobalt-nickel sulphide C	83
5.1.	Potentiostatic pulse circuit	108
5.2.	Galvanostatic pulse circuit	110
5.3.	The effect of double layer charging	112
5.4.	Voltage/current curves for cobalt-nickel sulphide in different porous electrode structures at 70°C	118
5.5.	Performance of cobalt-nickel sulphide in various porous electrode structures as a function of catalyst loading	120
5.6.	Performance of cobalt-nickel sulphide in teflon-bonded porous electrode structures as a function of teflon content	121
5.7.	Potentiodynamic and potentiostatic transient measurements for cobalt-nickel sulphide in dipping porous electrode structures at 25°C	122
5.8.	Potentiodynamic and potentiostatic transient measurements for cobalt-nickel sulphide in dipping porous electrode structures at 40°C	123
5.9.	Potentiodynamic and potentiostatic transient measurements for cobalt-nickel sulphide in dipping porous electrode structures at 70°C	124

		Page
5.10.	Potentiodynamic and potentiostatic transient measurements for cobalt-nickel sulphide in teflon-bonded porous electrode structures at 25°C	125
5.11.	Potentiodynamic and potentiostatic transient measurements for cobalt-nickel sulphide in teflon-bonded porous electrode structures at 70°C	126
6.1.	The plot of log i vs potential for cobalt-nickel sulphide dipping porous electrode in 5N KOH solution at 25°C	142
6.2.	The plot of log i vs potential for cobalt-nickel sulphide dipping porous electrode in 5N KOH solution at 40°C	143
6.3.	The plot of log i vs potential for cobalt-nickel sulphide dipping porous electrode in 5N KOH solution at 70°C	144
6.4.	The plot of log i vs 1/T, for cobalt-nickel sulphide dipping porous electrode in 5N KOH solution	145
6.5.	The plot of log i vs potential for cobalt-nickel sulphide dipping porous electrode in pH 14.32 KOH solution at 25°C, 40°C and 70°C	146
6.6.	The plot of log i vs potential for cobalt-nickel sulphide dipping porous electrode in pH 14.0 KOH solution at 25°C, 40°C and 70°C	147
6.7.	The plot of log i vs potential for cobalt-nickel sulphide dipping porous electrode in pH 13.06 KOH solution at 25°C, 40°C and 70°C	148
6.8.	The plot of log i vs 1/T for cobalt-nickel sulphide dipping porous electrode in pH = 13.42 KOH solution	152
6.9.	The plot of log i vs 1/T for cobalt-nickel sulphide dipping porous electrode in pH = 14.0 KOH solution	153
6.10.	The plot of log i vs 1/T for cobalt-nickel sulphide dipping porous electrode in pH = 13.06 KOH solution	154
6.11.	The plot of log i vs the pH at different potentials for cobalt-nickel sulphide dipping porous electrode at 25°C	158
6.12.	The plot of log i vs the pH at different potentials for cobalt-nickel sulphide dipping porous electrode at 40°C	159

Page

6.13. The plot of log i vs the pH at different potentials for cobalt-nickel sulphide dipping porous electrode at 70°C 160

CHAPTER ONE

EMERGING HYDROGEN ECONOMY

1. INTRODUCTION

In the light of todays uncertainty regarding future availability and price of conventional fossil fuels, much effort has been devoted to develop alternate energy sources, particularly new primary energy sources, such as nuclear fission, controlled fusion, geothermal energy and solar power. Other programmes are focused on the development of secondary fuels such as hydrogen, which can be manufactured on a large scale, using off-peak power from nuclear, solar or hydroelectric power stations.

Hydrogen is seen as the ultimate fuel to replace natural gas and gasoline. The principal advantage would be the absence of pollution after combustion. A second major attraction of hydrogen is its potential for the storage and cheap transmission of energy over long distances[1].

Before 1940, most hydrogen was produced by reacting steam with heated coke - the water gas. With the advent of low cost oil and naural gas, new processes were developed for hydrogen manufacture using these feedstocks. Today the bulk of hydrogen is produced by catalytic steam reforming of natural gas or naphtha and by the partial oxidation of heavy oils. A break down of total world production according to process employed is shown in Table 1.1.

Table 1.1. Hydrogen production process - worldwide

Hydrogen Production Process	%
Catalytic steam reforming	65
Partial oxidation	25
Coal/Coke based	7
Electrolytic	3

Electrolytic hydrogen (3% of world total) is obtained as a by-product of chlorine manufacture in the United Kingdom and elsewhere. Electrolysers specifically for hydrogen production have been built in regions of cheap hydro-electric power, e.g. Norway and Egypt (Aswan Dam).

At prices ruling today, hydrogen is employed almost exclusively for chemical purposes, generally in a plant situated in the same chemical complex as the reformer. As a fuel, it is unable to compete economically with fossil fuels and this situation is likely to continue until advances in nuclear reactor technology, solar energy etc. make these other primary energy sources substantially cheaper than fossil fuels. With the increasing cost of coal and the impending unavailability of oil and natural gas in as little as forty years[2], the only alternative method for hydrogen production on a large scale can be by water electrolysis using electricity derived from nuclear or solar energy. The other potential route to hydrogen production is thermal decomposition of water, which is still highly speculative; i.e. in basic research stage.

2. HYDROGEN PRODUCTION BY WATER ELECTROLYSIS

Hydrogen production technology has continually changed, due both to an increase in technical knowledge and because of economic factors. The electrolytic method is the simplest and cleanest method of hydrogen production from water, either on a small or large scale. The hydrogen produced contains only oxygen

(less than 0.3%) as impurity. On the whole, electrolysis is an off-the-shelf technology, which has received a lot of attention especially for the past five years.

The electrolysis of water was first demonstrated by Nicholson and Carlisle in 1800 and later by Faraday in 1820. An electrolysis cell for the production of hydrogen from water consists of an electrolyte, circulating between two electrodes. A basic solution as electrolyte is used in preference to pure water so as to increase the conductivity of the solution. This could also be accomplished using an acidic solution but the corrosion problems would be more severe. In a basic solution, the cathode reaction is,

$$2H_2O + 2e \longrightarrow H_2 + 2HO^- \qquad (1)$$

and oxygen is produced at the anode

$$2OH^- \longrightarrow 1/2\ O_2 + H_2O + 2e \qquad (2)$$

The cell reaction is the combination of cathode and anode reactions, in which a current is passed through a basic solution to produce hydrogen and oxygen:

$$H_2O + \text{electrical energy} \longrightarrow H_2 + 1/2\ O_2 \qquad (3)$$

The electrical energy is thereby converted into chemical energy as hydrogen with a change in enthalpy at 25°C and 1 atmosphere of

$$\Delta H = 68{,}320 \text{ cal./g-mole}$$

The first law of thermodynamics for a steady flow system is,

$$Q - W_s = \Delta H \tag{4}$$

in which Q = heat added to the system

W_s = useful work done by the system

For the electrolysis unit, the work term is the electrical energy to the cell, and is given by,

$$W_s = -nFE \tag{5}$$

in which n = 2, the number of electrons transferred.

F = the Faraday constant = 96,500 coulombs/g-equiv.

= 23,074 cal/volt-g-equiv.

E = the electrical potential applied to the cell, volts

Combining equations (4) and (5) gives

$$E = \frac{\Delta H - Q}{nF} \tag{6}$$

Consider in the reversible cases (i.e. cell operation at thermodynamic equilibrium) for which equation (6) becomes

$$E = \frac{\Delta H - Q_{rev}}{nF} \tag{7}$$

Since an electrolysis cell operates isothermally, from thermodynamics,

$$Q_{rev} = T\Delta S \tag{8}$$

So that

$$E_{rev} = \frac{\Delta H - T\Delta S}{nF} \tag{9}$$

The numerator of equation (9) is simply the change in Gibbs free energy reaction, and at 25°C, 1 atmosphere.

$$\Delta G = \Delta H - T\Delta S = 56{,}690 \text{ cal/g-mole}$$

The reversible cell potential is then,

$$E_{rev} = \frac{\Delta G}{nF} \tag{10}$$

and at 25°C, 1 atmosphere,

$$E_{rev} = \frac{56{,}690}{2(23{,}074)} = 1.229 \text{ volts} \tag{11}$$

Consider actual (not reversible) operation, i.e. equation (6), the cell potential, E, however, depends upon cell design parameters approaching E_{rev} for a well-designed system. The actual cell potential required is always greater than the reversible cell potential corresponding to the same conditions of pressure, temperature and electrolyte concentration. For reversible operation, Q is a positive quantity over the range of interest since the enthalpy change is greater than the Gibb's free energy change, ΔG, which by equation (10) is the same as nFE. As the operation becomes more irreversible, the cell potential increases thereby decreasing Q. Eventually, a point is reached where Q vanishes and no heat need be added to the system. This is called thermoneutral operation, and by equation (6), corresponds to a cell potential,

$$E_t = \frac{\Delta H}{nF} \tag{12}$$

in which E_t is the thermoneutral cell potential. For even greater irreversibility of operation, Q becomes negative. That is, in reversible operation heat is required, but cell inefficiency eventually leads to a situation where cooling is required.

Electrolysis cell thermal efficiency, ε_t is always calculated based on a comparison of the actual cell potential with the cell potential for thermoneutral operation:

$$\varepsilon_t = \frac{E}{E}t \times 100 \qquad (13)$$

The voltage efficiency, E_v of a water electrolysis cell operating at the current density i may be defined by:

$$E_v = \frac{E}{E}rev \times 100 \qquad (14)$$

2.1. Main Causes for Efficiency Losses in Water Electrolysis

At present, the energy efficiency for hydrogen by water electrolysis is about 75%. Theoretically, minimum energy required for the dissociation of water into its component gases can be calculated by assuming that no polarisation losses occur in an electrolysis cell. That is, the voltage applied to the cell is 1.229V at 25°C and 1 atmosphere pressure, independent of current flow. In practice, most industrial electrolysers require appreciably higher voltages than this, usually in the range of 1.7V to 2.2V cell. For hydrogen production to become an economical fuel base, technology efforts must be directed towards decreasing the electrical energy required to electrolyse water. This energy is a direct function of the terminal cell voltage, E. This voltage can be expressed as:

$$E = E_{rev} + \eta_a + \eta_c + \eta_{iR} \qquad (15)$$

in which η_a = activation polarisation at the electrodes.

η_c = concentration polarisation in the electrolyte.

η_{iR} = ohmic losses in the electrolyte and across membrane.

The difference between the actual cell voltage and the reversible cell voltage is the main cause for efficiency losses in water electrolysis.

2.1.1. Activation Polarisation

Activation polarisation at the electrodes results from charge transfer inhibition at the electrodes and is determined by the catalytic activity of the electrodes and surface roughness.

2.1.2. Ohmic Polarisation

Ohmic losses in the electrolysis cell is the sum of the η_{iR} terms due to electrolyte, membrane resistance and electrode resistance. Gas bubbles also contribute to the ohmic losses. In addition, vapour bubbles (water) will also be produced further increasing the ohmic resistance. The volume rate of bubbles produced will depend upon pressure, temperature, electrolyte concentration and current density, and these factors, together with electrolyte conductivity, membrane resistance and cell design considerations determine the ohmic loss in the electrolysis cell.

2.1.3. Concentration Polarisation

Concentration polarisation results from concentration gradients

which exist in the neighbourhood of the electrodes and is small for a cell with circulating electrolyte. Since this term arises due to a resistance to mass transfer, anything that tends to reduce mass transfer resistance will reduce the effect of this term. Thus, concentration polarisation may be reduced in any of the following ways:

(a) increasing the temperature,

(b) increasing the electrolyte flow rate,

(c) increasing the concentration of the species being transported, i.e. use greater strength potassium hydroxide solutions,

(d) decreasing the spacing between electrodes,

(e) decreasing the current density.

2.2. Areas of Research to Improve Energy Efficiency of Water Electrolysis Approaching 100%

(a) In fuel cell research and development, conclusive results have indicated that maximisation of the surface areas of the electrodes can reduce activation overpotential of the cell considerably. In general, porous electrodes can provide more of the electrode surfaces to be utilised as compared to planar electrodes. However, Tseung and Vassie[3,4] have showed that teflon-bonded platinum black porous electrode gives significantly higher performance than platinized porous electrode by measuring the effectiveness factor. (Transient pulse current immediately after double layer charging/steady state current at the same potential or overvoltage). This suggests that there is an urgent

need to optimise the porous electrode structure.

(b) By operating the electrolysis cell at higher temperatures, it is again possible to reduce activation polarisation considerably. This will also have the effect of reducing the ohmic losses in the cell. However, at higher operating temperatures, material problems will arise.

(c) The influence of gas bubbles on cell resistance can be minimised by optimising the spacing of the electrodes, by use of perforated electrodes or by operating the cell under pressure so as to reduce the actual volume of the bubbles. Other methods for reducing concentration polarisation have been described in Section 2.13.

(d) It is necessary to develop new separator materials in alkaline electrolyser cells to replace asbestos. Asbestos can not be used once the operating temperature exceeds 100°C. Also, there is a strong indication that asbestos will be banned because it is carcinogenic.

(e) The search for better electrocatalysts will speed up the rate of the reactions at the electrodes and thus reduce activation polarisation. Electrode material significantly influences the Tafel constants for activation polarisation, particularly the "a" values. For example, the choice of nickel and nickel-plated steel for the oxygen evolution anode is made based on consideration of these Tafel constants vs. availability and cost. Exotic materials such as platinum can reduce these

losses somewhat, but not economically, for large scale usage.

3. PRESENT WORK

The ultimate aim of this work has been to contribute towards the research and development of alkaline electrolyser cells. The line of approach to the problems have been outlined earlier in Section 2.2.

The primary target of this work is to select and evaluate potential materials for hydrogen cathode electrocatalysts in basic media. e.g. 5N KOH. As growth in technology application in electrocatalysis, especially in fuel cell technology, is more advanced than the degree of understanding, the need of experimental verifications is necessary. Therefore, another task in the present work is to correlate the catalytic activity for the hydrogen evolution reaction in an alkaline media, with different porous electrode structures. Two porous electrode structures are considered, namely the porous electrode structure, prepared by the dipping[5] method, and the teflon-bonded porous electrode structure.

On the whole, electrocatalytic phenomena are similar to chemical catalysis, and are governed by many parameters (electronic structure of the solid state body, conductivity, surface states, crystal faces, lattice defects, adsorption energy, surface mobility, steric effects, structure of double layer) that it is not possible to put forward a general theory at this stage. However, with a view to understanding and developing hydrogen evolution electrodes, fundamental kinetic parameters are also

determined in the present work for the most promising cathode electrocatalyst under investigation.

CHAPTER TWO

HYDROGEN CATHODE ELECTROCATALYST

1. GENERAL SURVEY ON THE HYDROGEN EVOLUTION REACTION (h.e.r.)

The Hydrogen Evolution Reaction, i.e. equation (1) is of considerable importance in water electrolysis and chlor-alkali cells, and is the most extensively studied reaction[6,7]. The majority of processes in the electrochemical industry are accompanied by hydrogen evolution, and the overvoltage of this electrode reaction significantly influences the energy requirements and the efficiency with respect to energy.

Bockris[8,9,10] and Conway[11] published correlations of overvoltages varied periodically with atomic number of various metals. Parson[12] and Breiter[13] showed that the variation of the rate of hydrogen evolution bears a relationship to the heat of hydrogen adsorption on the metal. In papers by Trasatti[14], Kita[15], Kita and Kurisu[16], Kuhn et al[17] and Miles and Thomason[18], the catalytic activity was related to a series of properties of the catalyst such as, atomic number, atomic radius, metal-hydrogen bond and compressibility, certain trends were found. Kita and Kurisu[16] showed that the activity is related to the work function and on this basis divided metal catalysts into two groups: the d and sp metals each having entirely different behaviour in phenomena related to the h.e.r. Kita showed volcano-type relationships to exist between heat of atomisation, boiling point and melting point with activity. A catalytic mechanism was proposed for the d metals whilst an electrochemical mechanism, with discharge of the adsorbed hydrogen molecule ion rate-determining, was proposed for the sp metals.

Kuhn et al[17] claimed that such correlations were subjective

and only data should be quoted where strict criteria are laid down for selection. Miles and Thomason[18] recently collected data of their own on this reaction on a series of metal catalysts. A correlation was found between hydrogen overpotential and the transition metal work function, this was less precise for non-transition metals. A volcano-type relationship was found between metal-hydrogen bond strength and overpotential similar to Trasattis'[14] results. The hydrogen overpotentials have minimum values for Ni, Pd and Pt which have d^8s^2, $d^{10}s^0$ and d^9s^1 electronic configurations, respectively. High hydrogen overpotentials are observed for Zn, Cd and Hg all with d^{10} s^2 electronic configurations. The experimental results confirm that electronic factors play a major role in electrocatalysis and that these factors can be favourably modified by combining the proper elements.

Bagotsky et al[19] found that coverage of the catalyst support with the catalyst influenced catalytic activity owing to activation of the Pt by the support. Tungsten oxide doped with Pt by implantation[20] had an enhanced catalytic activity attributed to either bronze formation or reduction of the oxide thus exposing more Pt. Vondrak and Balej[21] also found that hydrogen/tungsten bronzes accelerated the evolution reaction. Randin and Vijh[22] have also studied the reaction on Na_xWO_3. Kerovin et al[23] have also found an influence of support on catalytic activity.

Miles[24] evaluated various metallic elements, compounds and alloys as electrocatalysts for the h.e.r. and concluded that electronic properties are a major factor affecting catalytic activity. Brooman and Kuhn[25] also correlated the reaction rate

with alloy properties. Bockris, Damjanovic and Mannan[26] recently showed that electronic factors markedly influence the heat of activation in reactions involving chemisorbed species.

At present, the most common material used for cathodes in alkaline electrolyser cells is steel, but there are disadvantages. If cells are misconnected even for a few hours, considerable destructive attack can occur. Also, the typical performance of such electrodes is only 250 mA/cm^2 at -300 mV vs reversible hydrogen electrode (R.H.E.). Cathode catalytic problems can be solved most easily with platinum metal catalysts (1-2 mg/cm^2). However, it is very susceptible to poisoning by trace impurities from the cell components and electrolyte. Moreover, if the platinum metal is supported on catalyst supports, such as carbon, it would be impractical to use them in a hydrogen evolution mode, since the carbon or graphite would disintegrate once the hydrogen pressure built up inside the pores of the carbon aggregates[27].

Therefore, the alternative is the use of inexpensive Raney nickel[28] or nickel boride as cathode catalysts. These materials, though adequate in terms of performance improvement and reduced susceptibility to poisoning (because of the very much higher loadings used, 20-30 mg/cm^2), are not satisfactory since they tend to oxidise when they are at open circuit. The oxidation of the catalyst is particularly serious when such electrodes are accidentally exposed to air during non-scheduled shutdowns or breakdown of the separators. The presence of a NiO film on the catalyst surface will lead to drastic deactivation of the cathode catalyst; this is because NiO is non-conducting and extremely

difficult to reduce electrochemically. Hence any search for a new cathode catalyst must take this point into consideration. Another factor which must be considered is the ease and cost of fabricating the catalyst into high surface area form.

Taking the above considerations into account, the transition metal sulphides may be of particular interest, since they are normally good conductors and are known to be more oxidation resistant than Raney nickel and nickel boride. Furthermore, they can be synthesized into a high surface area form more readily.

2. LITERATURE SURVEY ON Ni-S SYSTEM

The Ni-S[29,30,31] system has been studied extensively. The mono-sulphide is dimorphic, and can be prepared by precipitation from aqueous solutions. The primary precipitate from a Ni^{2+} solution (α - NiS) is almost amorphous $Ni(SH,OH)_2$. At low pH it crystallises to give mainly rhombohedral (γ - NiS) of millerite type, and if traces of oxygen are present, nickel sulphide of Ni_3S_4 is formed. At a somewhat higher pH, the product of crystallisation is hexagonal $Ni_{1-x}S$ (β - NiS) of the NiAs type. The precipitate from alkaline solutions does not crystallise spontaneously, it oxidises to give NiS_2 and basic salts[32,33].

Nickel disulphide (NiS_2) has the pyrite structure[34]; it is an antiferromagnetic[35] semiconductor[36,37].

Ni_3S_4 (polydymite) has a spinel[29] structure at ordinary pressure, but a hexagonal structure at about 0.5 bars[38]. At c. 620K, Ni_3S_4 decomposes to NiS_2 and the NiAs type $Ni_{1-x}S$.

Ni_3S_2 (heazlewoodite) is rhombohedral at room temperature. Above 820K, Ni_3S_2 has a face-centred cubic structure[39] and a broad range of homogeneity ($Ni_{2.5}S_2$ - $Ni_{3.4}S_2$ at 970K). Ni_3S_2 is a metallic conductor[40].

The phase Ni_6S_5 (called Ni_7S_6 or Ni_9S_8 by some authors) is also dimorphic. It undergoes a transition at c. 670K. The high temperature form (stable up to 848K) is orthorbombic[41] and the low temperature form is possibly hexagonal.

Stoichiometric NiS converts at 650K to a rhombohedral form (millerite)[29], which is metallic[42] with temperature-independent paramagnetism[43], and the same is true of the NiAs type which undergoes a first order transition[45], the unit-cell dimensions change discontinuously[46], and the phase becomes semi-conducting[44] and antiferramagnetic [45,47].

Kato and Oki[48,49] and Gerlach[50] studied the anodic polarisation of nickel sulphides in acid solutions and found that nickel sulphides were oxidised with the formation of both elemental sulphur and the sulphates. Ranter and Breckpot[51] showed that nickel can be extracted or added, practically reversible, by electrochemical anodic or cathodic polarisation on the amorphous nickel sulphide suspended around a platinum electrode in the nickel ion solution.

A comprehensive electrochemical study of sulphide minerals was carried out by Peter[52], who showed that most sulphides can be characterised according to their reversibility along thermodynamically predicted reaction paths that yield elemental sulphur, or a mineral of higher sulphur activity.

Rand[53] studied the reduction of oxygen on sulphide minerals

and suggested that at negative potential, sulphides can be reduced to give metal rich sulphides or even elemental metal.

Huq and Rosenberg[54] studied the h.e.r. on nickel sulphide (NiS) and various nickel compounds. Experimental results revealed that NiS behaves similarly to nickel metal. Jasinki[55] used Ni_3S_2 as a fuel cell catalyst for anodic oxidation of carbon monoxide and found that it is also active towards h.e.r. in an alkaline solution of 6N KOH.

Since there is a wide range of possible nickel sulphide compositions, the initial evaluation has been mainly concentrated on compositions which are easily obtainable, commercially.

3. EVALUATION OF NICKEL SULPHIDES AS POTENTIAL HYDROGEN CATHODE ELECTROCATALYSTS IN ALKALINE MEDIA

3.1. Materials Used in Half-Cell Electrochemical Testing

3.1.1. The Electrolyte

The electrolyte used was 5N potassium hydroxide solution and was prepared from potassium hydroxide ((85%) analar grade, supplied by B.D.H.) and deionised water of resistance greater than 4 M-ohm-cm^{-1}. For normal steady state operation, the solution does not require further purification, but is is essential to purify the solution by electrolysis if pulse work is involved. This is done by passing a constant current of 5 mA for ten hours between two platinum foil electrodes (supplied by Johnson Matthey Co. Ltd.).

3.1.2. Electrocatalysts and Their Sources

(a) Platinum black powder (supplied by Johnson Matthey Co. Ltd.).

(b) Nickel sulphide, prepared by precipitation from 10% nickel nitrate solution saturated with hydrogen sulphide.

(c) Nickel(II) sulphide, (99% pure, obtained from Alfa Ventron Products).

(d) Nickel(IV) sulphide, (99% pure, also obtained from Alfa Ventron Products).

(e) NiS (technical grade, supplied by Fisons).

3.1.3. The Gases

Four gases were used, hydrogen, nitrogen, air and hydrogen sulphide. Hydrogen and nitrogen were white spot grade (supplied by B.O.C.). The air supply was obtained from the atmosphere without purification. The hydrogen sulphide was used to synthesize sulphides and was obtained from Cambrian Chemicals Ltd.

3.1.4. Fabrication of Teflon-Bonded Porous Electrode

A weighed amount of the electrocatalyst powder and aqueous polytetrafluoroethylene dispersion (60% PTFE content, manufactured by I.C.I. under the trade name "Fluon") were mixed with a few drops of methanol. The mixture was then dispersed in an ultrasonic bath for 10 minutes. A paste-like slurry is formed and is applied onto

a clean 1 cm^2, 100 mesh nickel screen (supplied by Begg and Cousland Co. Ltd.), the electrode was then dried in air with a hair dryer and cured in a stagnant air oven at 300°C for one hour. The electrocatalyst/teflon ratio is 10/3 in each case. This is because the most satisfactory PTFE content has been shown to be 25-35% by weight of the electrocatalyst[56].

3.1.5. The Half-Cell Design

The half-cell used was similar to the galvanostatic hydrogen stripping cell used by Vassie[57] and Hobbs[58], and consists of three compartments; a luggin capillary connected to the working compartment with the reference compartment. The counter electrode or current collector is a big piece of 100 mesh nickel screen welded onto a nickel wire, (supplied by Fisons). This kind of cell design offers major advantages over the conventional floating electrode cell design[59] because, firstly, it is more easy to handle and it also minimises the chances of carbonation of the electrolyte by the atmosphere. The half-cell is shown in Figure 2.1.

3.1.6. The Reference Electrode System

The dynamic hydrogen electrode[60] (D.H.E.) was used as the reference electrode in this work. The preparation of the D.H.E. has been described elsewhere[61]. The voltage between the D.H.E. against a normal bubbling hydrogen electrode (R.H.E.) in the same electrolyte, is about -25 to -33 mV. In order to maintain the D.H.E. in tip-top condition, it is best kept in diluted

Figure 2.1. Half-cell design.

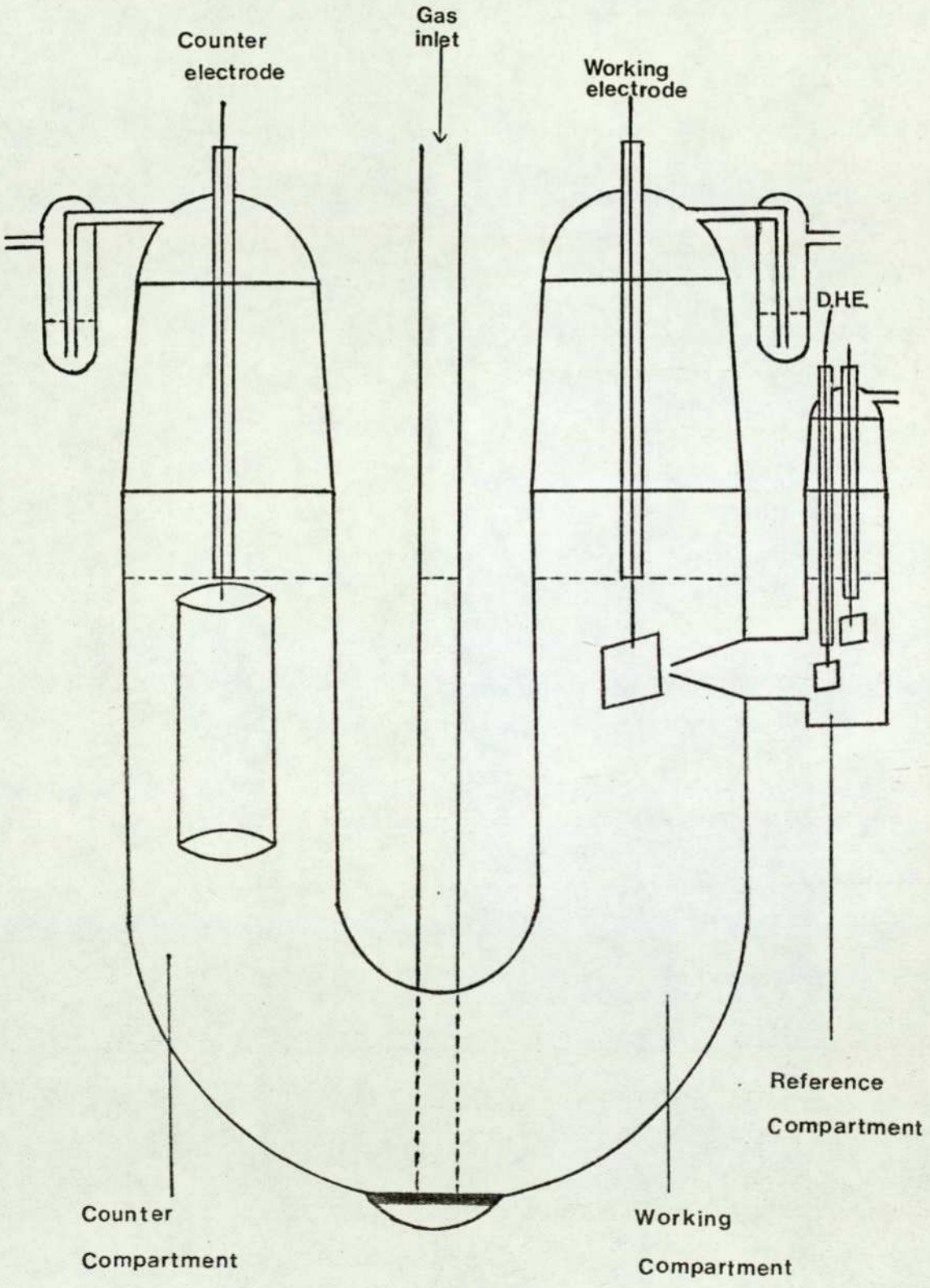

sulphuric acid when not in use, and it is necessary to platinise the D.H.E. at fortnightly intervals.

3.2. Half-Cell Electrochemical Testing

3.2.1. Steady State Polarisation Techniques

The use of potentiostatic and galvanostatic steady state polarisation techniques in electrochemistry have been described in detail by other workers[57,58]. A voltage/current relationship is obtained by stepwise polarisation using a potentiostat (model TR40-3A, made by Chemical Electronics Ltd.), with the aid of a digital voltameter (model DMM7, made by Gould Advance) either for the measurement of voltage between the working electrode and the D.H.E. or the current passing between the working electrode and the counter electrode. The circuit diagrams of the steady state potentiostatic and galvanostatic polarisation are shown in Figures 2.2 and 2.3. For each stepwise polarisation, readings are taken when they become steady, normally at five to ten minute intervals.

3.2.2. Potentiodynamic Polarisation Technique

Potentiodynamic technique is basically similar to potentiostatic steady state technique, the difference being the change of the applied voltage of the working electrode against the D.H.E. is driven by an external power generator, so that the change of voltage is a linear function with time. It is essentially the same as linear sweep voltammetry[62]. By selecting a sufficiently slow scan rate on the linear sweep generator (made

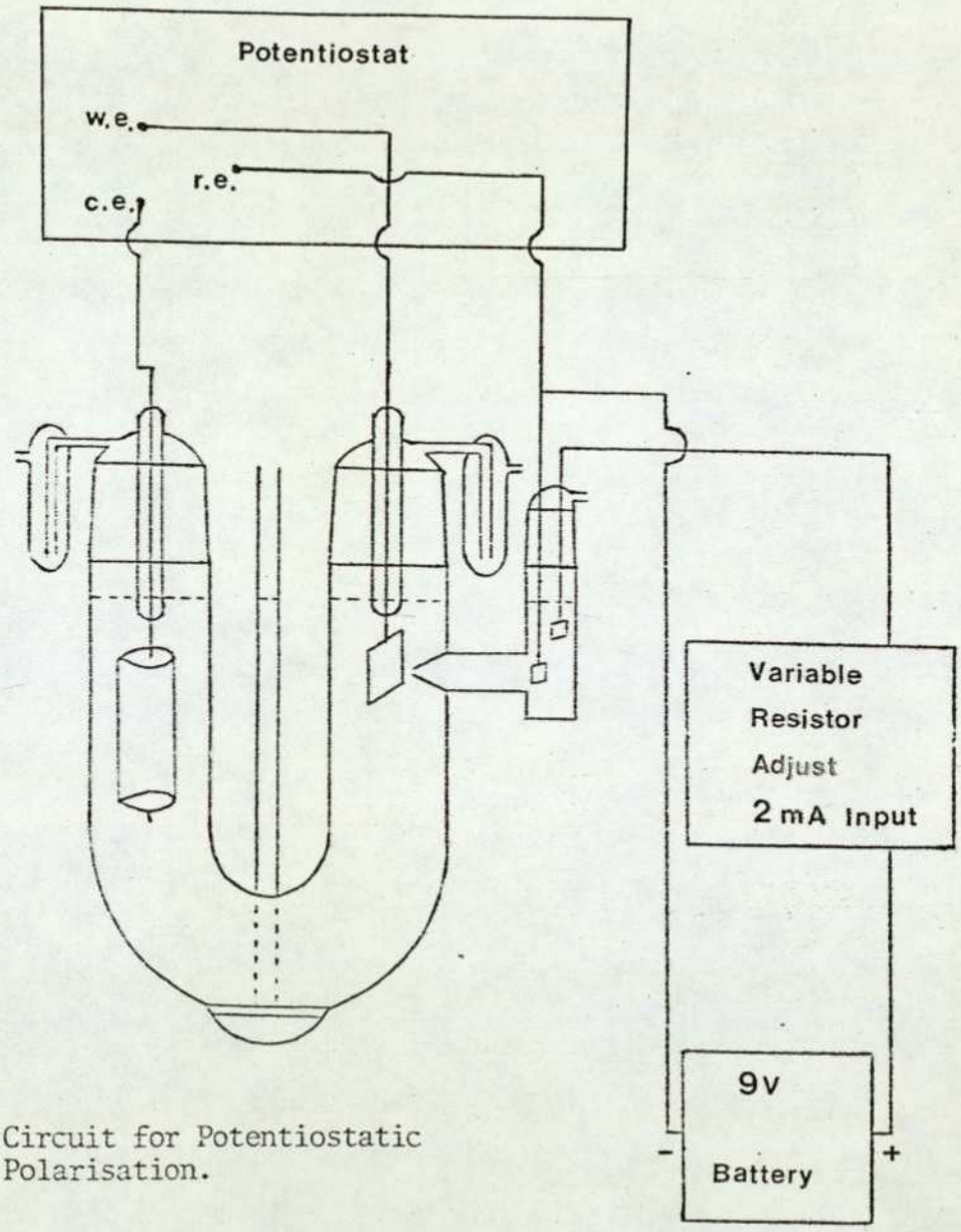

Figure 2.2. Circuit for Potentiostatic Polarisation.

Figure 2.3. Circuit for Galvanostatic Polarisation.

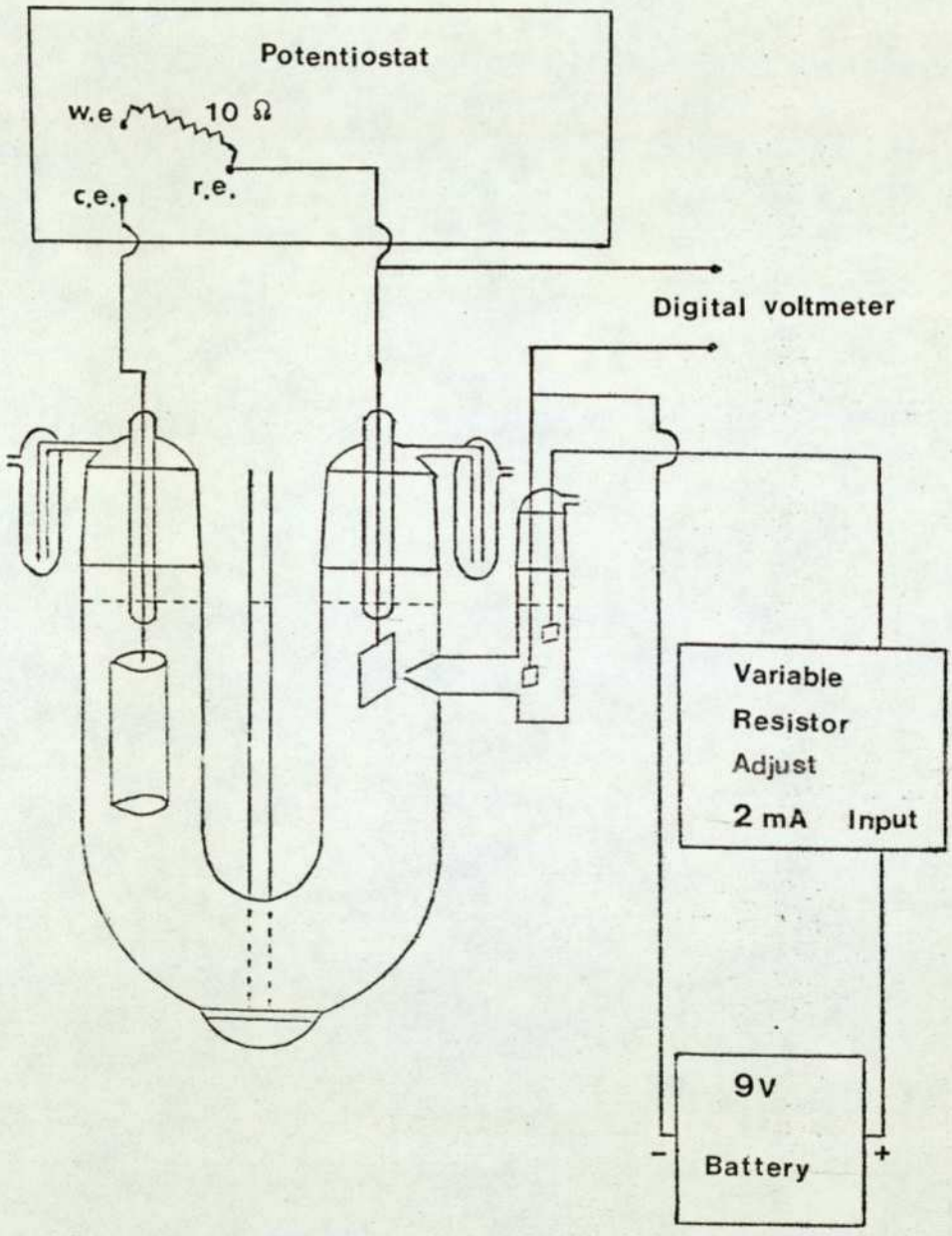

by Chemical Electronics Ltd.), the steady state potentiostatic voltage/current curve can be recorded on an X-Y pen recorder. (Model 29000 A4, made by Bryans).

3.2.3. Potentiostatic and Galvanostatic Stability Tests

Current/time relationship at constant voltage and voltage/time relationship at constant current are the most simple and practical methods to study the stability of the electrodes. The current/time voltage/time relationships can be recorded on an X-t plotter, (made by Smiths Industries) either using galvanostatic or potentiostatic circuits. (See Section 3.2.1.).

3.2.4. The Correction of Ohmic Overvoltage (iR drop)

The existence of ohmic overvoltage has been described in Chapter One. The most common method for the ohmic overvoltage correction is the interrupter method[63], although other techniques such as the measurement of the luggin-electrode geometry and A.C. conductivity bridge are also used[64,65]. The iR drop correction is most important when the electrodes are operated at high current density ranges, since more hydrogen bubbles arise at a higher current density, thus forming resistive layers and increasing the overvoltage of the electrodes. The circuit diagram and the interpretation of the iR drop correction by the interrupter method is shown in Figures 2.4 and 2.5.

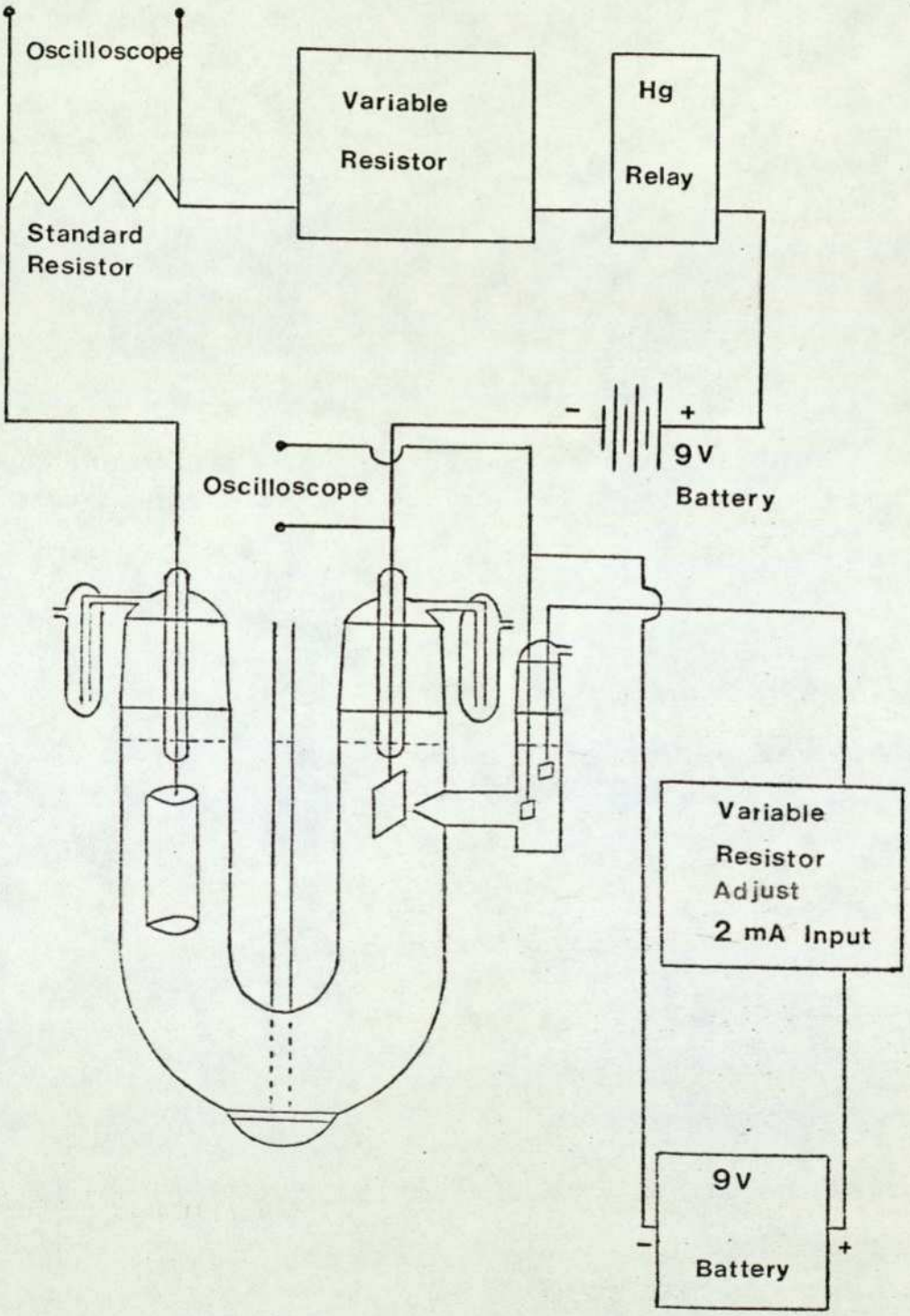

Figure 2.4. Interrupter Circuit.

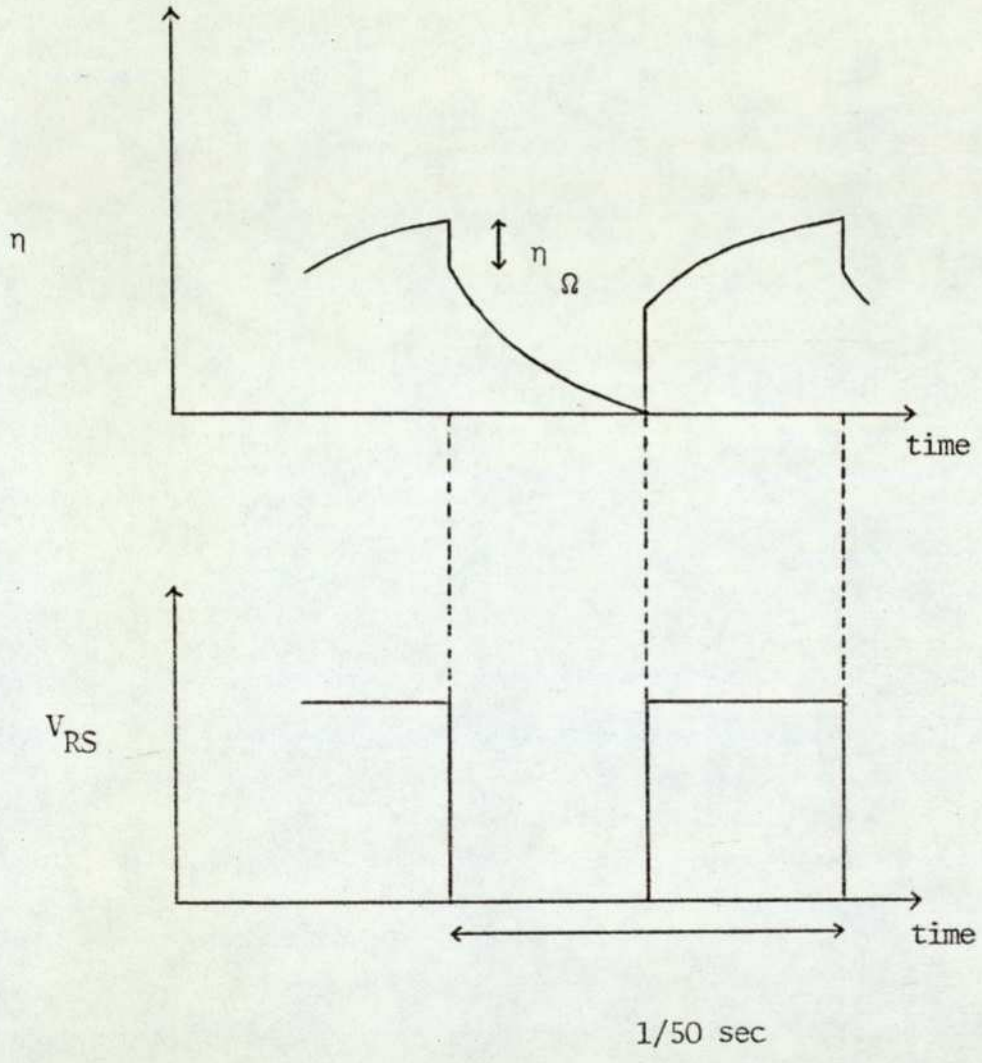

Figure 2.5. Voltage and current decay curves in interrupter measurements.

3.3. Electrocatalyst Characterisation

3.3.1. Aggregate Size Measurements

Apparatus for the measurement of particle size of the electrocatalyst was not available. Therefore, electrocatalyst power samples were sent to Coulter Electronics Ltd. for Coulter Counter size analysis. The average aggregate size of the electrocatalyst powders were calculated from Coulter Counter[66] measurements.

3.3.2. X-ray Powder Diffraction

Debye-Scherrer powder diffraction[67] photographs were obtained for many of the electrocatalysts used in this work with the help of the x-ray diffraction unit, (model PW1010, made by Phillips). Initially, the choice of x-ray sources, and the exposure time was by trial and error until a good diffraction photograph was obtained. Although accurate crystallographic measurements were not possible, there was little difficulty in identifying phases present and observing major differences in unit cell dimensions in the majority of the electrocatalysts under investigation. The limit of detection of trace phases is about 5%.

3.3.3. Atomic Absorption Spectroscopy[68]

Atomic absorption spectroscopy is the most frequently used method for the detection of trace metals dissolved in solution.

Metallic ions of concentration from 0.5 to 10 p.p.m. can be easily determined by this method. The metallic component is detected by analysing a sample of the nickel sulphide, dissolved in an acid solution. A systematic check for other transition metal ions which might be present as impurities in the sample, was also carried out using the atomic absorption spectrometer, (Model 290, made by Perkin Elmer).

4. RESULTS

4.1. X-ray Analysis

All samples were exposed to copper K_α radiation for five hours. X-ray diffraction patterns in Table 2.1., show that laboratory prepared nickel sulphide gives identical x-ray patterns as nickel(II) sulphide (purchased from Alfa Ventron Products). They all show the structure (γ - NiS) of the millerite type[69]. NiS (technical grade, obtained from Fisons) gave more complicated patterns, which suggested that mixed phases are likely to be present. By comparing the strong lines of the x-ray patterns of NiS with other related nickel compounds, it seemed that nickel sulphate monohydrate ($NiSO_4.H_2O$), nickel sulphide (Ni_3S_4), nickel-iron sulphide $(Ni, Fe)_3S_4$, nickel-cobalt sulphide $(Co, Ni)_3S_4$ and possibly other forms of nickel sulphide, may be present as impurities. The x-ray patterns of nickel(II) sulphide and nickel(IV) sulphide agree with the Literature[70]. The x-ray powder data of some related nickel compounds are listed in Table 2.2.

TABLE 2.1. X-ray Powder Data for Different Nickel Sulphides

NiS				Nickel Sulphide		Nickel(II) Sulphide		Nickel(IV) Sulphide	
dÅ	I	dÅ	I	dÅ	I	dÅ	I	dÅ	I
5.78	vf	1.90	vf	4.83	s	4.83	s	2.83	s
5.49	vf	1.85	vf	2.94	m	2.94	m	2.53	s
4.77	s	1.82	m	2.86	vf	2.86	vf	2.32	s
4.23	f	1.78	vf	2.78	vs	2.78	vs	2.00	s
4.03	vf	1.72	vf	2.51	s	2.51	s	1.91	s
3.83	m	1.67	m	2.40	m	2.40	m	1.72	vs
3.67	vf	1.61	f	2.23	s	2.23	s	1.66	f
3.56	vf			1.86	vs	1.86	vs	1.59	m
3.45	f			1.82	vs	1.82	vs	1.53	m
3.33	vs			1.73	s	1.73	s	1.32	s
3.23	f			1.63	m	1.63	m	1.29	m
3.10	vf			1.60	s	1.60	s	1.17	vs
3.00	m			1.55	m	1.55	m		
2.82	s			1.41	vf	1.41	vf		
2.61	vf			1.39	m	1.39	m		
2.53	vf			1.33	f	1.33	f		
2.48	f			1.30	m	1.30	m		
2.43	vf			1.26	m	1.26	m		
2.37	f			1.21	f	1.21	f		
2.14	m			1.20	m	1.20	m		
2.09	f			1.18	m	1.18	m		
2.02	f			1.14	m	1.14	m		
1.94	f			1.11	s	1.11	s		

I = intensity estimated visually
vs = very strong
s = strong
m = medium
f = faint
vf = very faint

TABLE 2.2. A.S.T.M. d-spacings for Some Related Nickel Compounds

[redacted]

TABLE 2.2. (continued)

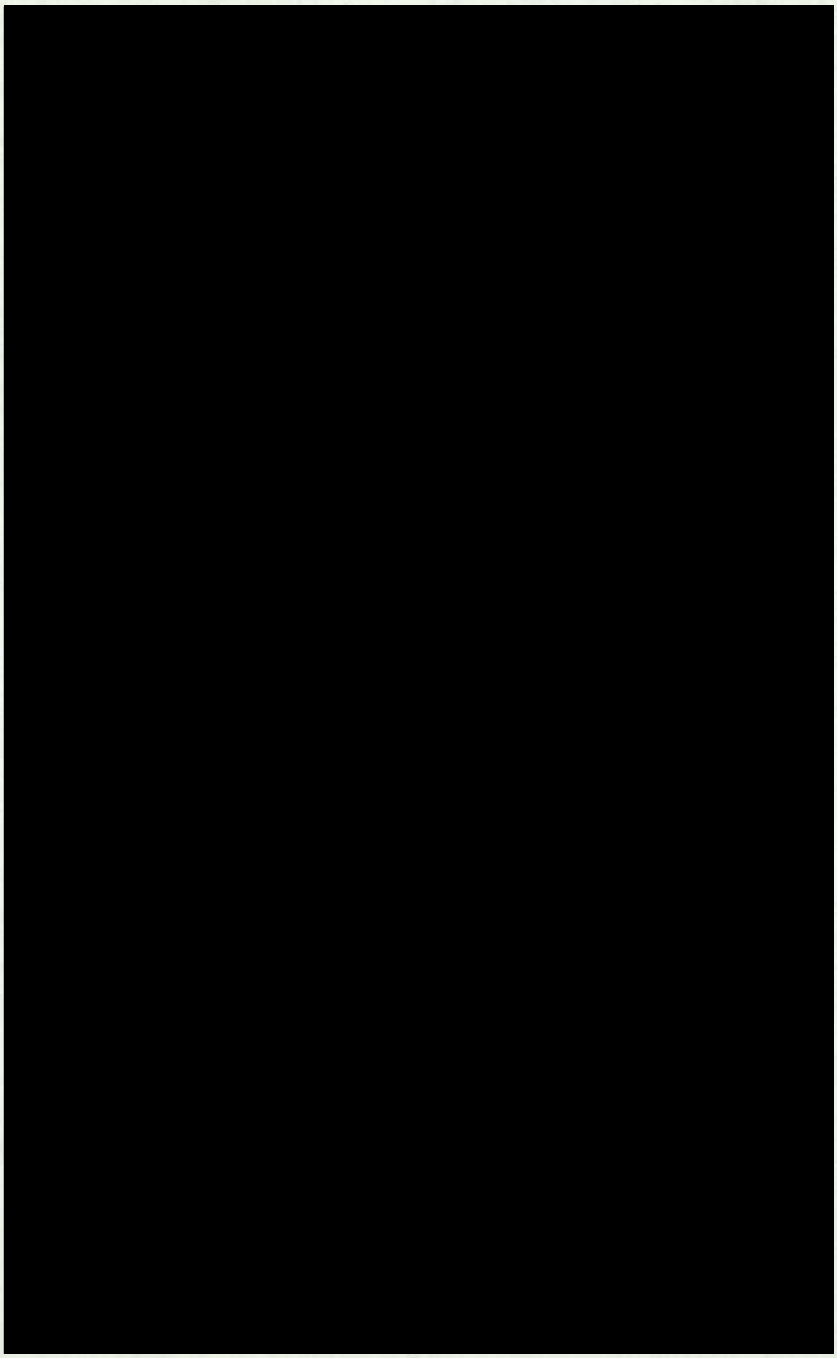

4.2. Aggregate Size Measurements

Table 2.3 lists the average aggregate diameter of various nickel sulphides, together with the result on cobalt-nickel oxide ($NiCo_2O_4$), for comparison. Cobalt-nickel oxide was prepared by freeze drying[71] (see Chapter Three, Section 2) and the reason for its inclusion will be seen more clearly later. (See Section 5).

4.3. Atomic Absorption Analysis

X-ray results showed that only NiS (technical grade) was contaminated with impurities while all other nickel sulphides were very pure. As it is impossible to detect the sulphur content directly by this method, the exact chemical composition of NiS (technical grade) is therefore not possible to deduce. However, it is possible to detect other metallic ions as impurities by analysing a series of solutions, each with different amounts of dissolved NiS sample. A relative ratio of nickel ions concentration with respect to other metallic ions concentration in each solution can be measured.

4.4. Half-Cell Electrochemical Results

Different nickel sulphide powders in teflon-bonded porous structures were investigated using the potentiodynamic polarisation technique. (See Section 3.2.2.). Immersed teflon-bonded porous electrode was mounted vertically in the working compartment of the half-cell, which was kept at a constant temperature with the aid of a thermostat (made by Techne Ltd.). The half-cell was purged with

TABLE 2.3. Average Aggregate Diameter (μ) for Various Nickel Sulphides and Freeze Dried Cobalt-Nickel Oxide

Sample	Average Aggregate diameter (micron)
$NiCO_2O_4$ (freeze dried)	1.27
Nickel sulphide (Laboratory prepared)	4.6
Nickel(II) sulphide (obtained from Alfa Venton Products)	15.1
NiS (technical grade, obtained from Fisons)	4.6
Nickel(IV) sulphide (obtained from Alfa Venton Products)	14.9

bubbling hydrogen thoroughly for an hour and a stable open circuit voltage (O.C.V.) or rest potential was then taken. The O.C.V. value was set on the potentiostat and the negative voltage limit was set on the linear sweep generator. The electrode was then potentiodynamically polarised at a sweep rate of 30 mV/minute in the cathodic direction. When the negative voltage limit of -300 mV (vs D.H.E.) was reached, a reverse sweep commences automatically. After sweeping between 25 mV to -300 mV (vs. D.H.E.) for several cycles, a reproducible voltage/current curve was then recorded on an X-Y plotter. The next step was the correction of iR drop by the interrupter method. (See Section 3.2.4). Potentiostatic current/time curves were also measured immediately after the iR drop correction.

iR Corrected potentiodynamic voltage/current curves in Figure 2.6, show that all tested samples of nickel sulphide have much better activity for h.e.r. than 100 mesh nickel screen. The order of activity was NiS > nickel(IV) sulphide > nickel sulphide > nickel(II) sulphide. In all cases, the final potentiostatic currents at the end of ten hours testing were higher than the potentiodynamic currents at the same potential. Figure 2.7 shows the iR corrected potentiostatic current/time curves of different samples of nickel sulphide. After leaving in the electrolyte of 5N KOH, saturated with bubbling air, for eight hours, the activities of nickel(II) sulphide, NiS and nickel sulphide, recover to within 10% of their original value in the course of the testing period. For nickel(IV) sulphide, the original activity cannot be reproduced. These effects are shown in Figure 2.8.

Figure 2.6. Voltage/current curves for different nickel sulphides in teflon-bonded porous electrode structures.

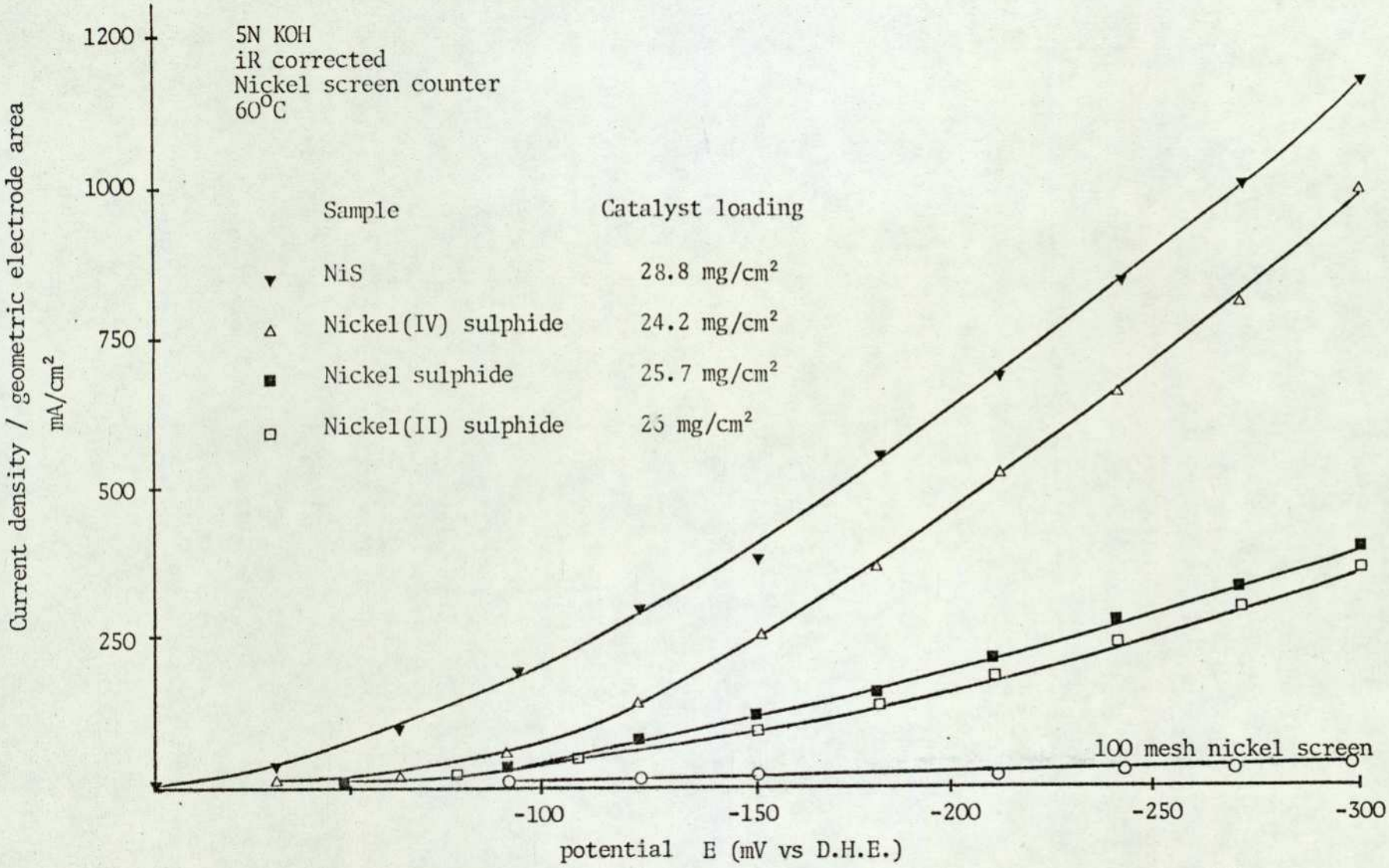

structures

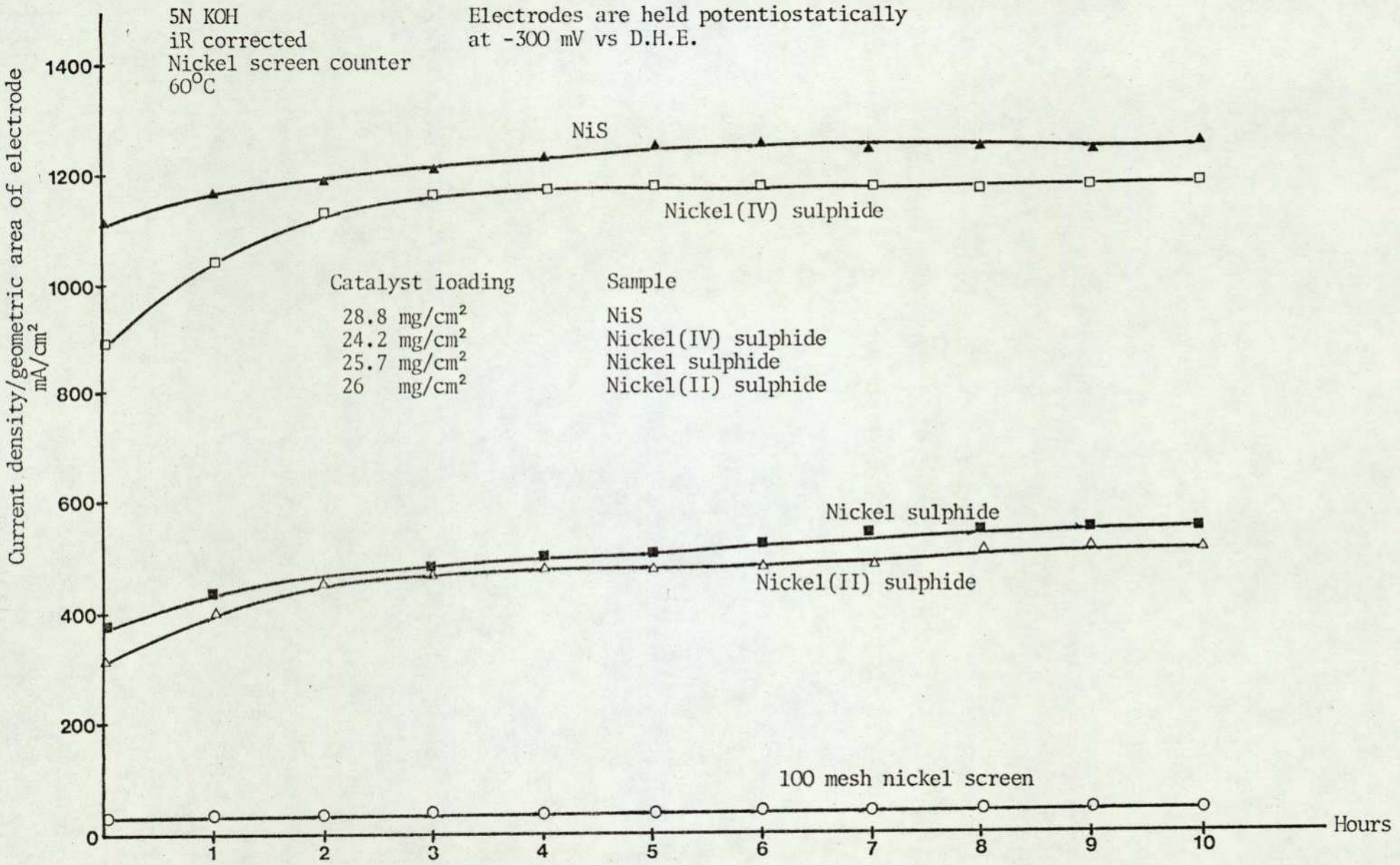
5N KOH
iR corrected
Nickel screen counter
60°C
Electrodes are held potentiostatically
at -300 mV vs D.H.E.
Current density/geometric area of electrode
mA/cm²
1400
1200
1000
800
600
400
200
0
NiS
Nickel(IV) sulphide
Catalyst loading
Sample
28.8 mg/cm²
NiS
24.2 mg/cm²
Nickel(IV) sulphide
25.7 mg/cm²
Nickel sulphide
26 mg/cm²
Nickel(II) sulphide
Nickel sulphide
Nickel(II) sulphide
100 mesh nickel screen
1
2
3
4
5
6
7
8
9
10
Hours

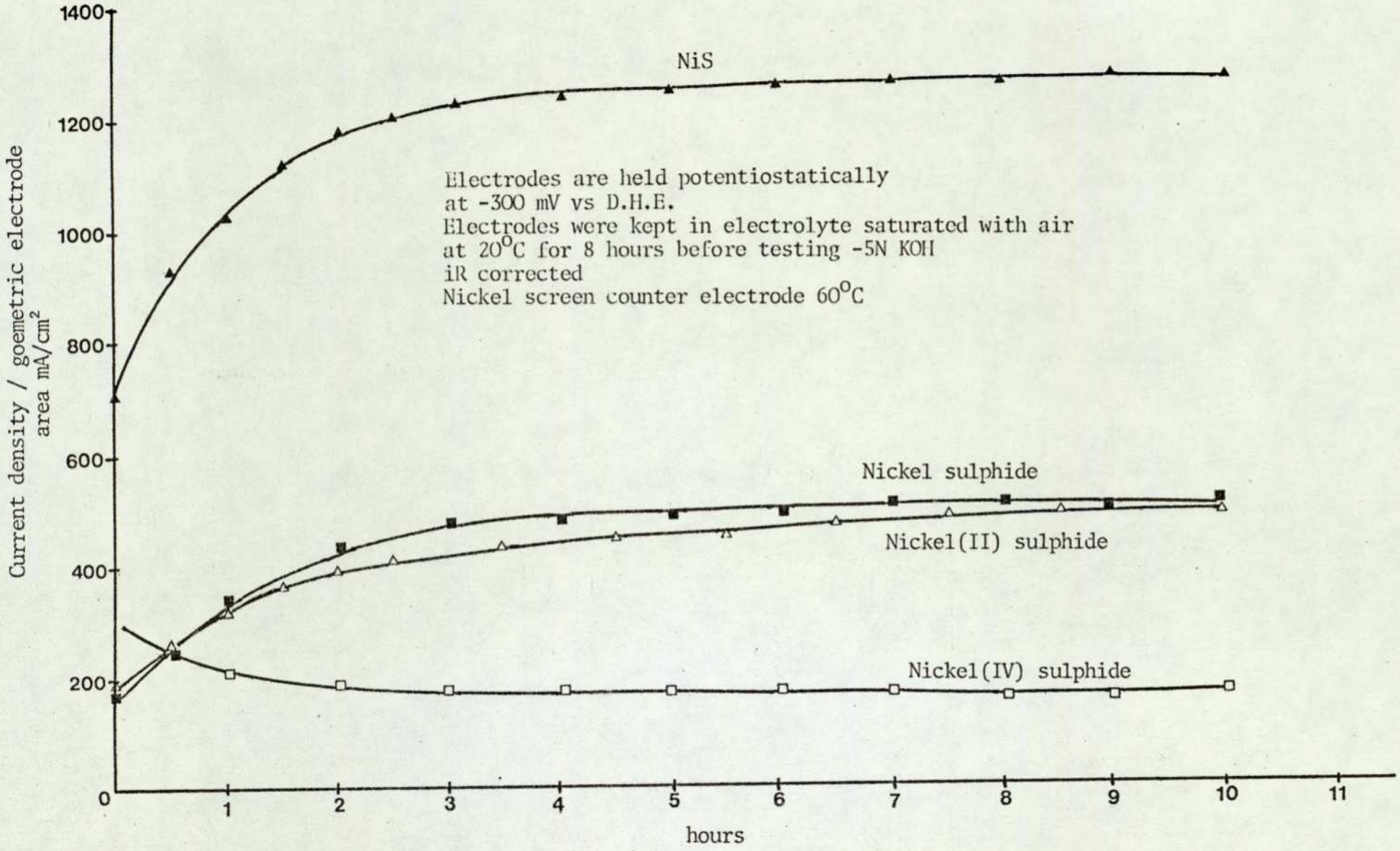
NiS
Electrodes are held potentiostatically
at -300 mV vs D.H.E.
Electrodes were kept in electrolyte saturated with air
at 20°C for 8 hours before testing -5N KOH
iR corrected
Nickel screen counter electrode 60°C
Nickel sulphide
Nickel(II) sulphide
Nickel(IV) sulphide
Current density / goemetric electrode area mA/cm²
hours
0
200
400
600
800
1000
1200
1400
1
2
3
4
5
6
7
8
9
10
11

5. DISCUSSION

The half-cell electrochemical testing showed that NiS (technical grade) gave the highest performance and that its activity was unaffected by exposure to air when it is left at open circuit. Nickel(IV) sulphide also possesses good activity, but unfortunately on exposure to air, the activity is markedly decreased. Nickel sulphide and nickel(II) sulphide, prepared in the laboratory and purchased from Alfa-Ventron Products, gave very low performance by comparison. X-ray results showed that NiS (technical grade) is very impure, containing possibly Ni_3S_4, $(Ni, Fe)_3S_4$. The presence of Fe_3S_4 either in solid solution with Ni_3S_4 or as a mixture may be significant, since iron oxides are more readily reduced electrochemically and this may be responsible for the recovery in performance after exposure to air. However, atomic absorption spectroscopy clearly indicated that the major impurity in NiS is in the form of cobalt salts. The atomic absorption results are listed in Table 2.4. The relative ionic concentration of nickel/cobalt is about 19/1 i.e. the maximum impurity of cobalt salts is about 5%. Together with the complicated x-ray patterns of NiS, it is therefore likely that the majority of the impurity could be cobalt-nickel sulphide $(Co, Ni)_3S_4$.

Earlier observations[72] showed that the very much higher utilisation of the available surface in a teflon-bonded porous electrode was related to the fact that during gas evolution, although the electrolyte inside the catalyst aggregate is pushed

TABLE 2.4. Atomic Absorption Analysis of NiS (Technical Grade)

Solution	Ni concentration (p.p.m.)	Co concentration (p.p.m.)	Fe concentration (p.p.m.)
1	5.4	0.2	nil
2	12	0.6	nil
3	12.4	0.68	nil
4	5.0	0.35	nil
Average	19	1	nil

out of the pores, the gas can readily escape on reaching the surface of the aggregate through the dry porous channels. This ensures that the electrolyte will not be completely pushed out of the electrode, and hence the catalyst on or near the surface of the aggregate can still function. Thus, for an electrocatalyst of given surface area, the smaller the aggregate size, the greater will be the total external surface of the aggregate available for electrochemical reaction. The aggregate size measurements showed that the various nickel sulphide samples have aggregate sizes very much larger than the cobalt-nickel oxide ($NiCo_2O_4$) prepared by freeze-drying. Therefore, it is of interest to use freeze dried or similar high surface area cobalt-nickel oxide ($NiCo_2O_4$) as starting material to produce the sulphides. There are two possible advantages: (a) smaller aggregate size, (b) $NiCo_2O_4$ is fairly conducting (less than 10 ohm-cm). If the nickel-cobalt sulphide is oxidised, the nickel-cobalt oxide that is formed on the surface can be reduced electrochemically. Besides, crystal structure may also be responsible for the high activity since Ni_3S_4, $(Ni,Fe)_3S_4$, Fe_3S_4, $(Co, Ni)_3S_4$ and $NiCo_2O_4$ are of similar spinel structures. Therefore, it may be possible to prepare $NiCo_2S_4$ directly from $NiCo_2O_4$.

1. INTRODUCTION

A number of thiospinels of the type AB_2S_4, where A and B are transition metals, have been reported in the literature[73,74,75]. The classical method of synthesizing thiospinels is the high temperature method of direct combination of metals and sulphur. The reactions are carried out in evacuated silica tubes and the desired structure is obtained by annealing the product for a defined period. Thiospinels of various stoichiometric compositions can be prepared in this way.

Lotgering[73] synthesized sulphocobalties, $NiCo_2S_4$ by the above method, and various physical parameters were measured. From the low susceptibility and low atomic moment, it was concluded that the metal atoms are not in the pure ionic state. The lattice parameter, a = 9.392Å, is slightly less than the theoretically postulated lattice parameter, a = 9.85Å, (based on ionic S^{2-} close packing). This means that the sulphur atoms are much nearer to each other than corresponds to the sum of ionic radii (Goldschmidt radius = 1.74Å for the S^{2-} ions).

Later, Bouchard, Russo and Wold[76] repeated the same preparation of the sulphocobalties, $NiCo_2S_4$ and confirmed Lotgering's findings. Further measurements showed that $NiCo_2S_4$ is a metallic conductor with a low resistivity at room temperature of 8×10^{-4} ohms-cm, and the small cell sizes indicate considerable covalency characteristics. It appears that metallic conductivity in $NiCo_2S_4$ may be due to partially filled band states extending throughout the lattice of the type proposed by Goodenough[77].

CHAPTER THREE

ELECTROCATALYTIC HYDROGEN EVOLUTION WITH COBALT-NICKEL SULPHIDE

Brehret, Binder and Sandstede[78] attempted to prepare a thiospinel of composition Co_3S_4 at low temperature, by bubbling air through an aqueous solution of cobalt thiosulphate. In spite of correct stoichiometric composition, no spinel type compound was formed. Furthermore, a model was put forward to explain electrocatalytic oxygen reduction with thiospinels and other sulphides of transition metals.

Most of the useful preparation method for $NiCo_2S_4$, mentioned earlier, involved high temperature synthesis. A low temperature preparation method is preferred in the interest of electrocatalyst technology, since further reduction in preparation temperature means an increase in the active surface area of the final product.

2. PREPARATION OF SULPHOCOBALTIES, $NiCo_2S_4$.

Since the high temperature of direct combination of the metals and sulphur to synthesize $NiCo_2S_4$ is ruled out as a suitable technique to obtain a high surface area electrocatalyst, the only alternate method would be the reduction of the spinel cobalt-nickel oxide ($NiCo_2O_4$) by hydrogen sulphide according to the equation:

$$NiCo_2O_4 + 4H_2S \rightarrow NiCo_2S_4 + 4H_2O$$

This method has been used successfully in the preparation of some of the sulphochromites[76], i.e. $MnCr_2S_4$ and $CoCr_2S_4$. The pure spinel oxides can be prepared by the method of Whipple and Wold[79], but King[80] showed that the high surface area spinel oxide, $NiCo_2O_4$ is best prepared by the freeze-drying and co-precipitation method. Therefore, four samples of high surface area $NiCo_2O_4$ were

prepared as follows:

(1) Cobalt-nickel Sulphide A

An aqueous solution of 150 mls containing 24.4 gm of cobalt chloride ($CoCl_2 \cdot 6H_2O$, analar grade, B.D.H. Chemicals) and 12.13 gm nickel chloride ($NiCl_2 \cdot 6H_2O$, analar grade, B.D.H. Chemicals) was added, while constantly stirring, to 100 mls of 5N KOH. The pH was adjusted (by dilution) until the chloride ion was no longer detected in the filtrate. The clean precipitate of mixed hydroxides (Co/Ni = 2/1) was then heated in an oven, with flowing oxygen, at 400°C for 21 hours. This gave cobalt-nickel oxide A, which was then heated with hydrogen sulphide (see Chapter Four Section 2) at 550°C for 5 hours to give cobalt-nickel sulphide A.

(2) Cobalt-nickel Sulphide B

A similar composition and preparation method as mentioned in (1), was used but the clean precipitate of mixed hydroxides (Co/Ni = 2/1) was heated in an oven, without flowing oxygen, at 400°C for 21 hours. This gave cobalt-nickel oxide B, which was then sulphided with hydrogen sulphide at 350°C for 8 hours to give cobalt-nickel sulphide B.

(3) Cobalt-nickel Sulphide C

A 100 mls solution containing 39.49 gm of cobalt nitrate ($Co(NO_3)_2 \cdot 6H_2O$, analar grade, B.D.H. Chemicals), and 19.79 gm of

nickel nitrate ($Ni(NO_3)_2.6H_2O$, analar grade, B.D.H. Chemicals) was sprayed onto a dish containing liquid nitrogen. The frozen metallic salt solution was rapidly transferred into a round-bottomed flask containing liquid nitrogen and then subjected to freeze-drying. The apparatus is shown in Figure 3.5.

After drying, the mixed nitrate powder (Co/Ni = 2/1) was subjected to vacuum decomposition at 250°C for 3 hours, followed by thermal heat treatment in an oven at 400°C for 21 hours. This gave cobalt-nickel oxide C, which was then sulphided with hydrogen sulphide at 400°C for 2 hours and finally at 550°C for a further 5 hours to give cobalt-nickel sulphide C.

(4) Cobalt-nickel Sulphide D

The same freeze-drying method as above was used, but the thermal heat treatment step was omitted, i.e. after vacuum decomposition at 250°C for 3 hours, the product cobalt-nickel oxide D (Co/Ni = 2/1) was sulphided with hydrogen sulphide at 350°C for 8 hours to give cobalt-nickel sulphide D.

3. ELECTROCATALYST CHARACTERISATION

3.1. Electrical Conductivity Measurements

One of the fundamental requirements for an electrocatalyst to function efficiently is to have adequate electrical conductivity. Although it is difficult to lay down rigid standards, it is possible to say that a resistivity of 10 ohm-cm^{-1} is good and one of 10^6 ohm-cm^{-1} is unacceptable. For this reason, it is desirable to have an estimate of the order of magnitude of the electrical conductivity of the

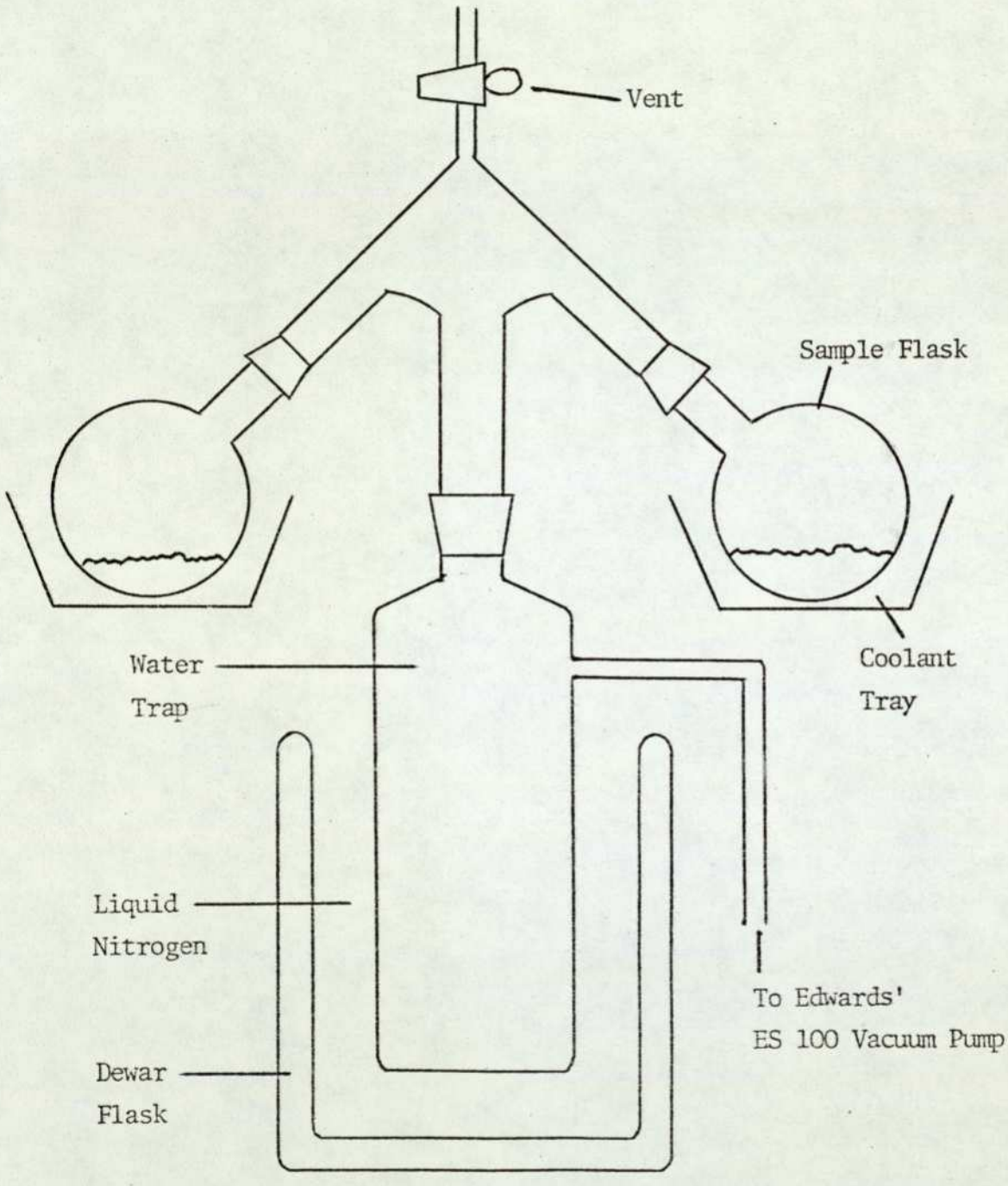

FIG. 3.5 Freeze Drying Apparatus

electrocatalyst before further electrochemical evaluation are carried out. Electrical conductivity of powder sample can be easily measured by means of a conductivity bridge (Wayne kerr) and a simple apparatus comprising of two identical metal rigs and a PTFE ring. This apparatus has been described[81,82] previously, and shown in Figure 3.6. Although accuracy in the measurement of electrical conductivity is highly dependent on the degree of compression of the powder sample, good reproducible measurements can be obtained if a fixed mass of powder sample and the degree of compression is strictly followed throughout.

3.2. X-ray Powder Diffraction (see Chapter Two, Section 3.1.2.).

4. HALF-CELL ELECTROCHEMICAL TESTING

The potentiodynamic polarisation technique (see Chapter Two, Section 3.2.2.) at very slow potential sweep rate, is used for the steady state electrochemical testing of various cobalt-nickel sulphides in teflon-bonded porous electrode structures (see Chapter Two, Section 3.1.4.). The potentiostatic current/time relationship was also studied.

A teflon-bonded platinum black porous electrode was also investigated at the same experimental conditions for activity comparison with a teflon-bonded cobalt-nickel sulphide porous electrode. The experimental procedures and testing sequences are the same as in Chapter Two. (See Chapter Two, Section 4.4.).

Figure 3.6. Apparatus for the measurement of electrical conductivity on powder sample.

(a) metal rigs (two in all)

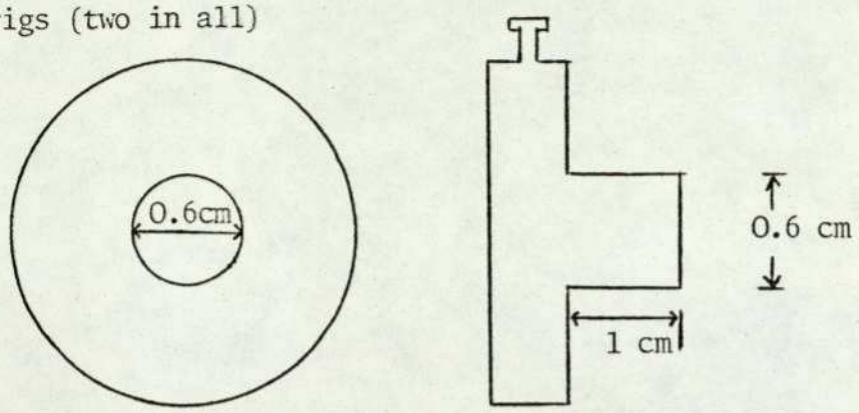

(b) PTFE ring

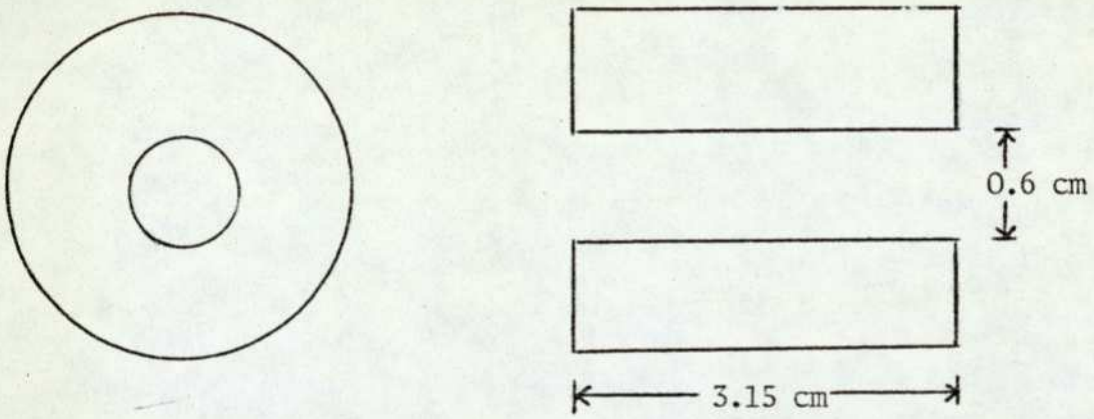

(c) Metal rigs with powder sample in PTFE ring

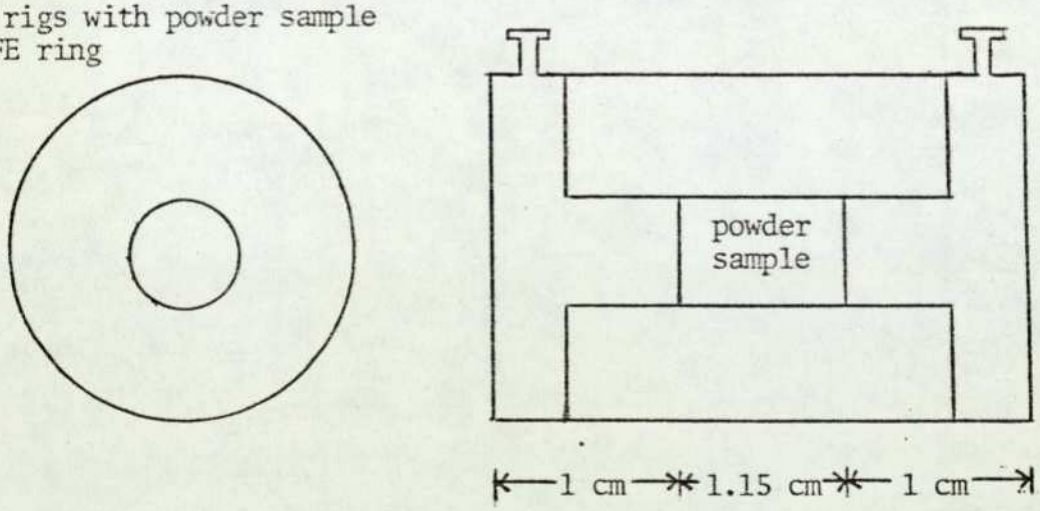

5. RESULTS

5.1. X-ray Analysis

All cobalt-nickel sulphide samples, together with their corresponding starting oxides, were exposed to molybdenum K_α radiation for 3 hours. X-ray data of various cobalt-nickel oxides and cobalt-nickel sulphides are listed separately in Table 3.1 and 3.2. Related oxides are also listed for comparison.

Regardless of different preparation methods, all the starting materials, cobalt-nickel oxides show predominately spinel structure. The contamination with other phases such as NiO, Co_3O_4 and CoO seems possible, and is dependent on preparation temperatures.

The x-ray patterns of the cobalt-nickel sulphides are more complicated. The lines on the x-ray photographs are more well defined for samples prepared at 550°C even though all samples were exposed to the same x-ray source for the same period of time. It has been suggested that this may be due to the following reasons:

(1) different orientation of the samples to x-ray radiation;

(2) cobalt-nickel sulphides prepared at higher temperature, i.e. at 550°C, are more crystalline and the structures are better formed;

(3) cobalt-nickel sulphides prepared at lower temperature, i.e. at 350°C, are less crystalline and the structures are less well formed.

Moreover, by comparing with the x-ray data of different nickel

TABLE 3.1. X-ray Powder Data for Different Cobalt-Nickel Oxides

[redacted]

TABLE 3.2. X-ray Powder Data for Different Cobalt-Nickel Sulphides

[redacted]

sulphides and cobalt sulphides, the possibility of other phases present in all the prepared cobalt-nickel sulphide samples cannot be ruled out. The calculated lattice parameter of all the cobalt-nickel sulphide samples are also listed in Table 3.2.

5.2. Electrical Conductivity Measurements

Electrical conductivity results for various cobalt-nickel oxides, together with their corresponding cobalt-nickel sulphides are tabulated in Table 3.3. These measurements are not the absolute values of electrical resistivity since 100% dense material cannot be obtained from the powder samples. However, by adopting a standard procedure for all powder samples, the measurements of resistivity can be compared with one another.

5.3. Half-Cell Electrochemical Results

Near steady-state potentiodynamic performance of cobalt-nickel sulphide A and platinum black at different temperatures is shown in Figure 3.1. At 70°C, the electrocatalytic activity of cobalt-nickel sulphide A is comparable to platinum black at high overpotential (i.e. at -300 m vs D.H.E.). The voltage/current curves show linear relationships for platinum black while a non-linear relationship is observed for cobalt-nickel sulphide A. In both cases, no limiting current was observed.

Figure 3.2 shows the potentiostatic current/time plots at cathodic potential of -300 mV (vs D.H.E.) for the platinum black and cobalt-nickel sulphide A. Steady state performance

TABLE 3.3. Electrical Resistivity for Cobalt Nickel Oxides and Their Corresponding Sulphides

Cobalt nickel oxide	Resistivity ohm-cm^{-1}	Cobalt nickel sulphide	Resistivity ohm-cm^{-1}
A	90	A	2×10^{-2}
B	75	B	4.2×10^{-1}
C	10	C	3×10^{-2}
D	18	D	3.6×10^{-1}

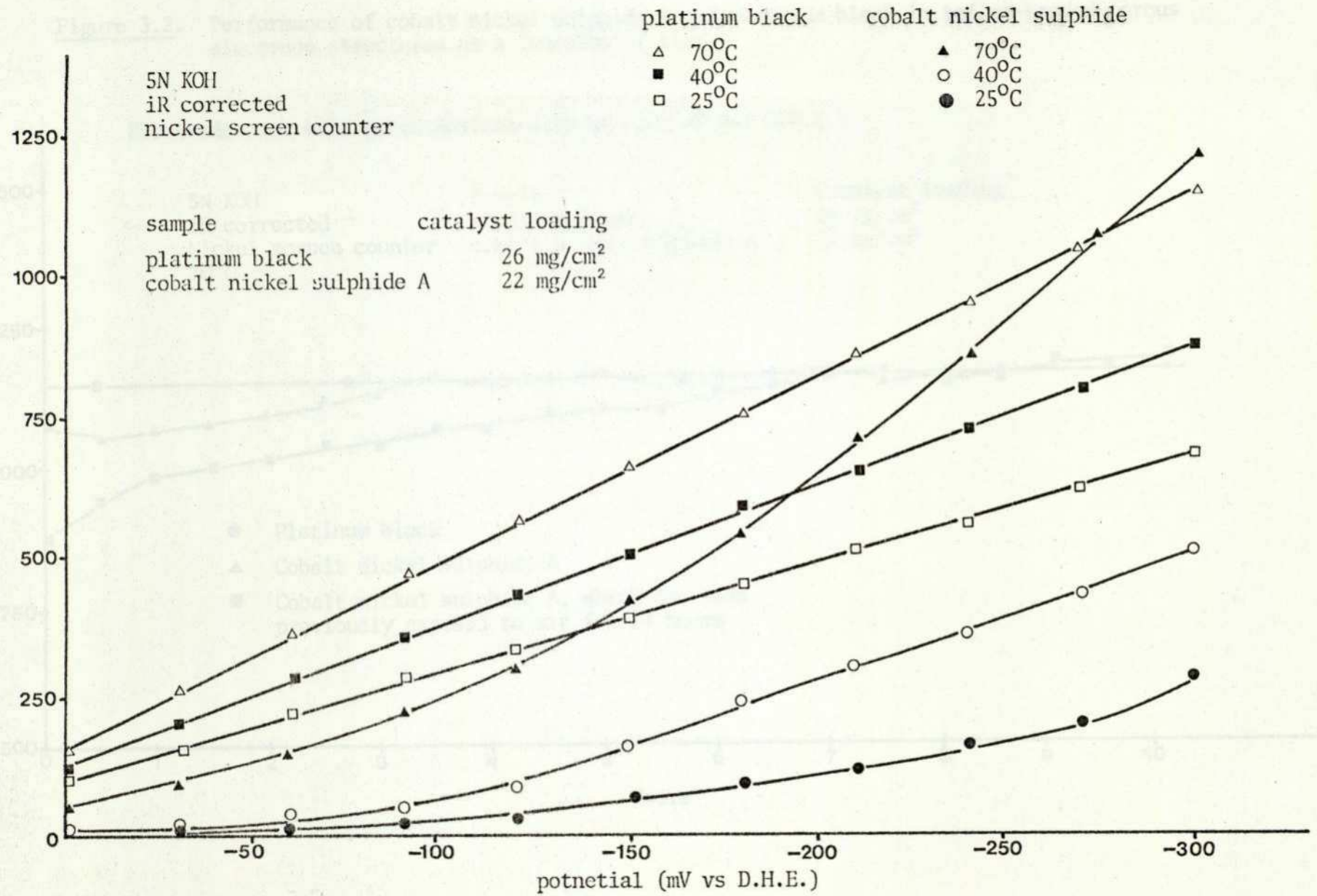

Figure 3.1. Voltage/current curves for cobalt nickel sulphide A and platinum black in teflon-bonded porous electrode structures.

Figure 3.2. Performance of cobalt nickel sulphide A and platinum black in teflon-bonded porous electrode structures as a function of time.

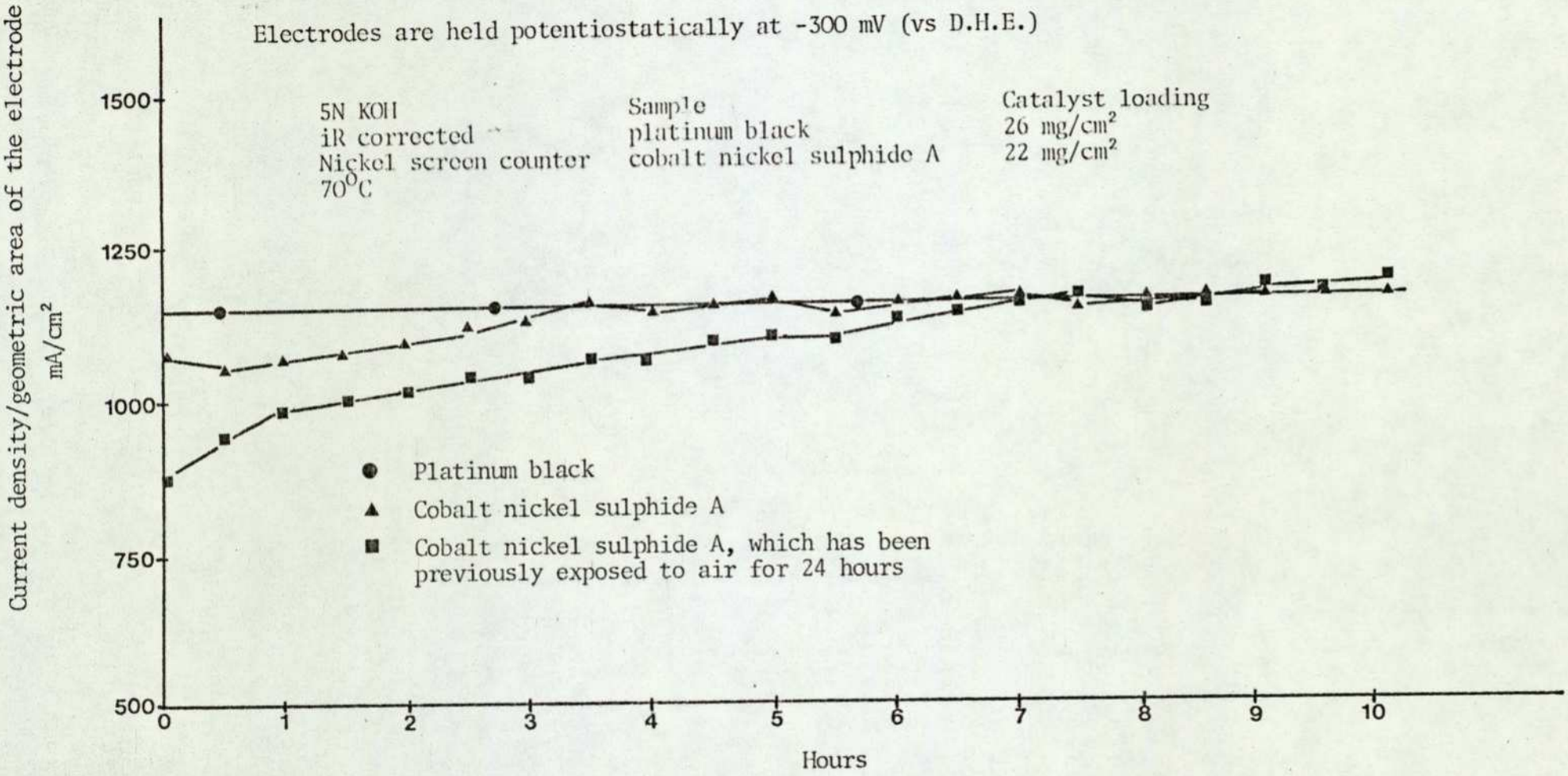

for the cobalt-nickel sulphide A increases gradually with time. Even after exposure to bubbling air for 24 hours at open circuit, cobalt-nickel sulphide A can recover to its original performance during the course of the test period of 8 hours.

A comparison of potentiodynamic activity for different cobalt-nickel sulphides at 60°C is shown in Figure 3.3. Figure 3.4 shows the changes in performance of cobalt-nickel sulphide D over a period of 2 days.

6. DISCUSSION

Prior to potentiodynamic electrochemical testing, it has been established that all cobalt-nickel sulphides behave as irreversible hydrogen electrodes. When they are initially equilibriated in electrolyte saturated with hydrogen, they show no affinity towards hydrogen chemisorption. Consequently, the open circuit voltage (O.C.V.) or rest potential is normally between 600-800 mV (vs D.H.E.) in hydrogen saturated electrolyte of 5N KOH at temperatures between 25°C to 70°C. Activation of these electrodes by cathodic polarisation at -300 mV (vs D.H.E.) for fifteen minutes usually improves the O.C.V. value somewhat nearer to the reversible hydrogen electrode potential (i.e. 25 mV vs D.H.E.), but in a short time, it drifts upward again.

The complex x-ray patterns for the cobalt-nickel sulphides are more difficult to interpret than that of their corresponding oxides. The calculated lattice parameters for all the cobalt-nickel sulphides are listed in Table 3.2. Though varying from 9.38Å to 9.41Å,

electrode structures.

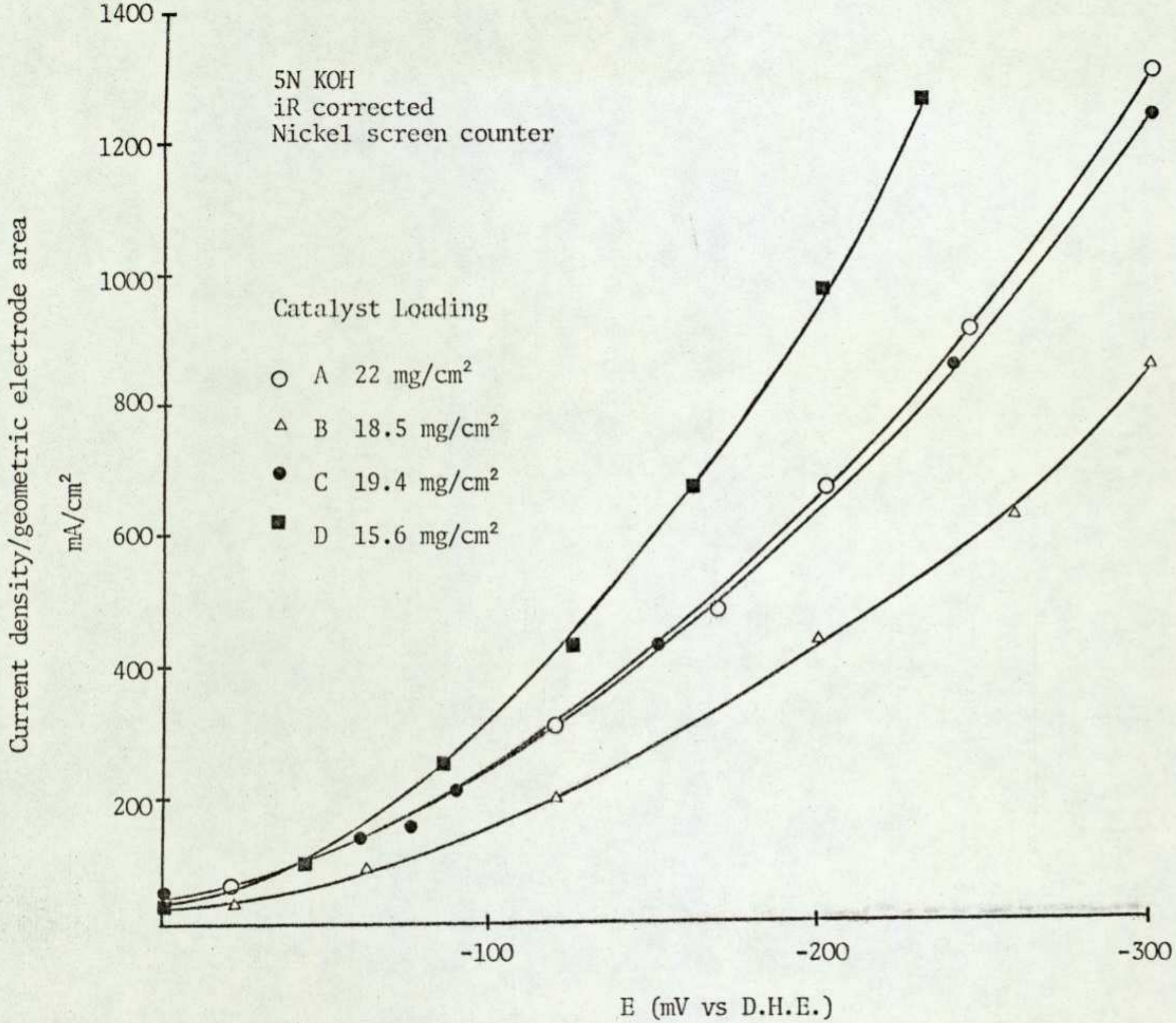

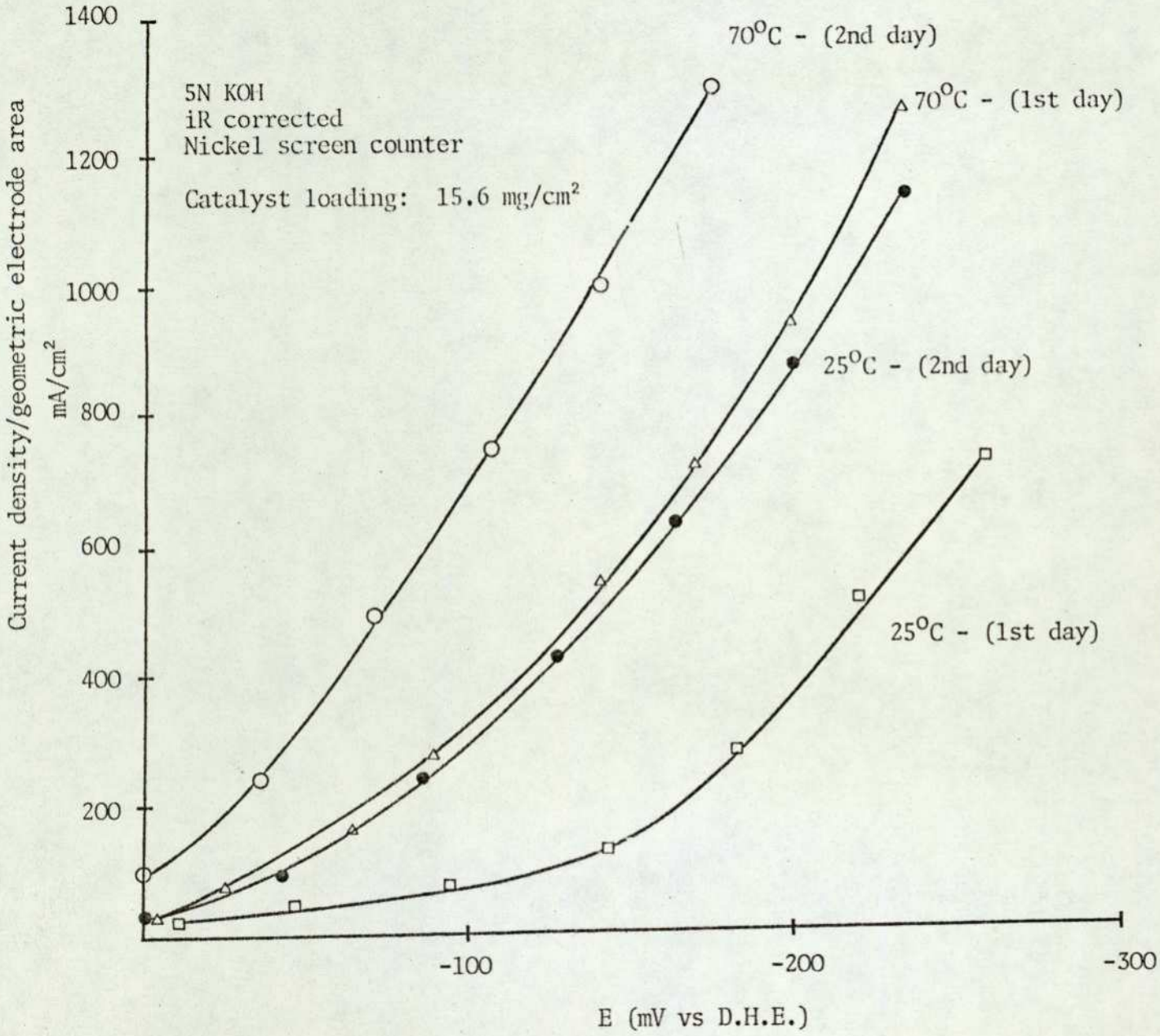
1400
1200
1000
800
600
400
200
Current density/geometric electrode area
mA/cm²
5N KOH
iR corrected
Nickel screen counter
Catalyst loading: 15.6 mg/cm²
70°C - (2nd day)
70°C - (1st day)
25°C - (2nd day)
25°C - (1st day)
-100
-200
-300
E (mV vs D.H.E.)

they all show a spinel type of structure. Nevertheless, the d-spacings (Å) of all the cobalt-nickel sulphides are more irregular, especially at low Bragg angles. The calculated lattice parameters for the cobalt-nickel oxides are also listed in Table 3.1. They all show extremely close agreement with literature[84].

From Table 3.3, electrical conductivity measurements show a sharp decrease in resistivity in the order of 100 to 1000 folds for all the cobalt-nickel sulphides as compared to their corresponding spinel cobalt-nickel oxides, which show only semi-conducting properties.

Electrochemical evaluation of different cobalt-nickel sulphides show that the highest electrocatalytic activity is in the order of cobalt-nickel sulphide D > cobalt-nickel sulphide A > cobalt-nickel sulphide C > cobalt-nickel sulphide B. However, when comparing with platinum black, the performance of cobalt-nickel A becomes stable after only a few hours of hydrogen evolution at a constant cathodic potential. It is suggested that this is due to the electrochemical reduction of the oxide layers, which may be formed during the curing process at 300°C in stagnant air, in the preparation of teflon-bonded porous electrodes. It is also suggested that passive oxide layers may be formed as soon as the cobalt-nickel sulphide electrodes are placed in the strongly alkaline electrolyte[83] and that they can be easily reduced electrochemically. If the passive oxide films are formed chemically when the electrodes are at the open circuit, this would give a certain degree of protection towards further oxidation of the cobalt-nickel sulphide to give elemental sulphur and other oxidation products. Another possibility is that

during h.e.r., the cobalt-nickel sulphide catalyst is being reduced with the electrochemical discharge of hydrogen sulphide. Thermodynamic calculation[52] shows that this route is very plausible. Removal of all sulphide from the cobalt-nickel sulphide catalyst, in the form of hydrogen sulphide would leave the electrode only covered with finely divided cobalt and nickel powders, which are known to have a low hydrogen overvoltage. However, analysis of the out coming gases during the electrolysis show no evidence of hydrogen sulphide. It is also worth noting that the performance of cobalt-nickel sulphide D improves significantly over a test period of two days and it is not affected by continuous exposure to bubbling air between each test. For cobalt-nickel sulphide A, original steady state activity can also be recovered even after it has been exposed to bubbling air for 24 hours.

The small differences in the electrical resistivities amongst different cobalt-nickel sulphides may be attributed to interference from non-conducting mixed phases such as NiO and Co_3O_4 present as impurities. X-ray analysis also confirms the possibility of mixed phases present in the predominantly spinel cobalt-nickel sulphide products. Since all the cobalt-nickel sulphides are prepared by different routes and sulphided under different conditions, it is difficult at this stage to speculate on the fundamental factors affecting the activity of cobalt-nickel sulphide catalysts. However, from the experimental data obtained so far, it is established that spinel cobalt-nickel sulphides can be prepared by reduction of spinel oxides with hydrogen sulphide. Therefore, a fundamental study of the parameters that affect the

formation of pure spinel-cobalt-nickel sulphide is necessary for a further evaluation of cobalt-nickel sulphide as a potential hydrogen cathode catalyst.

CHAPTER FOUR

THE INFLUENCE OF PREPARATION PARAMETERS ON THE ELECTROCATALYTIC ACTIVITY OF COBALT-NICKEL SULPHIDE

1. INTRODUCTION

It has been reported in Chapter 3 that cobalt-nickel sulphides in teflon-bonded porous electrode structures, show promising performance for the h.e.r. in alkaline media. It has also been shown that cobalt-nickel sulphides, prepared under different conditions, have some effect on electrocatalytic activity. A correlation between the preparation parameters and the structure of the final products is one of the immediate aims of this investigation, since it should lead to a better understanding of the cobalt-nickel-sulphur system. Also, an investigation is conducted to study the kinetics of the reaction of cobalt-nickel oxide with hydrogen sulphide.

In order to study this effect in more detail, it is necessary to select and fix certain preparative parameters; i.e. reaction time and temperature. Although it is logical to assume that longer time is required for complete conversion of oxide to sulphide by hydrogen sulphide at a lower temperature than at a higher temperature, it is felt that the time period of 12 hours is sufficient for completion of the sulphiding process, even at a temperature as low as 300°C. The next problem that needs to be considered is the choice of the reaction temperature.

Kal'mutskaya et al[85] studied the kinetics on the reduction of cobalt chromite ($CoCr_2O_4$) and nickel chromite ($NiCr_2O_4$) and found that the temperature for complete sulphiding of chromites into sulphochromites (i.e. $CoCr_2S_4$ and $NiCr_2S_4$) is below the temperature for complete sulphiding of Cr_2O_3 into Cr_2S_3. A mechanism was thus

proposed for the formation of sulphide spinels. Bouchard et al[76] prepared $CoCr_2S_4$ successfully by using Kal'mutskaya et al's temperature criteria. In analogy, since Co_2O_3 is unstable and Co_3S_4 decomposes at 680°C to give CoS and CoS_2,[86] together with the possibility that $NiCo_2S_4$ also decomposes at relatively low temperatures; the firing temperature for the sulphiding of cobalt-nickel oxide is kept under 600°C. It is also considered that above 600°C surface areas could begin to be seriously affected. Temperatures of 300°C, 350°C, 400°C and 550°C were therefore chosen.

At each temperature, the surface area would reach its equilibrium values as soon as the reaction goes into completion. This value is reached faster at a high temperature rather than at a low temperature. Beyond this value, any heating would mean sintering of the product to the extent that it is a function of temperature and time. Therefore, samples prepared from different temperatures would have different surface areas. Also, they can have different structures if either the reaction time is not sufficiently long enough for the sulphiding process to go into completion or, the product may have various stable structures at different temperatures.

2. PREPARATION OF COBALT-NICKEL SULPHIDES

Cobalt-nickel oxide is first prepared by the freeze drying method. (See Chapter 3, Section 2). Sulphiding of the cobalt-nickel oxide is carried out in a tubular electric furnace (model MTF 1 ELP, made by Carbolite Ltd.) over the range of 300°C - 550°C. Samples

of cobalt-nickel oxide were placed in porcelain boats and inserted into the tube furnace, which was purged thoroughly with nitrogen for 20 minutes before hydrogen sulphide was admitted. The cobalt-nickel oxide samples were sulphided in hydrogen sulphide at a constant flow rate of 60-65 mls/min. for 12 hours at the desired temperatures. Samples of cobalt-nickel sulphide were prepared at temperatures of 300°C, 350°C, 400°C and 550°C. In all cases, the maximum reaction time was fixed at 12 hours.

3. ELECTROCATALYST CHARACTERISATION

3.1. Analysis of Cobalt-nickel Sulphides

Three analytical methods were used for direct and indirect determination of the sulphur contents in the prepared cobalt-nickel sulphide samples. Nickel(II) sulphide and nickel(IV) sulphide were used as standards in all of the analytical experiments. They were obtained from Alfa Ventron Products and have purity of 99.9%.

(1) Determination of insoluble sulphides in the form of hydrogen sulphide gas

A weighed amount of cobalt-nickel sulphide was reacted with concentrated hydrochloric acid, which was activated either by aluminium or zinc metals. Hydrogen sulphide is liberated and carried by a stream of nitrogen to react with an iodine solution of known concentration according to the equation:

$$H_2S + I_2 \longrightarrow S + 2H^+ + 2I^-$$

During the course of this reaction, iodine was consumed in

the formation of elemental sulphur. The amount of iodine consumed can be calculated by back titrating the iodine solution against a standard sodium thiosulphate solution according to the equation:

$$2S_2O_3^{2-} + I_2 \longrightarrow 2I^- + S_4O_6^{2-}$$

A freshly prepared starch solution was used as an indicator. The apparatus for this experiment is shown in Figure 4.1. This method has the distinct advantage of differentiating between elemental sulphur and sulphide so that any free sulphur mixed with the cobalt-nickel sulphide is not detected, i.e. there is no reaction between sulphur and concentrated hydrochloric acid to yield hydrogen sulphide gas.

(2) Determination of sulphur by the oxygen flask (Schöniger) combustion method.

This technique was originally designed to analyse organically bound sulphur, but it is also applicable to analyse insoluble inorganic sulphides. A weighed amount of cobalt-nickel sulphide specimen was first oxidised and combusted in oxygen, the combustion gases are then absorbed and dissolved in a solution of hydrogen peroxide of known concentration, to form sulphate ions, which were titrated against a standard barium chloride solution, using thorin solution as indicator. The reactions take place according to the following equations:

$$S + O_2 \longrightarrow SO_2$$

$$SO_2 + H_2O_2 \longrightarrow H_2SO_4$$

$$BaCl_2 + H_2SO_4 \longrightarrow BaSO_4 + 2HCl$$

Figure 4.1. Apparatus for the determination of sulphide contents in insoluble metallic sulphides.

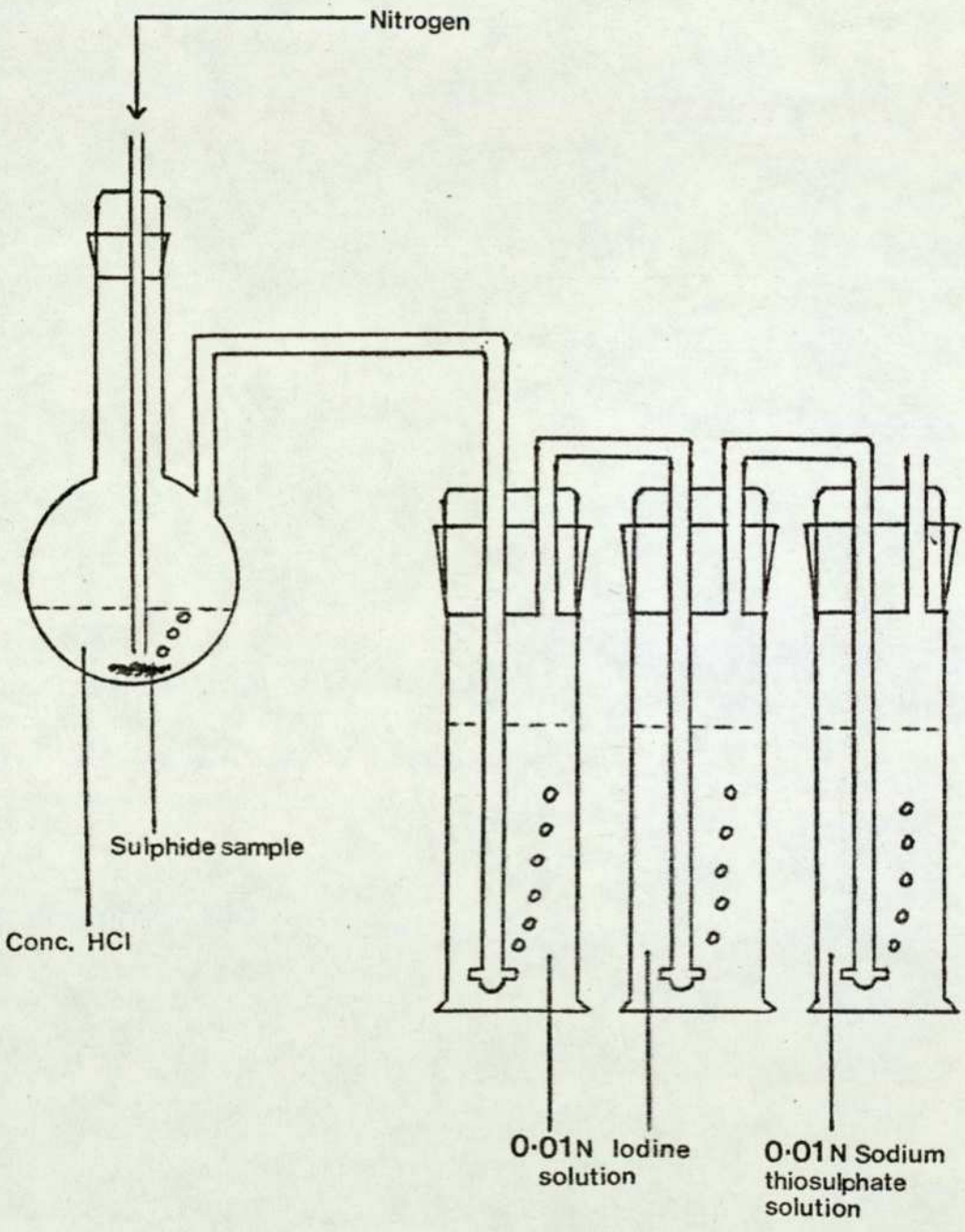

(3) Determination of sulphur by electron microscopy

This is a quick and qualitative method for the determination of the empirical composition of most compounds. For all cobalt-nickel sulphide samples, the relative atomic ratio of each chemical component can be determined accurately if no other phases are present. Also, electron microscopy is very useful for particle size determination from which the surface area can be calculated.

3.2. X-ray Powder Diffraction

(See Chapter 2, Section 3.3.2).

4. HALF-CELL ELECTROCHEMICAL TESTING

Potentiodynamic polarisation technique (see Chapter 2, Section 4.3.) is used for the evaluation of electrocatalytic activity of different cobalt-nickel sulphides in teflon-bonded porous electrode structures.

5. INVESTIGATION OF THE THERMAL BEHAVIOUR OF FREEZE DRIED COBALT-NICKEL OXIDE AND SOME OF ITS SULPHIDED PRODUCTS

5.1. Apparatus

Samples of catalyst powder were heated in a Mettler

'Thermoanalyser II' thermobalance. This gives a continuous record of the weight of a sample, the rate of weight change, the temperature of the sample and the difference in temperature between the sample and an inert standard material. The latter technique, known as Differential Thermal Analysis (DTA), gives an indication of the heat of the reaction, of the reactions which occur as the sample is heated at a linear heating rate. In all cases in the present work, an empty Pt/10 % Rh crucible, identical to the sample crucible, was used as the DTA reference point. This has been found to give, for small samples at least, a reduced base-line drift when compared with the more normally used Al_2O_3 standard. Calibration experiments carried out for DTA have shown that a sensitivity of $1\mu V mg^{-1}$ is approximately equal to 30 cal. g^{-1}.

The sensitivity of the various measurements made during the present investigation are as follows:

(1) Temperature: better than 1 mm chart width per $1^{o}C$.

(2) Weight of sample: 0.2 mg per 2.5 cm of chart width: For the 20 mg samples used in this work, with which about half the initial weight of material was lost from the crucible, this gave a sensitivity of better than 0.5% of the weight-loss per 2.5 cm of chart width.

(3) Rate of weight change (DTG): 0.5 mg min^{-1} per 25 cm of chart width for the studies in nitrogen, where very fast reactions occurred, as with the mixed oxide/sulphides in air, the sensitivity needed to

be reduced by a factor of 10. In each case division by the weight of material lost in each degradation reaction gives the rate of weight-loss for that stage in %/min, the figure quoted in the results.

(4) DTA. Again, the occurrence of very fast reactions was the important factor in the choice of sensitivity. For the reactions occurring during the oxidation of the cobalt-nickel sulphide materials, the sensitivity was limited to 200μV. per 25 cm of chart width, for all the other reactions studied it was increased by 10.

5.2. Materials

Two different types of powder were examined in order to give an understanding of the behaviour of the metal oxides and metal sulphides. Two metal oxides were examined and they were prepared by the freeze drying method. i.e. cobalt-nickel oxide C and cobalt-nickel oxide D. (See Chapter 3, Section 2). Two samples of metal sulphide were also examined, i.e. cobalt-nickel sulphide C and cobalt-nickel sulphide D. (See also Chapter 3, Section 2).

5.3. Procedure

Initial studies carried out with cobalt-nickel sulphide C showed that about 50% of the material originally present was lost when the samples were heated to ca. 950°C. Thereafter, ca. 20 mg of each sample was heated to this temperature in air or nitrogen. A heating rate of 5°C min^{-1} gave the optimum combination of sensitivity

of reaction temperature (requiring low heating rates) and ease of separation of the individual stages in the decomposition (which requires high heating rates). Before each of the reactions in nitrogen the balance housing and the furnace area were purged until the concentration of oxygen, as measured by an oxygen sensor, was below ca. 0.1%. This took about 5 minutes at a flow rate of about 3ml min^{-1}; if moisture was present in the sample, much if not all of the moisture was lost during this purging. In this case, the initial stages in the decomposition of the samples could not easily be defined. A flow rate of 60 ml min^{-1} of gas was passed over the samples as they were heated. This was sufficient to keep the furnace area saturated with the required atmosphere, but low enough not to cause noise on the 'rate of reaction' trace. The flow of gas also prevented any of the gaseous products of the decomposition entering the balance housing and causing corrosion of the balance mechanism. The disadvantage of the gas flow was that, for metal oxides heated in a flow of nitrogen, the gas flow encourages decomposition by causing such equilibria as:

$$\text{metal oxide} \rightarrow \text{metal} + \text{oxygen} \uparrow$$

to be pushed to the right thereby leading to reduction of the metal oxide. This, in turn leads to the apparent volatilisation of 'metal oxide' at temperatures much below its normal boiling point. The volatilisation at 690°C of antimony oxide (B.Pt 1450°C) is known to occur in this way. In the present investigation, samples of cobalt-nickel sulphide heated to 950°C in a nitrogen atmosphere lead to a residue of metal which then appears to 'alloy' with the platinum crucible, from which

it can not be removed by any of the normal cleansing agents for platinum. For this reason, subsequent decompositions in nitrogen were heated only to a temperature of about 850°C (i.e. the end of the reaction preceding the reduction reaction).

6. RESULTS

6.1. X-ray Analysis

All cobalt-nickel sulphide samples prepared from different temperatures for 12 hours, together with the starting freeze-dried cobalt-nickel oxide ($NiCo_2O_4$) were exposed to molybdenum K_α radiation for 3 hours. Their x-ray powder data are listed in Table 4.1. For comparison, thermal decomposed cobalt-nickel oxide (see Chapter 5, Section 2) was sulphided and characterised under similar conditions. Their x-ray powder data are listed in Table 4.2.

6.2. Analytical Results

A transmission electron microscope (model JEM 100 B, made by Joel) was used for qualitative analysis of the cobalt-nickel sulphides and their corresponding oxides. The scanning system was used since the particle size of all the samples was larger than 0.1 micron. The microscope was switched to the secondary electron mode with an accelerating voltage of 40 KeV. The magnification set at 10,000 times. The samples were thoroughly dispersed in an ultrasonic bath with methanol before transferring onto graphite grids. X-ray fluorescence analysis was made with an Edax analysis system. The concentration of each elemental component was estimated

Table 4.1. X-ray Powder Data for the Freeze Dried Cobalt-Nickel Oxide and its Sulphided Products.

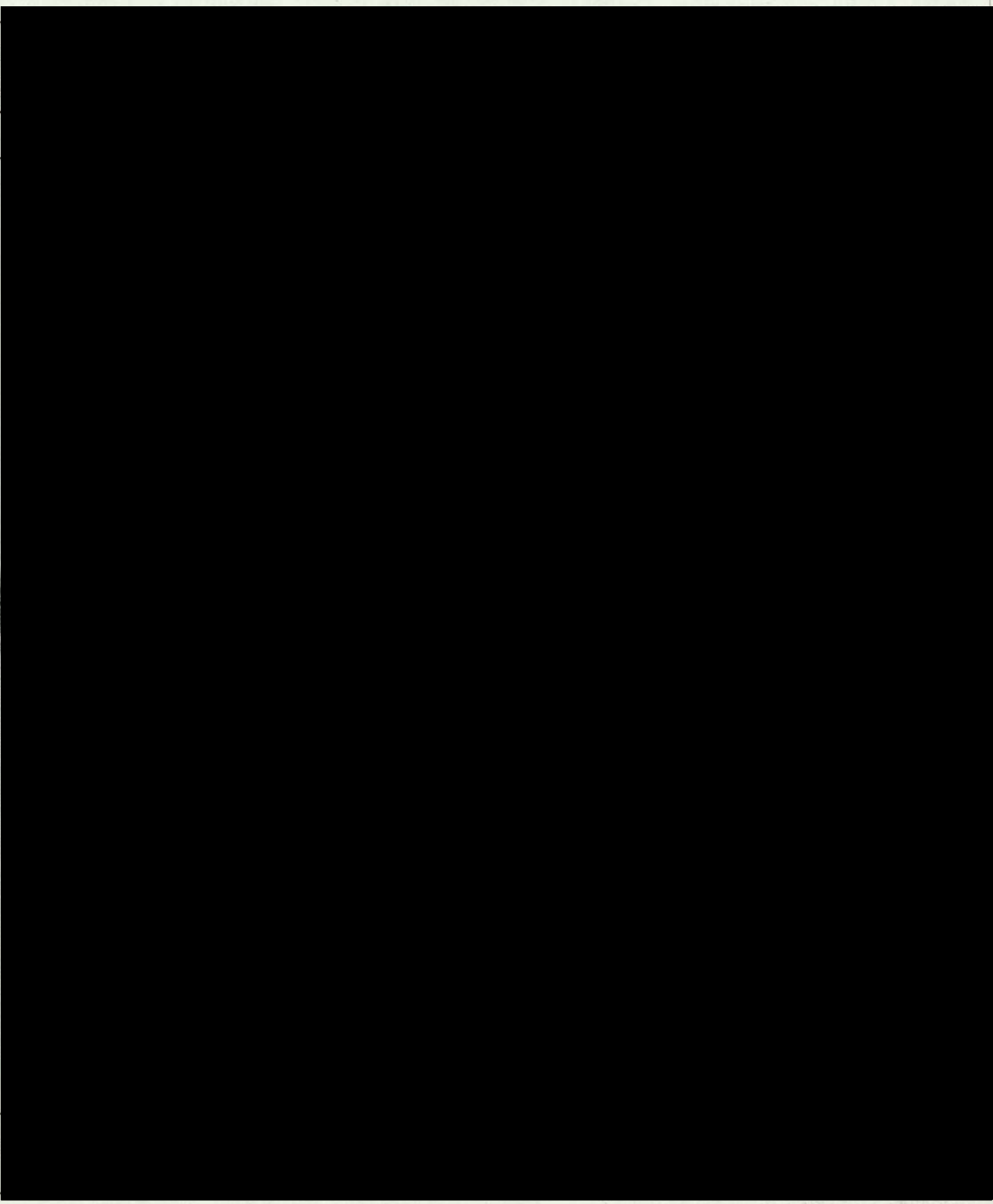

lculated lattice parameter

Intensity estimated visually

TABLE 4.2. X-ray Powder for the Thermal Decomposed Cobalt-Nickel Oxide and its Sulphided Products.

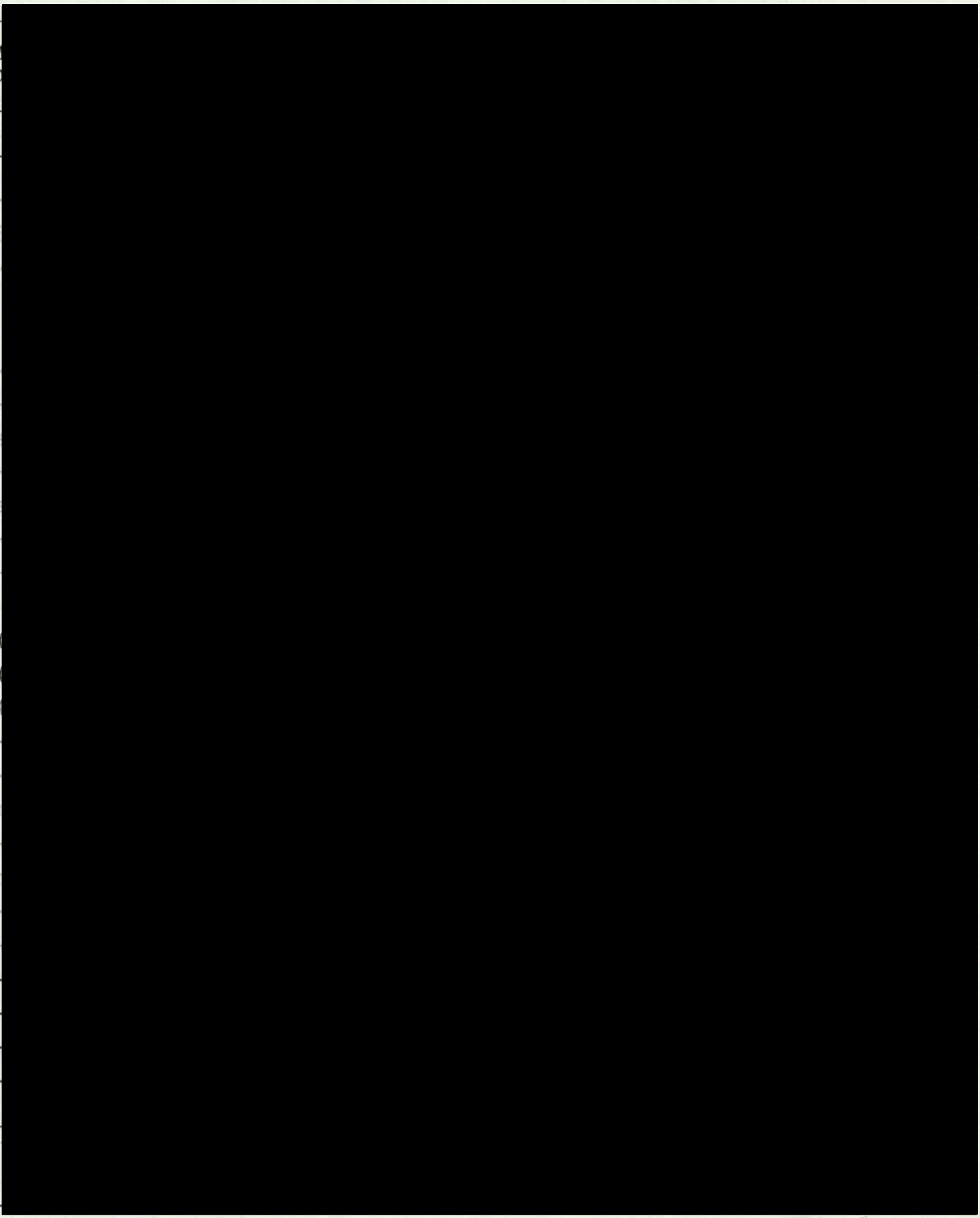

Calculated lattice parameter

I = Intensity estimated visually

by peak height/background measurements corrected for atomic number and specimen tilt.

Electron microscopy analytical results are listed in Table 4.3. A typical Edax analytical concentration count of cobalt, nickel and sulphur are shown in Figure 4.2. Calculation for each individual element from the peak height measurements in Figure 4.2 were estimated according to the following equation:

$$\frac{\text{Number of counts - background counts}}{\text{Correction factor x atomic weight}} = \text{atoms}$$

where correction factor for nickel = 0.93, cobalt = 1.01 and sulphur = 1.35.

Electron micrographs for some of the cobalt-nickel sulphide samples prepared from the freeze dried cobalt-nickel oxide and thermal decomposed cobalt-nickel oxide are shown in Figures 4.3 and 4.4 respectively.

The rate of sulphiding was measured by analysing for sulphur in the sulphided products, with the assumption that oxygen atoms are replaced either partially or completely by sulphur atoms during the sulphiding process. Figure 4.5 shows the kinetic curves for sulphiding of freeze dried cobalt-nickel oxide ($NiCo_2O_4$) at different temperatures: 1) 300°C, 2) 350°C, 3) 400°C and 4) 550°C.

Two chemical analytical methods (see Section 3.1 (1) and 3.1 (2)) were used for sulphur analysis of the final sulphided products and the results are tabulated in Table 4.4. The sulphiding index were calculated in three different ways:

(1) Assume the sulphided products have the empirical

TABLE 4.3(a) Edax Analysis of Nickel-Cobalt and Sulphur in Freeze Dried Cobalt-Nickel Oxide and its Sulphided Products.

Sulphided Products		S Conc. Count	Ni Conc. Count	Co Conc. Count	S background Count	Ni and Co background Count	Atomic Ratio		
(°C)	(hrs)						S Atom	Ni Atom	Co Atom
300	12	4624	1300	2479	120	169	104.26	20.71	38.81
400	12	1579	353	664	167	113	32.69	4.40	9.26
550	12	2964	1238	2064	165	164	64.79	19.67	32.01
freeze dried cobalt-nickel oxide		229	1062	2141	198	182	0.72	16.12	32.91

TABLE 4.3(b) Edax Analysis of Nickel-Cobalt and Sulphur in Thermal Decomposed Cobalt-Nickel Oxide and Its Sulphided Products.

Sulphided Products		S Conc. Count	Ni Conc. Count	Co Conc. Count	S background Count	Ni and Co background Count	Atomic Ratio		
(°C)	(hrs)						S Atom	Ni Atom	Co Atom
300	12	6092	4939	9564	321	597	135.67	79.52	150.66
400	12	2798	963	1783	179	163	60.63	14.65	27.22
550	12	3334	879	1655	163	153	73.40	13.30	25.24
thermal decomposed cobalt-nickel oxide		303	5289	10253	345	520	-0.97	87.31	163.53

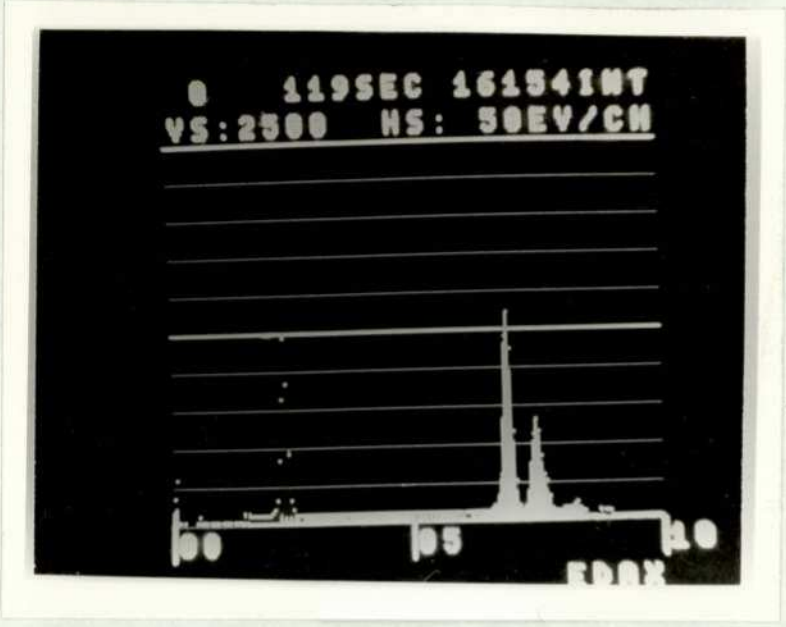

Figure 4.2. A typical Edax analytical concentration count for cobalt, nickel and sulphur.

Figure 4.3. Electron micrographs of sulphided products prepared from freeze dried cobalt-nickel oxide. Magnification = 10,000 times (1 cm = 10 μ), 40 KeV.

(a). Cobalt-nickel sulphide prepared at 300°C for 12 hrs.

(b). Cobalt-nickel sulphide prepared at 400°C for 12 hrs.

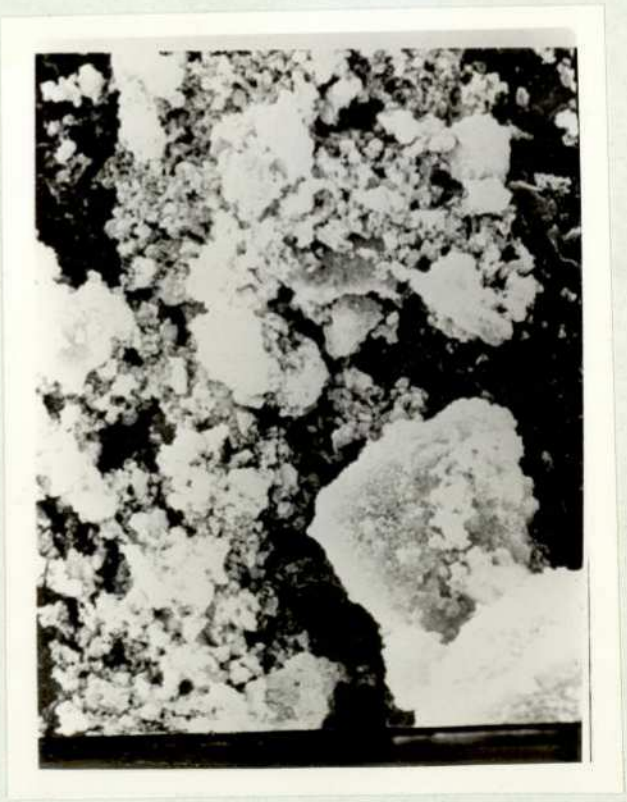

(c). Cobalt-nickel sulphide prepared at 550°C for 12 hrs.

Figure 4.4. Electron micrographs of thermal decomposed cobalt-nickel oxide and its sulphided products. Magnification 10,000 times (1 cm = 10 μ), 40 KeV.

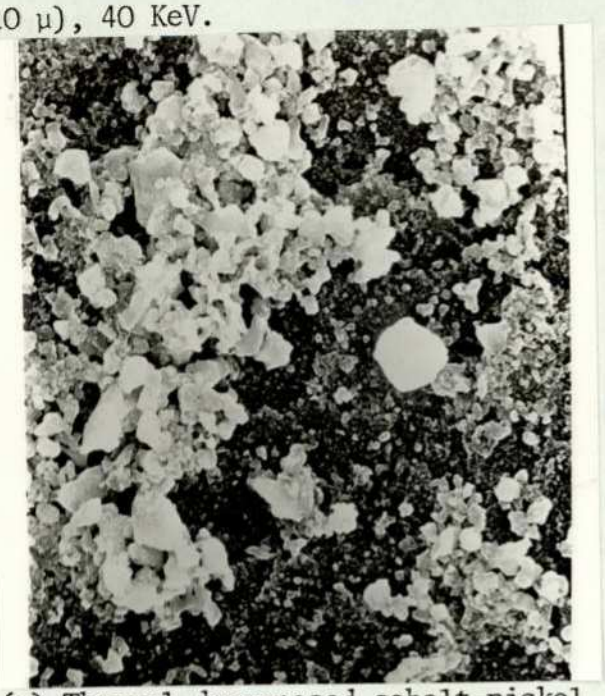

(a) Thermal decomposed cobalt-nickel oxide.

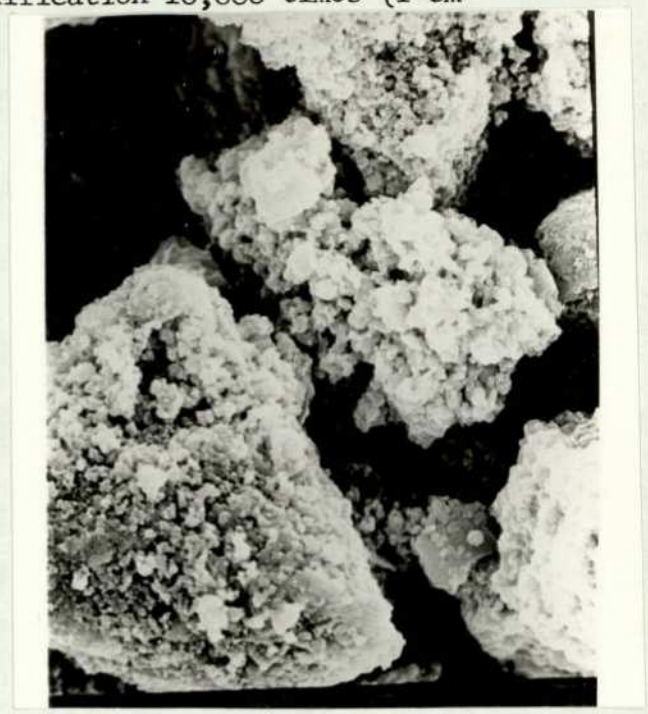

(b) Cobalt-nickel sulphide prepared at 300°C, 12 hrs.

(c) Cobalt-nickel sulphide prepared at 400°C, 12 hrs.

(d) Cobalt-nickel sulphide prepared at 550°C, 12 hrs.

Figure 4.5. Kinetic curves of sulphiding freeze dried cobalt-nickel oxide.

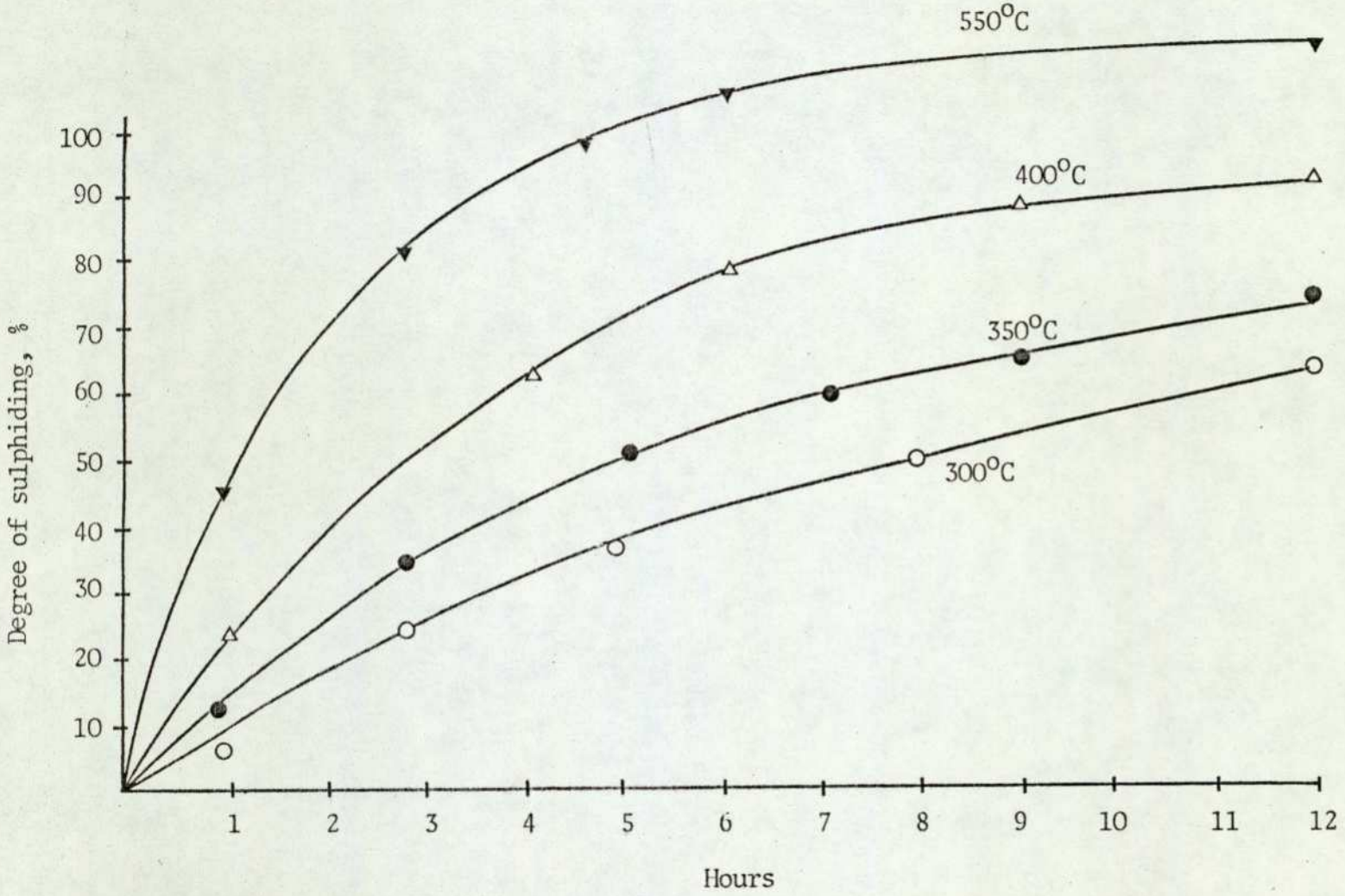

TABLE 4.4. Chemical Analysis of Different Cobalt-Nickel Sulphides

lphided oducts at (hrs)		OXYGEN FLASK ANALYSIS*				INSOLUBLE SULPHIDE ANALYSIS**						
		Sulphur found % (w/w)	Assume $NiCo_2O_xS_y$ x	y	Assume $NiCo_2S_x$ x	Sulphide found % (w/w)	Assume $NiCo_2O_xS_y$ x	y	$NiCo_2S_x$ x	Assume $NiCo_2O_xS_y + S_z$ x	y	z
)	1	3.4	3.74	0.26	0.19	3.4	3.74	0.26	0.19	3.74	0.26	-
)	2¾	9.3	3.27	0.73	0.56	9.3	3.27	0.73	0.56	3.27	0.73	-
)	5	16.0	2.70	1.30	1.05	15.8	2.71	1.29	1.03	2.71	1.29	0.02
)	8	23.0	2.05	1.95	1.64	22.6	2.09	1.91	1.61	2.08	1.92	0.03
)	12	29.8	1.37	2.63	2.33	27.9	1.57	2.43	2.13	1.51	2.49	0.17
)	2	10.9	3.14	0.86	0.67	10.7	3.15	0.85	0.66	3.15	0.85	0.02
)	5	22.1	2.14	1.86	1.56	22.0	2.15	1.85	1.55	2.14	1.86	0.01
0	7	25.7	1.79	2.21	1.90	25.2	1.84	2.16	1.85	1.83	2.17	0.04
0	9	27.4	1.62	2.38	2.08	25.8	1.78	2.22	1.91	1.74	2.26	0.14
0	12	32.4	1.10	2.90	2.64	32.2	1.12	2.88	2.61	1.11	2.89	0.02
0	1	10.1	3.20	0.80	0.62	10.0	3.21	0.79	0.61	3.21	0.79	0.01
0	4	26.5	1.71	2.29	1.98	25.4	1.82	2.18	1.87	1.79	2.21	0.10
)	6	23.7	0.96	3.04	2.80	32.2	1.12	2.88	2.61	1.07	2.93	0.14
0	9	37.1	0.58	3.42	3.24	36.4	0.66	3.34	3.15	0.63	3.37	0.06
0	12	38.9	0.38	3.62	3.50	37.6	0.53	3.47	3.31	0.47	3.53	0.12
0	1	19.0	2.43	1.57	1.29	18.2	2.50	1.50	1.22	2.49	1.51	0.07
0	3	36.0	0.71	3.29	3.09	34.8	0.84	3.16	2.94	0.79	3.21	0.11
0	4½	44.8	-	-	4.46	41 6	0.06	3.94	3.92	-	-	-
0	6	45.4	-	-	4.57	43.0	-	-	4.15	-	-	-
0	12	46.5	-	-	4.78	44.2	-	-	4.36	-	-	-

* see section 3.1.(2)

** see section 3.1.(1)

composition if $NiCo_2S_x$, where $4 > x > 0$.

(2) Assume the sulphided products are a mixture of oxide and sulphide. i.e. $NiCo_2O_xS_y$, where $x + y = 4$.

(3) Assume the sulphided products are a mixture of oxide, sulphide and some elemental sulphur. i.e. $NiCo_2O_xS_y + S_z$, where $x + y = 4$ and $z > 0$.

6.3. Half-Cell Electrochemical Results

Potentiodynamic voltage/current curves for various cobalt-nickel sulphides in teflon-bonded porous electrode structures at 70°C, are shown in Figure 4.7. The effect on the electrocatalytic activity at a constant cathodic potential of -300 mV (vs D.H.E.) for different cobalt-nickel sulphide electrodes with respect to catalyst loading is shown in Figure 4.8.

6.4. DTA Analysis

The results for the thermal decomposition of cobalt-nickel oxides are shown diagrammatically in Figure 4.10 - celluloid sheet - and quantitatively in Table 4.5. The results suggest that the mixed oxides decompose in three stages when they are heated to 950°C, and the temperature is then held constant for one hour. No decomposition occurs with these materials above 850°C. During the first two weight-loss stages, cobalt-nickel oxide C behaves similarly when heated in air or nitrogen. The weight-losses are probably due to loss of moisture and interstitial oxygen respectively. Definition

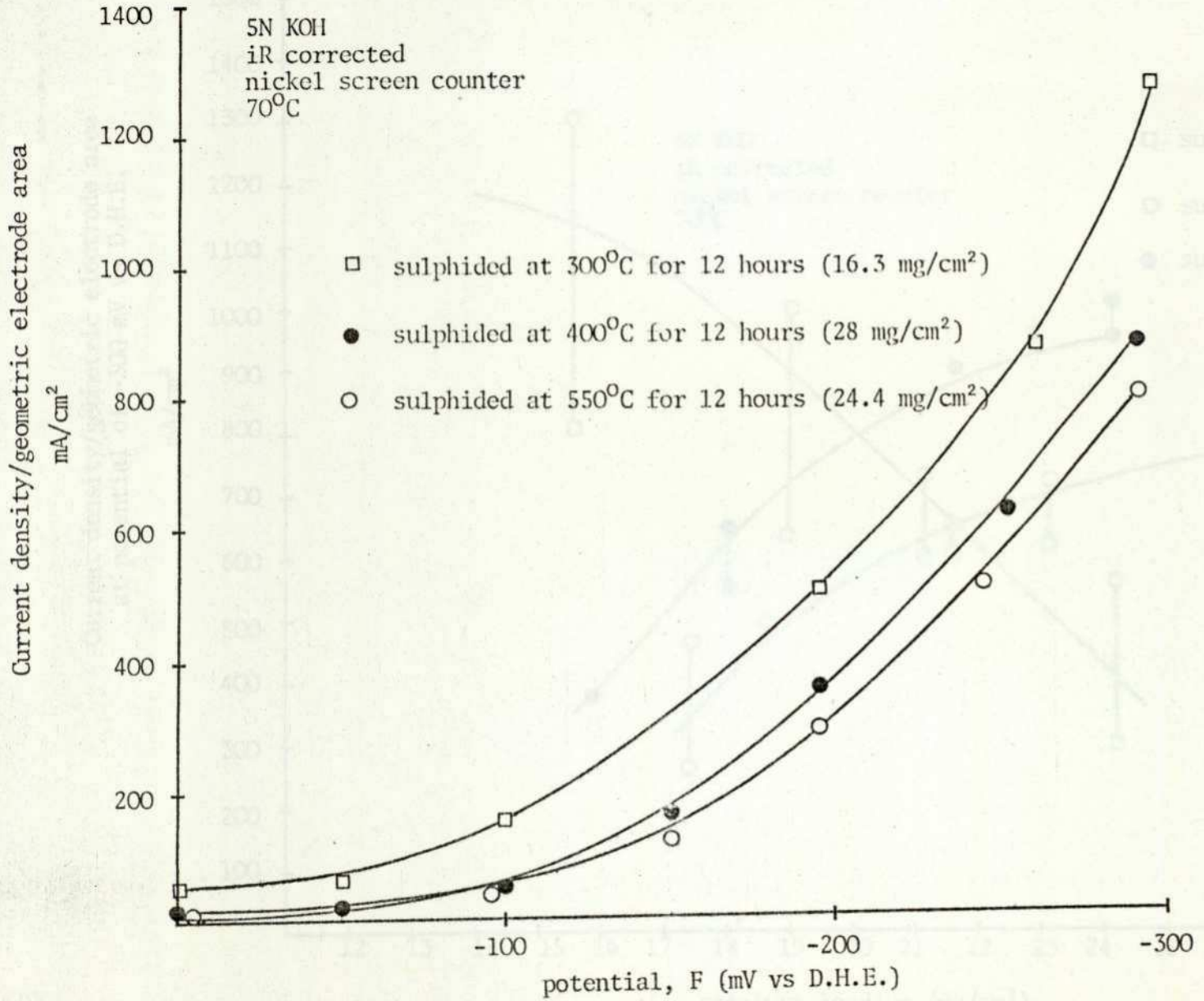

Figure 4.7. Voltage/current curves for various cobalt-nickel sulphides in teflon-bonded porous electrode structures at 70°C.

Figure 4.8. The plot of performance vs catalyst loading for different [illegible] nickel sulphides in teflon-bonded porous electrode structures.

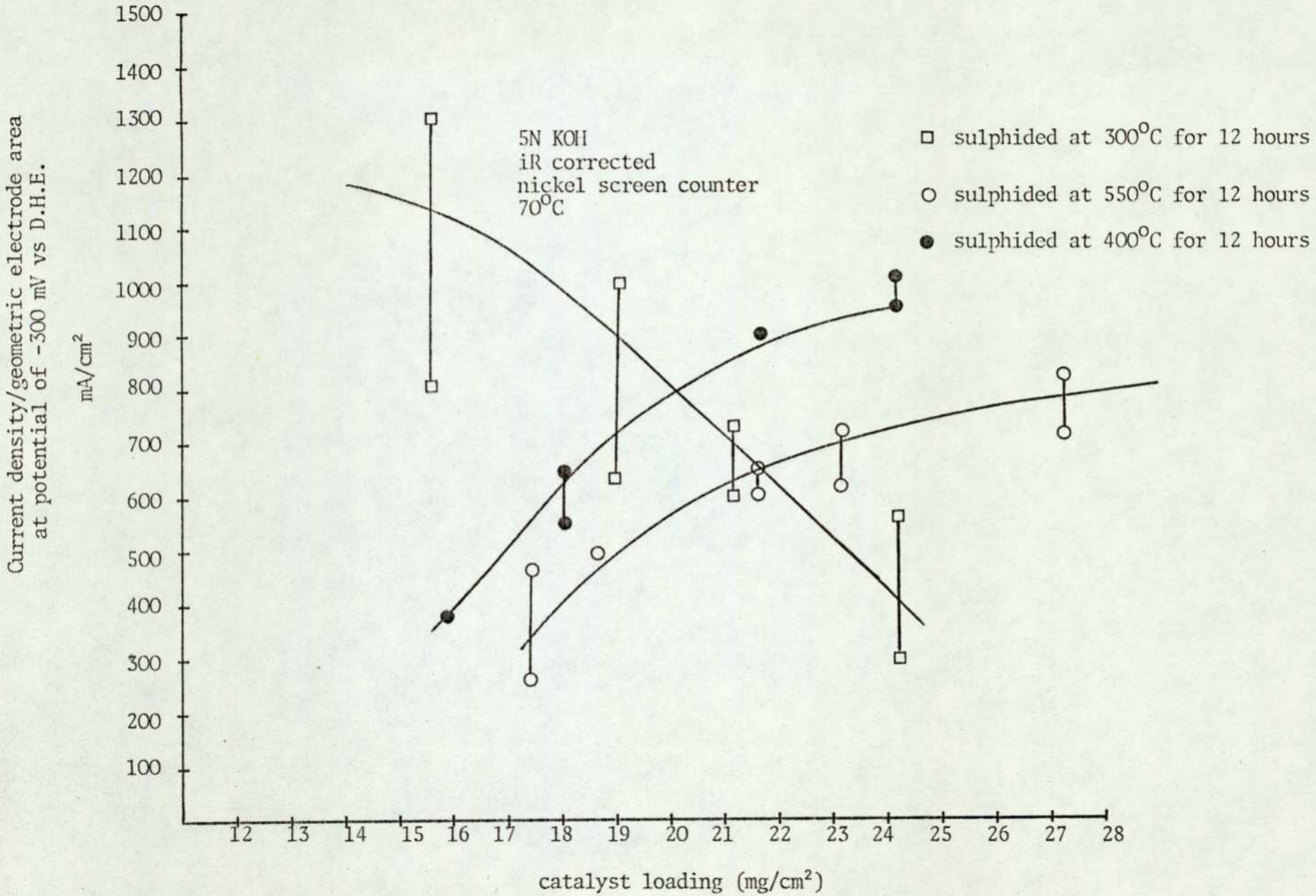

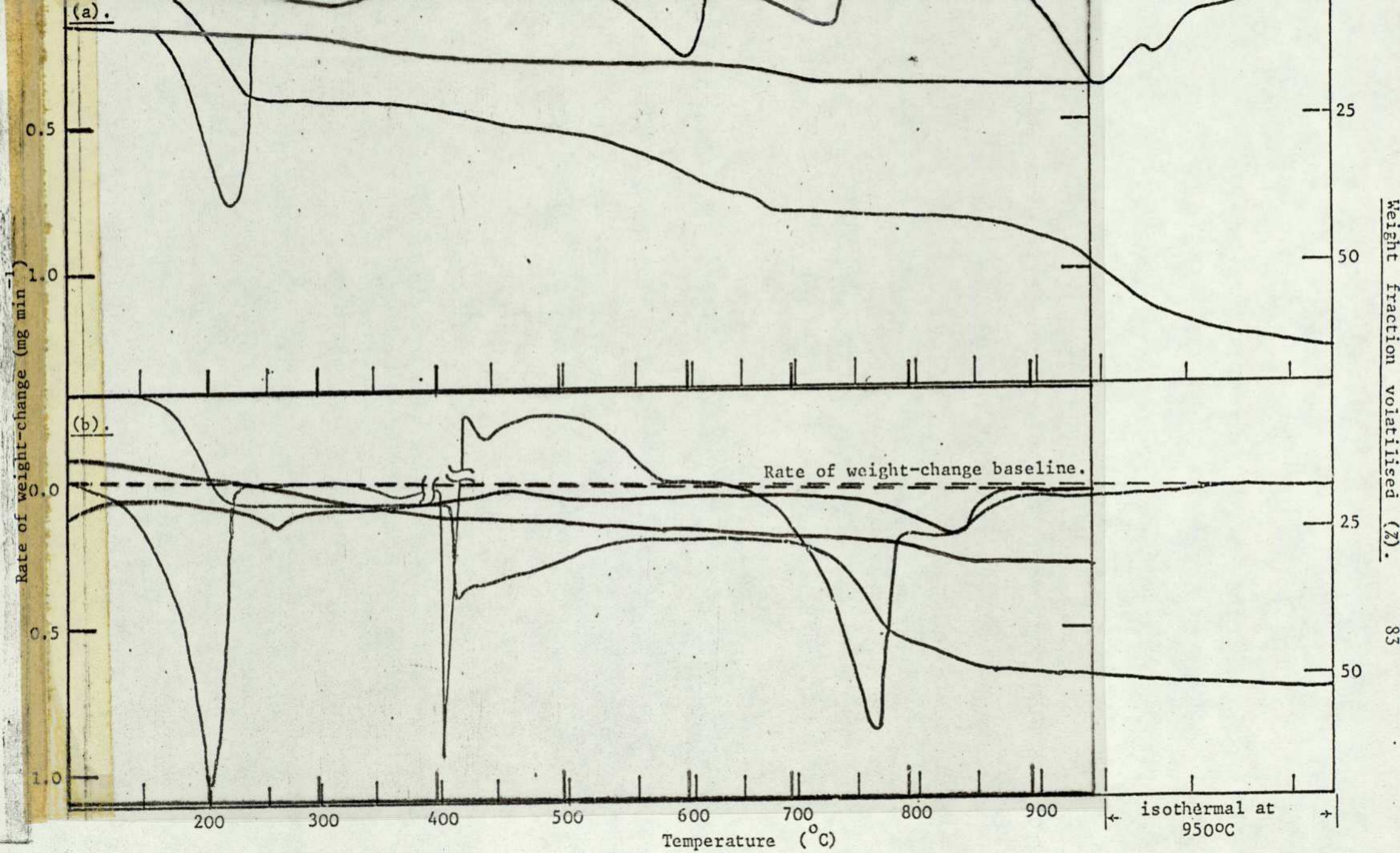
(a).
(b).
Rate of weight-change baseline.
Rate of weight-change (mg min⁻¹)
0.5
1.0
0.0
0.5
1.0
25
50
25
50
Weight fraction volatilised (%).
200
300
400
500
600
700
800
900
Temperature (°C)
isothermal at 950°C

TABLE 4.5. The Thermal Decomposition of Cobalt-Nickel Oxides in Nitrogen and Air (Sample size, ca. 20 mg; heating rate, 5°C min^{-1}; gas flow rate, 60 ml min^{-1}; crucible diameter, 8 mm; crucible material, Pt/10% Rh).

Sample number:	D	C	D	C
Atmosphere (A = air, N = nitrogen)	A	A	N	N
First weight-loss stage				
Temperature range (°C):	RT-162	RT-229	RT-212	RT-155
Weight-fraction volatilised (%):	11.4	1.5	6.2±0.8	1.7±0.8
Maximum rate of weight-loss (% min^{-1}):	10.8	12.2	3.3±0.1	8.1±0.8
Temperature of max. rate (°C):	100	69	75±18	86±12
Second weight-loss stage				
Temperature range (°C):	162-710	229-671	212-496	155-580
Weight-fraction volatilised (%):	11.4	1.7	4.8±0.9	2.6±0.2
Maximum rate of weight-loss (% min^{-1}):	4.4	4.2	4.0±0.6	[a]SWL/2.6
Temperature of max. rate (°C):	266/577*	553	305±5	[a]SWL/514
Third weight-loss stage				
Temperature range (°C):	710-854	671-849	496-747	580-755
Weight-fraction volatilised (%):	4.8	4.8	4.1±0.3	4.4±0.1
Maximum rate of weight-loss (% min^{-1}):	9.2	7.9	9.6±0.6	9.4±0.1
Temperature of max. rate (°C):	815	816	730±5	727±5
Maximum exothermicity (kcal g^{-1}):**	0.20	0.21	0.22	0.18
Temperature of max. exothermicity (°C):	818	820	736	735

Key: a, slow weight-loss occurs rather than a well defined reaction rate maximum: *, weight-loss occurs in two stages; **, calculated by a linear calibration procedure rather than the more accurate area procedure; ±, indicates the values quoted are the average of two experiments.

of the initial temperature and final temperature of the reactions, and of the weight-fractions volatilised at each stage, is difficult because of the low rates of weight-loss. However, cobalt-nickel oxide C appears to lose ca. 1.5 - 2.0 % (w/w) moisture, and between 1.7 and 2.8% (w/w) at a higher temperature. Cobalt-nickel oxide D appears to be anomalous in that its behaviour is different in air and nitrogen. The greater weight-loss from cobalt-nickel oxide D compared with cobalt-nickel oxide C is probably due to the 'conditioning' that the latter had received. Cobalt-nickel oxide D loses ca. 11.0 % (w/w) in the first two stages in nitrogen and about twice as much in air. The difference suggests that cobalt-nickel oxide D may not be homogeneous, the values in air should probably be more similar to the values in nitrogen by analogy with cobalt-nickel oxide C. The values in nitrogen were duplicated; the run in air was not. The third (main) weight-loss stage was similar for both samples, but the range of temperatures over which it occurs depends on the nature of the gaseous atmosphere. This stage, probably due to 'reduction' or oxygen loss from the mixed oxides occurs with a maximum rate of ca. 9% min^{-1} at ca. 730°C in nitrogen and ca. 815°C in air. The reaction is moderately exothermic (ca. 0.2 kcal. (g. of oxygen-loss)$^{-1}$) and is the only one of the three reactions which shows any significant DTA signal. About 4.5% of the initial weight of mixed oxide is lost during this stage; this corresponds to about 5.5% of the weight of material remaining at the beginning of the third weight-loss stage. Conversion of pure $NiCo_2O_4$ to $NiCo_2O_3$ would require a weight-loss of ca. 6.7% at this stage.

Table 4.6 shows that the initial stages in the decomposition

TABLE 4.6. The Thermal Decomposition of Cobalt-Nickel Sulphides in Nitrogen and Air.

(Sample size, ca. 20 mg; heating rate, 5°C min^{-1}; gas flow rate, 60 ml min^{-1}; crucible diameter, 8 mm; crucible material, Pt/10% Rh).

Sample number	C	C	D	D
Atmosphere (A = air, N = nitrogen)	A	N	A	N
TABLE IIA - Initial stages in air and nitrogen				
Moisture loss				
Temperature range (°C):	-	-	RT-82	RT-91
Weight-fraction volatilised (%):	-	-	1.4	1.4
Second weight-loss stage				
Temperature range (°C):	102-214	105-279	82-176	91-250
Weight-fraction volatilised (%):	18.0±0.1	18.0±0.1	2.0±0.1	6.2
Maximum rate of weight-loss (% min^{-1}):	17.2±3.0	11.0±0.5	9.8	9.8
Temperature of max. rate (°C):	197±3	218±1	162±1	135
Maximum exothermicity (k cal.g^{-1}):	0.22	-	0.65	-
Temperature of max. exothermicity (°C):	200±7	-	168±1	-
Third weight-loss				
Temperature range (°C):	294-388	268-404	284-413	250-313
Weight-fraction volatilised (%):	0.6	1.2±0.5	13.3±2.4	1.6
Maximum rate of weight-loss (% min^{-1}):	SWL	9.4±0.2	ca.160.0	10.5
Temperature of max. rate (°C):	365	386±6	413±2	318

of cobalt-nickel sulphide C and cobalt-nickel sulphide D in air and nitrogen. For cobalt-nickel sulphide C, no moisture loss occurred and the decomposition below ca. 400°C occurs in two stages. About 18% (w/w) of the initial weight of material is volatilised from ca. 100°C to ca. 220°C (in air) or ca. 280°C (in nitrogen). This weight-loss stage is probably due to excess sulphur present in the catalyst. This is followed by a much slower weight-loss upto ca. 390°C in air or ca. 400°C in nitrogen. In air, the main reaction is faster than in nitrogen (ca. 17% min^{-1}. vs ca. 11% min^{-1}), occurs at a lower temperature (197°C vs 218°C) and is moderately exothermic, whilst in nitrogen, the reaction is approximately thermoneutral. This suggests that the reaction is at least partially oxidative in nature. Subsequent experiments in which pure sulphur was heated in air under the same conditions have provided further evidence that this reaction stage is likely to be due to the volatilisation of excess sulphur from the catalyst. Cobalt-nickel sulphide D loses ca. 15% moisture below ca. 90°C, thereafter the reactions are somewhat different in air and nitrogen. The rates of reaction are low, so that the accuracy of measurement of temperature range and weight-loss is limited. However, the weight of excess sulphur volatilised from cobalt-nickel sulphide D is about 6% (w/w). The results for the later stages of the decomposition of cobalt-nickel sulphide C are shown graphically in Figure 4.10(a) and quantitatively for both samples in Table 4.8. In Table 4.8, as in Table 4.7, the weight-fraction volatilised has been calculated in two ways. The first value quoted is calculated using the total initial weight of material as denominator, that is:

TABLE 4.7. The Thermal Decomposition of Cobalt-Nickel Sulphides (the later Stages of the Decomposition in Air).

(Sample size, ca. 20 mg; heating rate, 5°C min^{-1}; gas flow rate, 60 ml min^{-1}; crucible diameter, 8 mm; crucible material, Pt/10% Rh).

	Sample C	Sample D
Main weight-loss reaction		
Temperature range (°C):	390-407	284-414
Weight-fraction volatilised (%):*	15.5±0.5(18.9±0.5)	15.5±0.4(18.5±0.6
Maximum rate of weight-loss (% min^{-1})	ca.200	ca.160
Temperature of max. rate (°C):	406±1	410±1
Maximum exothermicity (kcal.g^{-1}):	6.3±2.5	4.0±2.4
Maximum exothermicity (T, °C):	33±2	40±3
Baseline T for max. exothermicity (°C):	403	412±2
First weight-gain reaction		
Temperature range (°C):	407-431	414-428
Weight-fraction taken up (%):*	2.1±0.4(3.3±0.5)	2.8(4.2)
Maximum rate of uptake (% min^{-1}):	16.4±2.3	36.5±10.0
Temperature of max. rate (°C):	424±4	438±4
Maximum exothermicity (kcal.g^{-1}):	102±0.5	-
Temperature of max. exothermicity (°C):	431	-
Second weight-gain reaction		
Temperature range (°C):	431-635	442-640
Weight-fraction taken up (%):*	9.0±0.4(13.2±0.6)	12.2±0.8(14.4±0.8)
Maximum rate of uptake (% min^{-1}):	3.9±0.1	5.2±0.5
Temperature of max. rate (°C):	495±3	504±1
Fourth weight-loss reaction		
Temperature range (°C):	635-795	635-978
Weight-fraction volatilised (%):*	21.8±0.7(28.1±0.5)	23.1(30.0)
Maximum rate of weight-loss (% min^{-1}):	10.1±0.1	11.6±0.6
Temperature of max. rate (°C):	766±1	772±2
Fifth weight-loss stage		
Temperature range (°C):	795-952	789-911
Weight-fraction volatilised (%):*	7.0(12.0)	8.0(14.2)
Maximum rate of weight-loss (% min^{-1}):	8.5±1.1	9.8±1.7
Temperature of max. rate (°C):	817±1	822±10

Key: *, see Table 4.8; for both samples, the values quoted are the average of at least two experiments.

TABLE 4.8. The Thermal Decomposition of Cobalt-Nickel Sulphides (the later Stages of the Decomposition in Nitrogen)

(Sample size, ca. 20 mg; heating rate, 5°C min^{-1}; gas flow rate, 60 ml min^{-1}; crucible diameter, 8 mm; crucible material, Pt/10% Rh)

	Sample C	Sample D
Fourth weight-loss stage		
Temperature range (°C):	408-495	337-456
Weight-fraction volatilised (%):	3.8±0.3(4.8±0.3)*	1.3(1.6)*
Maximum rate of weight-loss (% min^{-1}):	11.6±1.6	10.5
Temperature of max. rate (°C):	439±2	438
Maximum exothermicity (cal. g^{-1}):	15.8	46.8
Temperature of exothermicity (°C):	439	438
Fifth weight-loss stage		
Temperature range (°C):	493-621	456-571
Weight-fraction volatilised (%):	8.4±0.8(11.0±1.0)*	6.6(8.9)*
Maximum rate of weight-loss (% min^{-1}):	9.9±0.3	12.4
Temperature of max. rate (°C):	596±6	475
Sixth weight-loss stage		
Temperature range (°C):	621-732	571-698
Weight-fraction volatilised (%):	3.6±0.6(5.3±0.6)*	2.7(4.0)*
Maximum rate of weight-loss (% min^{-1}):	16.6±1.7	15.4
Temperature of max. rate (°C):	663±2	638
Seventh weight-loss stage		
Temperature range (°C):	732-855	698-868
Weight-fraction volatilised (%):	2.8(4.4)*	4.3(6.1)*
Maximum rate of weight-loss (% min^{-1}):	7.6	7.7
Temperature of max. rate (°C):	831	840
Eighth weight-loss stage (including reactions which occur when sample held at 950°C)		
Temperature range (°C):	855-950 + iso.	868-950 + iso.
Weight-fraction volatilised (%):	23.6(42.3)*	15.8(26.0)
Maximum rate of weight-loss (% min^{-1}):	7.8	5.2
Temperature of max. rate (°C):	925	-
Maximum exothermicity (kcal.g^{-1}):	0.14	0.16
Temperature of max. exothermicity (°C):	921	923

Key: *, under 'weight-fraction volatilised' the first figure is calculated from the total initial weight of powder; the second figure in brackets is calculated from the weight of material remaining at the beginning of the reaction stage quoted.
±, indicates that the value quoted is the average of more than one experiment.

$$(W.F.)_a = (W_a/W_o) \times 100$$

where W_o is the total initial weight of material.

The value in parentheses was calculated using, as denominator, the weight of material on the crucible at the commencement of the weight-loss stage (or weight-gain stage) under discussion. This gives a 'running total':

$$(W.F.)_a = \frac{W_a}{W_o - \sum_{n=1}^{m} W_{(a-n)}} \times 100$$

where $m = a-1$.

For both stages, the decomposition occurred in five stages above 400°C in nitrogen. Only two of the stages show any DTA signal. The first stage above 400°C (the fourth stage in total) was slightly exothermic, the final weight-loss was much more exothermic. From the nature of the final product, the final weight-loss appeared to be due to the partial reduction of the metal oxide mixture formed in the previous stages, followed by the alloying of the metal product to the Pt/10 Rh crucible. Analysis of the solid products formed during each stage of the decomposition was necessary before the mode of anaerobic decomposition can be fully elucidated. Figure 4.10(b) and Table 4.8 show the later stages of the thermal decomposition of cobalt-nickel sulphide C and cobalt-nickel sulphide D when heated in air. The samples behave very similarly; the temperatures of maximum rate of weight-loss are within 10°C for all the reaction stages and the weight-fractions absorbed or volatilised at each stage are similar. The reaction stages, due to impurity of one

form or another, discussed earlier, were followed in turn by (a) a very exothermic weight-loss reaction, immediately followed by (b) two weight-gain (oxygen-uptake) reactions with (c) two further weight-losses occurring at higher temperatures. The decomposition in air was completed at a temperature of about 825°C; the product appeared to be a mixed metal oxide.

The very fast weight-loss reaction occurring over the narrow temperature range from 390-410°C was probably due to burn-off of sulphur from the catalyst. The reaction occurred only in air and was very exothermic, thus oxygen from the gas phase was undoubtedly involved in the mechanism of the reaction. The maximum rate of weight-loss occurred very close to the conclusion of the weight-loss reaction, and the temperature of the sample and crucible were raised by ca. 36°C. The maximum rate of weight-loss occurred, for most of the reactions studied, at a point where between 60 and 85% of the reactant originally present had reacted. Where the maximum rate of reaction occurred at the end of the reaction, as it did in this case, the normal reason would be that two reactions are occurring simultaneously over the same temperature range, one causing weight-loss and the other weight-gain. Initially, the weight-loss reaction was dominant, but as the temperature rose the weight-gain became energetically more feasible. Thus on a molecular level, in the present experiments, the loss of sulphur from the catalyst to form free valencies was the initial predominant reaction. As the temperature rose and the 'metal surface' became free from sulphur, weight-gain occurred as oxygen was absorbed to saturate the valencies. At a certain temperature, the rate of loss of sulphur

becomes equal to the rate of uptake of oxygen. As the loss of sulphur was not completed before the uptake reaction began, the measured amount of sulphur would be less than the actual amount of sulphur present in the catalyst. The reaction scheme for the full decomposition seems likely to be as follows:

$$NiCo_2O_xS_y + S_z \xrightarrow{A} NiCo_2O_xS_y \xrightarrow{B} NiCo\ O_x \xrightarrow{C} NiCo_2O_4$$

where $x + y = 4$.

If y = 4, loss at B = 42.1%, gain at C = 36.4%

3, loss at B = 33.3%, gain at C = 25.0%

2, loss at B = 23.5%, gain at C = 15.4%

1, loss at B = 12.5%, gain at C = 7.1%.

From Table 4.7, loss at B is ca. 18.5% for both samples and gain at C is about 15%. Thus it appears that y is approximately equal to 2. This would give a total sulphur content of ca. 42% for cobalt-nickel sulphide C and ca. 30% for cobalt-nickel sulphide D.

The later stages of the decomposition in air should be similar to the decomposition of cobalt-nickel oxides (cobalt-nickel oxide C and cobalt-nickel oxide D) except that the materials from cobalt-nickel sulphide C and cobalt-nickel sulphide D should have higher surfacea areas and thus be more reactive. Loss of each oxygen atom from the mixed oxide product (assumed to be $NiCo_2O_4$) would be equivalent to loss of ca. 6.7% of the initial weight at the beginning of the weight-loss above 635°C. In fact, over 40% of the material initially present at the end of the oxygen uptake reaction was volatilised below 950°C in air. The total weight-fraction

volatilised from cobalt-nickel sulphide C is 55.4% and from cobalt-nickel sulphide D is 61.6%. Thus, the final weight-loss stages in air appear to be due to the volatilisation of at least a portion of the metal originally present in the catalyst.

7. DISCUSSION

The kinetic curves in Figure 4.5 clearly show that freeze dried cobalt-nickel oxide ($NiCo_2O_4$) is completely sulphided to give cobalt-nickel sulphide of composition close to $NiCo_2S_4$ at 550°C with the optimum reaction time of 5-6 hours. At lower preparation temperatures, i.e. 300°C to 400°C, the degree of sulphiding is never completed, even though the reaction time is set for 12 hours. X-ray analysis of the cobalt-nickel sulphides prepared from different temperatures show that mixed phases are present, which is mainly due to NiO and Co_3O_4. The presence of these mixed phases is most likely to occur at lower sulphiding temperatures, but gradually diminishes if the optimum sulphiding conditions are reached. Parallel experiments were also carried out to sulphide NiO and Co_3O_4 using similar experimental procedures and conditions. Their kinetic curves are shown in Figure 4.6, and it was found that NiO and Co_3O_4 are completely sulphided to give NiS and Co_3S_4 at 500°C with the optimum reaction time of about 6 hours. NiO and Co_3O_4 are prepared by thermal decomposition of the corresponding nitrates.

For cobalt-nickel sulphides prepared at 550°C beyond the optimum reaction time of 5-6 hours, the sulphur content found in in these samples are always higher than the theoretical value of

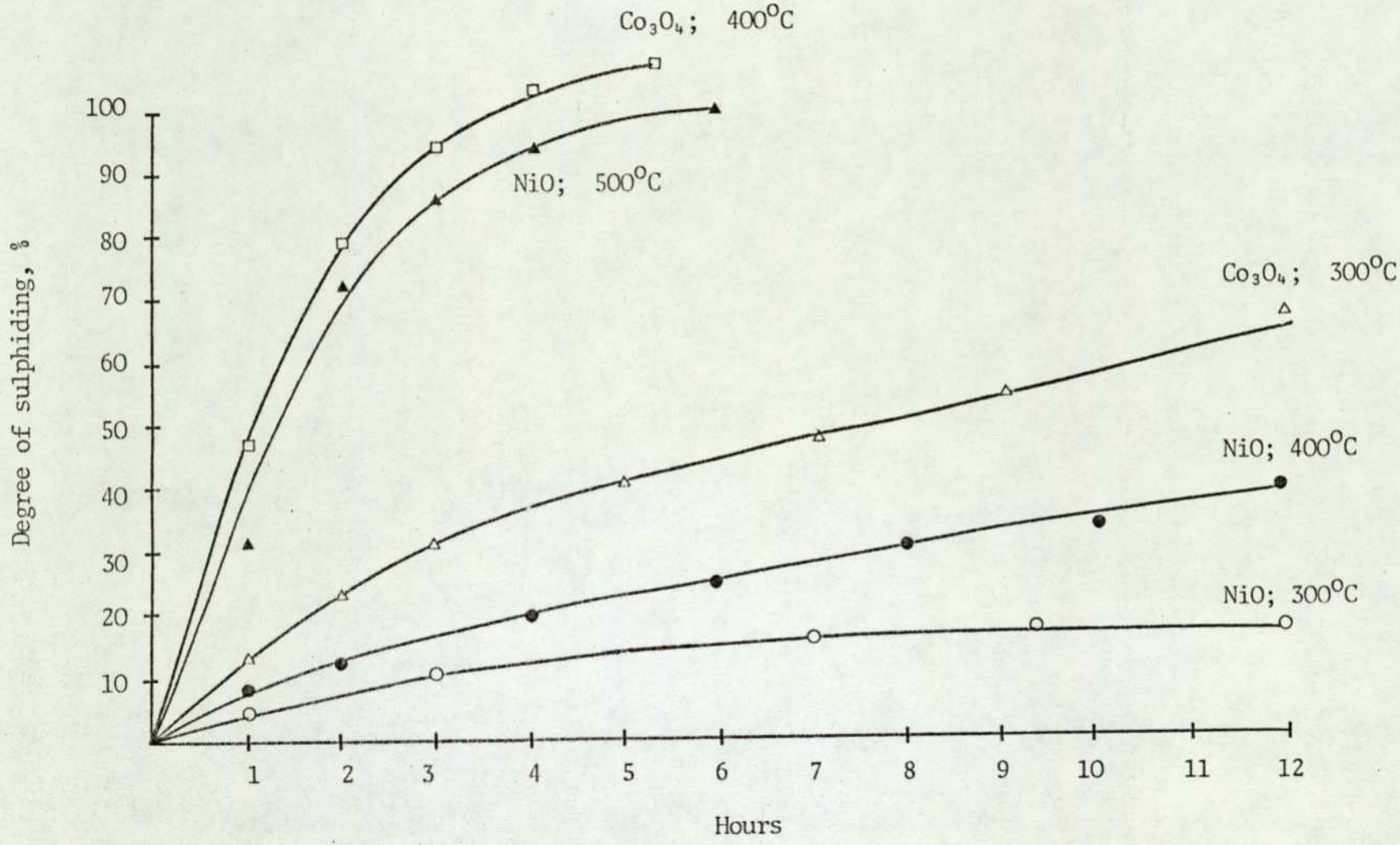

Figure 4.6. Kinetic curves of sulphiding NiO and Co_3O_4

maximum 42.08%, which corresponds to the composition of $NiCo_2S_4$. This can be explained by observing that free sulphur is deposited on the reaction tube during the sulphiding process. Therefore, decomposition of sulphur as a result of decomposition of hydrogen sulphide at high temperatures is most likely to happen at the same time. Chemical analysis by the reaction of cobalt-nickel sulphide with activated concentrated hydrochloric acid (see Section 3.1 (1)), gave a slightly lower sulphiding index than the results obtained from the oxygen flask analytical method. (See Section 3.1 (2)). This is especially significant for samples prepared beyond the optimum preparation conditions. This strongly suggests that free sulphur is deposited during the sulphiding process and is most significant at a higher temperature.

In all the cobalt-nickel sulphide samples, x-ray results cannot detect the presence of free sulphur. This may be due to the concentration of sulphur being too low to be detected or the deposition of sulphur only occurring on the surface of the powder sample. Therefore, the distribution of sulphur as mixed phase is very uneven and small. The calculated lattice parameters for some of the cobalt-nickel sulphide samples are listed in Table 4.1, and they all show predominately spinel structure. The kinetic of sulphiding $NiCo_2O_4$ to $NiCo_2S_4$ can be summarised as follows:

(1) The optimum conditions for sulphiding $NiCo_2O_4$ to give $NiCo_2S_4$ is at a temperature of 550°C and sulphiding time of 5-6 hours.

(2) The degree of sulphiding can be measured by the

weight-gain procedure, oxygen flask analytical method and from the amount of water liberated (see Chapter 3, Section 2), which can be trapped in tubes filled with calcium chloride. However, it is not possible to measure the amount of water liberated due to the design of the tube furnace, which is schematically shown in Figure 4.9.

(3) At temperatures below 400°C, Co_3O_4 and NiO are present as impurities with the partially sulphided products.

(4) At temperatures between 400°C and 550°C, the presence of Co_3O_4 and NiO as impurities is gradually diminished with increase in reaction time.

(5) The deposition of free sulphur takes place simultaneously during the sulphiding process and is most significant at a higher sulphiding temperature.

A mechanism can be proposed for the sulphiding of cobalt-nickel oxide ($NiCo_2O_4$) according to the following equations:

(a) $NiCo_2O_4 + H_2S \longrightarrow NiS + H_2O + Co_2O_3$

(b) $Co_2O_3 + 3H_2S \longrightarrow Co_2S_3 + 3H_2O$

(c) $Co_2S_3 + NiS \longrightarrow NiCo_2S_4$

Since $NiCo_2O_4$ decomposes[87] into NiO and Co_3O_4 at about 400°C to 450°C, it is not clear as to whether the sulphiding process occurs at the spinel cobalt-nickel oxide or at the decomposition

Figure 4.9 Apparatus for Sulphiding of Cobalt-Nickel Oxides

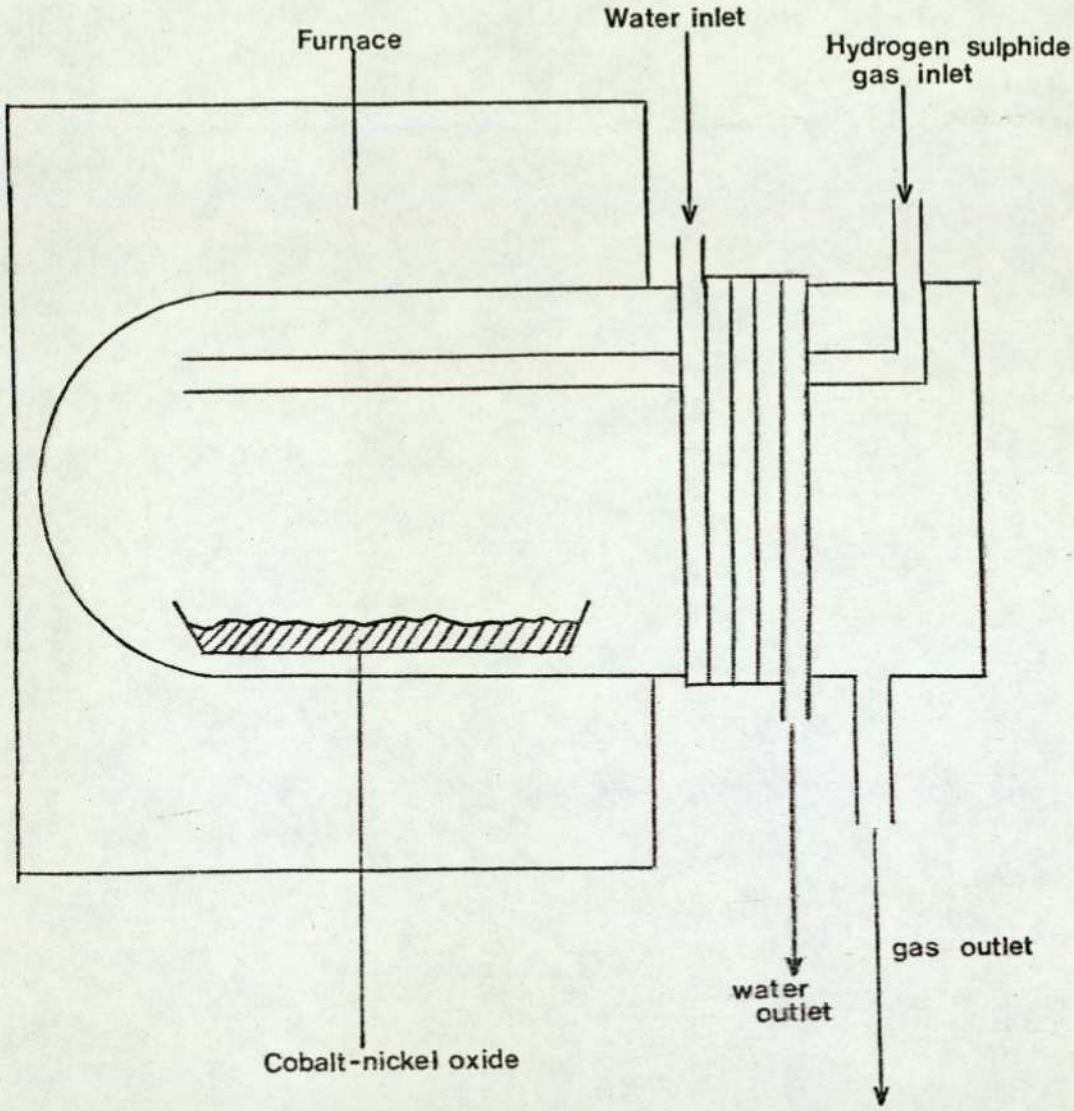

products of NiO and Co_3O_4. However, results show that at temperatures below 400°C, the sulphiding process is very slow and never completely sulphided during the reaction time of 12 hours, while the rate of sulphiding is sharply increased at a higher temperature. During the initial stage of the sulphiding process, the hydrogen sulphide is adsorbed on the oxide surface[88]. An exchange of sulphur and oxygen takes place at the hydrogen sulphide/oxide interphase and a layer of metal sulphide is formed between the oxide surface and the hydrogen sulphide. As the degree of sulphiding increases, the sulphide formation rate is decreased, due to the difficulty in diffusion through the layer of reaction products by sulphur and oxygen atoms. The counter diffusion of both sulphur and oxygen atoms and Co^{3+} and Ni^{2+} is negligible[89]. In the region shared by the oxide and the sulphide, stresses develop as a result of different unit-cell volumes. (i.e. lattice parameter for $NiCo_2O_4$ is 8.112Å, whilst that of $NiCo_2S_4$ is 9.392Å). These stresses can result in the formation of 'channels' in the sulphide layer, through which sulphide can enter and water can be removed.

Potentiodynamic voltage/current curves in Figure 4.7 show that electrocatalytic activity is highest for cobalt-nickel sulphide catalyst sulphided at 300°C for 12 hours, as compared to two other sulphide samples prepared at higher temperatures, regardless of catalyst loading. At the first instance, their differences in activity may be due to surface area and catalyst loading effects. However, by examining other results, such as chemical analysis, x-ray analysis and DTA analysis on the appropriate sulphided products, it is reasonably clear that electrochemical activity is

increased with decrease in the sulphur and sulphide content in the cobalt-nickel sulphide catalyst. The plot of performance as a function of catalyst loading in Figure 4.8, shows similar trends, but the degree of electrochemical reproducibility is best achieved with cobalt-nickel sulphide catalyst sulphided at 400°C for 12 hours, though the activity is less than that obtained for cobalt-nickel sulphide catalyst sulphided at 300°C for 12 hours. In contrast, the likelihood of mixed phases, such as NiO and Co_3O_4 contaminated in the sulphided products is increased with decrease in sulphiding temperature. In addition, the spinel structure of $NiCo_2S_4$ is more developed at higher sulphiding temperatures as indicated by the x-ray powder data, especially in the sulphiding of the thermal decomposed cobalt-nickel oxide. Therefore, a compromise of the impurity effect, the structural effect and electrochemical activity (taking the degree of reproducibility into account) is made and cobalt-nickel sulphide catalyst sulphided at 400°C for 12 hours was chosen for further studies.

CHAPTER FIVE

THE APPLICATION OF COBALT-NICKEL SULPHIDE ELECTROCATALYSTS IN DIFFERENT POROUS ELECTRODE STRUCTURES FOR THE HYDROGEN EVOLUTION REACTION IN ALKALINE MEDIA

1. INTRODUCTION

A porous electrode generally consists of an electrocatalyst, distributed uniformly in the form of small particles, in a porous and conducting substrate. The original idea is that such a porous electrode possesses a greater area which results in an increase in current density at any overpotential, but it is soon realised that the superior performance (i.e. higher power density and limiting current) sustained by such a porous electrode, as compared to a planar electrode, is partly due to the high ratio of the real to the apparent area and a much lower diffusion layer thickness.

The theory of electrode reaction in porous media is very complex as compared with planar electrodes. Current densities are not uniform within porous media because the ohmic overpotentials vary throughout the length of the pores. It is generally difficult to consider one form of rate control for reactions in porous electrodes, as the contribution of activation and diffusion overvoltages, in addition to the ohmic overvoltage, also vary throughout the pore structure.

Two types of porous electrode systems are known. They are the two-phase system which involves the liquid and the solid state, in which the reactant is dissolved in the electrolyte and is transported to the active sites of the electrode by diffusion and electrolyte migration. The three-phase system involves gas, liquid and solid, in which the gaseous reactant dissolves at the three-phase boundary and thus minimises the diffusion of the reactant through the electrolyte to the active sites of the electrode.

The main difference between these two types of porous electrode systems is the manner in which these electrodes are prepared. The three-phase

type of porous electrodes have been used successfully, especially in the field of fuel cell technology. Many physical models[90] have been proposed and studied, but due to lack of experimental verifications, except for a few simple models, the theory of porous electrodes is still considered as being in the development stage. The three_phase type of porous electrode can be prepared by mixing with a certain reagent which could decrease the wetting character of the electrode. (i.e. PTFE can provide a hydrophobic character to the electrode structures and can also function as a binder). The two-phase type of porous electrodes are normally prepared by annealing the catalyst with the porous catalyst support at elevated temperature. The chemical bonds that result in the sintering process serve as the binding force holding the catalyst and the porous catalyst support together.

It is the objective of this Chapter, to investigate which type of porous electrode structure can be used for the hydrogen evolution reaction, with the application of the newly evaluated cobalt-nickel sulphide electrocatalyst. The other aim is to correlate electrode performance and stability in terms of mechanical strength, and effectiveness in the utilisation of the available surface area between two types of porous electrode structures. The teflon-bonded porous electrode (i.e. the three-phase system) structure, and the dipping[6] porous electrode (i.e. the two-phase system) structure were chosen for the present study.

Porous electrodes are prepared by using a high surface area powder and have a biporous structure; that is they possess a dual scale of porosity. In the electrode the small particles of electrocatalyst of particle size of the order of 100 Å (diameter),

form aggregates, of particle size of the order of 1 μ. The dual scale of porosity consists of (a) the microporosity which is due to the voids within each aggregate and (b) the macroporosity which is due to the voids between the aggregates.

In general, the surface area associated with the micro-porosity is about 100 times greater than that associated with the macroporosity[91] . In teflon-bonded porous electrodes, the aggregates are held together by teflon particles situated between the aggregates, these produce hydrophobic gas channels which do not contain electrolyte. The micropores are completely filled with electrolyte. These teflon-bonded electrodes may be thought of as having certain advantages over the porous electrode containing no hydrophobic binder, in that they have a much greater mechanical strength and that the mass transfer of the gaseous reaction products, from the interior of the electrodes, should be increased by the presence of hydrophobic gas channels. This model predicts that all the gas will be produced in the micropores and consequently must find its way to the outer surface of the aggregate and flow away down the gas channels to escape from the electrode. If a single pore is considered, in order for the gas to escape, it is necessary for a certain gas pressure to develop which depends on the pore size, the surface tension and the contact angle according to the following equation:

$$p = \frac{2\sigma}{r} \cos \Theta$$

where σ = surface tension of the electrolyte

r = pore radius

Θ = contact angle

p = pressure of the gas

At lower pressures, the only method of escape is for the gas to dissolve in the electrolyte under pressure and move to the outer surface of the aggregate by diffusion through the electrolyte. When the required pressure is reached, the gas and most of the electrolyte will be forced out of the micropore. Hence it can be seen that a substantial part of the micropore surface area will not be in contact with the electrolyte for most of the time. This raises the problem of just how much of the available surface area is effectively used over a period of time. It is possible that most of the interior of the aggregates are usually dry and that the reaction only occurs on the film of liquid on the outer surface of the aggregates. If this is the case, then the advantage of using porous electrodes for gas evolution reactions would be seriously questioned. The teflon-bonded electrodes have proven to be most effective for the gas dissolution reaction, but its use for gas evolution have not been seriously considered. However, in terms of electrode fabrication, the dipping porous electrode is more easier and less costly to prepare than the teflon-bonded porous electrode.

2. PREPARATION OF THE ELECTROCATALYST AND ELECTRODES

In order to compare electrode activity directly between two different porous electrode structures, it is essential to fabricate both types of porous electrodes with a catalyst of similar surface area. Therefore, the preparation conditions for the two different porous electrode structures are kept as close as possible.

However, it is always difficult to control the exact catalyst loading on every electrode. Therefore, a series of porous electrodes of different catalyst loadings are examined.

2.1. Dipping Porous Electrode

A concentrated mixed nitrates solution is prepared by dissolving a 2/1 molar ratio of cobalt nitrate ($Co(NO_3)_2 \cdot 6H_2O$, analar grade, B.D.H. Chemicals), and nickel nitrate ($Ni(NO_3)_2 \cdot 6H_2O$, analar grade, B.D.H. Chemicals) in deionised water. A clean, 1 cm^2, 100 mesh nickel screen, welded with a piece of nickel wire, is dipped into the mixed nitrates solution. A thin layer of the mixed nitrates solution sticks to the nickel screen, which is quickly and carefully transferred to an oven and left for 5-10 minutes at 300°C until no more brown fumes (i.e. nitric oxide) are given off. The dipping and the thermal decomposition processes are repeated for several times until the desired loading of mixed oxides on the nickel screen is obtained. The porous electrode is then heat treated in an oven at 400°C for 21 hours so that the mixed oxide catalyst is completely transformed into the spinel cobalt-nickel oxide, ($NiCo_2O_4$) which is then sulphided by heating with a stream of hydrogen sulphide at 400°C for 12 hours. (See Chapter 4, Section 2). A piece of nickel wire and a 1 cm^2, 100 mesh nickel screen are used as a control in the sulphiding process. The analysis of loading is done by the weight-gain procedure.

2.2. Teflon Bonded Porous Electrode

The remainder of the mixed nitrates solution from Section 2.1.

is evaporated to dryness and then thermally decomposed in an oven at 300°C, until no more brown fumes are given off. The resulting black coloured, mixed oxides are firstly converted to spinel cobalt-nickel oxide ($NiCo_2O_4$) and finally to cobalt-nickel sulphide by using a similar preparation condition as mentioned in the last section. (See Section 2.1.).

Freshly prepared cobalt-nickel sulphide is made into the teflon-bonded porous electrode. The procedure for the fabrication of a teflon-bonded electrode has been fully described in an earlier Chapter. (See Chapter 2, Section 3.14).

3. HALF-CELL ELECTROCHEMICAL TESTING

So far, for the preliminary evaluation of the electrocatalytic activity of cobalt-nickel sulphides in teflon-bonded porous structures, only steady state electrochemical testing techniques are used. (i.e. potentiostatic current/time plot and near steady state potentiodynamic voltage/current plot). In order to obtain the intrinsic electrocatalytic activity of these electrodes in a mass transfer free condition, potentiostatic pulse, galvanostatic pulse and rotating disc electrode techniques are used. Mass transfer overvoltage is originated from the transport of reactants and products. i.e. water molecules migrate to the active sites at the electrode surface and hydrogen diffuses away from the electrode surface.

3.1. Rotating Disc Electrode (R.D.E.)

The theory of the Rotating Disc Electrode has been described

in detail by many workers[92]. It consists essentially of a disc electrode of known area, rotating horizontally under carefully controlled hydrodynamic conditions. Under mass transfer control condition, the effect of the rotating speed at a constant potential is linear in relation to the limiting current. i.e. obeyed Levich equation[93]. At a critical rotating speed, the limiting current is no longer depending on the rotating speed. Voltage/current relationship at this critical rotating speed is considered as being free of mass transfer. Any rotating speed over this critical value would make the system more complicated[94]. Due to the extreme difficulty in fabricating powder electrocatalysts into disc electrodes, it is therefore not possible to use this technique for the study of porous structures such as teflon-bonded electrodes.

3.2. Potentiostatic Pulse and Galvanostatic Pulse Technique

They are originally designed for planar electrodes to eliminate the mass transfer effect. But mass transfer through the porous media (i.e. teflon-bonded porous electrode) is more complex than mass transfer to a planar electrode. In view of present day achievements in the theory of fundamental electrochemistry of porous electrodes, mass transfer in porous structures is best eliminated by taking transient measurements at the shortest time intervals at which double layer[95] (see Section 4.2.1.) charging is completed. For planar electrodes, a more accurate measurement can be obtained from the mathematical relationship for the transient. (i.e. at the semi-linear diffusion condition[96]). This improved method has been widely

documented elsewhere[97].

3.2.1. Experimental : Potentiostatic Pulse Technique

The circuit diagram and apparatus used is shown in Figure 5.1. The potentiostat is coupled with a waveform generator. (Model RB 1, made by Chemical Electronics Ltd.). The reversible hydrogen electrode potential, (i.e. 25-33 mV vs D.H.E.) is first set on the potentiostat. The half-cell, containing the electrodes and electrolyte, is purged thoroughly with bubbling hydrogen and maintained at a constant temperature in a thermostatic water bath. The teflon-bonded working electrode is polarised to the pre-set voltage (i.e. 25-33 mV vs D.H.E.) by connecting the half-cell to the potentiostatic circuit. A stepwise increment of 5-10 mV in the cathodic direction, is set manually on the waveform generator. Also, by selecting the appropriate delay time and pulse length at each potential or overvoltage setting, a single shot of potential jump in the cathodic direction can be recorded on an oscilloscope (Remscope type SO 1, made by Cawkell Ltd.) in which the storage facility is used. The potential jump signals of different magnitudes are displayed on the storage scope in the form of square waves where the x-axis is corresponded to the current and the y-axis is corresponded to the time. By taking the transient currents immediately after the double layer charging time at different potentials or overvoltages, a voltage/current curve can then be constructed and is is considered as being under mass transfer free condition.

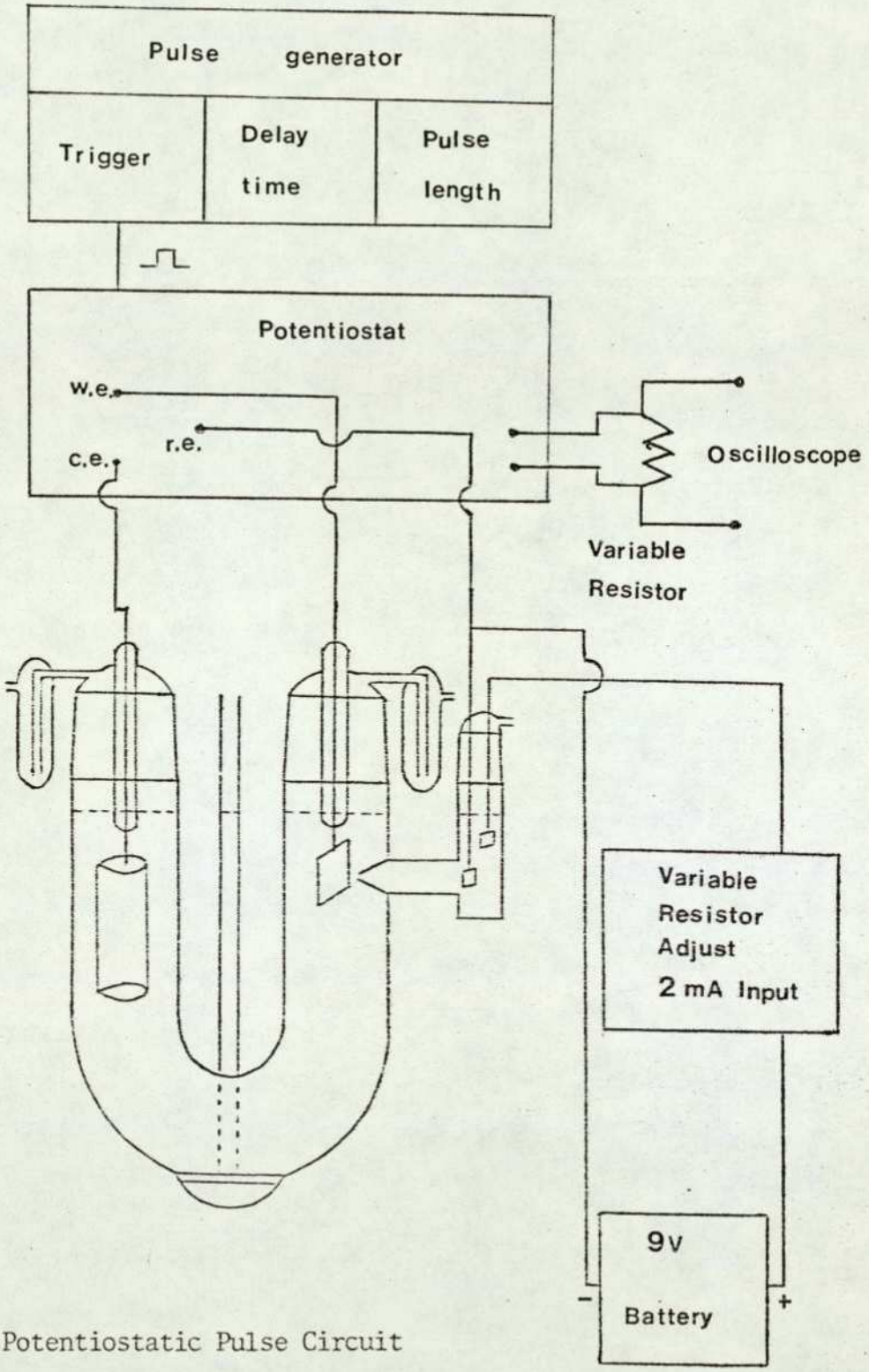

Figure 5.1. Potentiostatic Pulse Circuit

It is seen than the pre-set voltage on the potentiostat is the same as the reversible hydrogen electrode potential. (i.e. 25-33 mV vs D.H.E.). Therefore, for hydrogen evolution reaction, the potentiostatic pulse technique is the measurement of transient current at potentials which are deviated from the reversible hydrogen electrode potential in the cathodic direction. However, if the tested electrode does not behave similarly as the reversible hydrogen electrode, (i.e. does not chemisorb hydrogen), then the rest potential or the open circuit voltage (O.C.V.) in the hydrogen saturated electrolyte would be more positive than the reversible hydrogen electrode potential. Therefore, once the tested electrode is connected to the potentiostatic circuit, a quick potential jump occurs and the tested electrode is polarised from its rest potential to the reversible hydrogen electrode potential. The cathodic current resulting from this potential jump may be due to various possible electrochemical reactions. i.e. the reduction of the oxide film which may be formed on the electrode surface during the fabrication of teflon-bonded structure; the reduction of electro-active species which may be present as impurities in the electrolyte; the reduction of the electrocatalyst and etc.

For a non-reversible hydrogen electrode, the use of potentiostatic pulse technique for transient measurement is highly advantageous over the galvanostatic technique, since the former does not include other transient measurements other than that of the hydrogen evolution reaction. The circuit diagram for the galvanostatic pulse technique is shown in Figure 5.2.

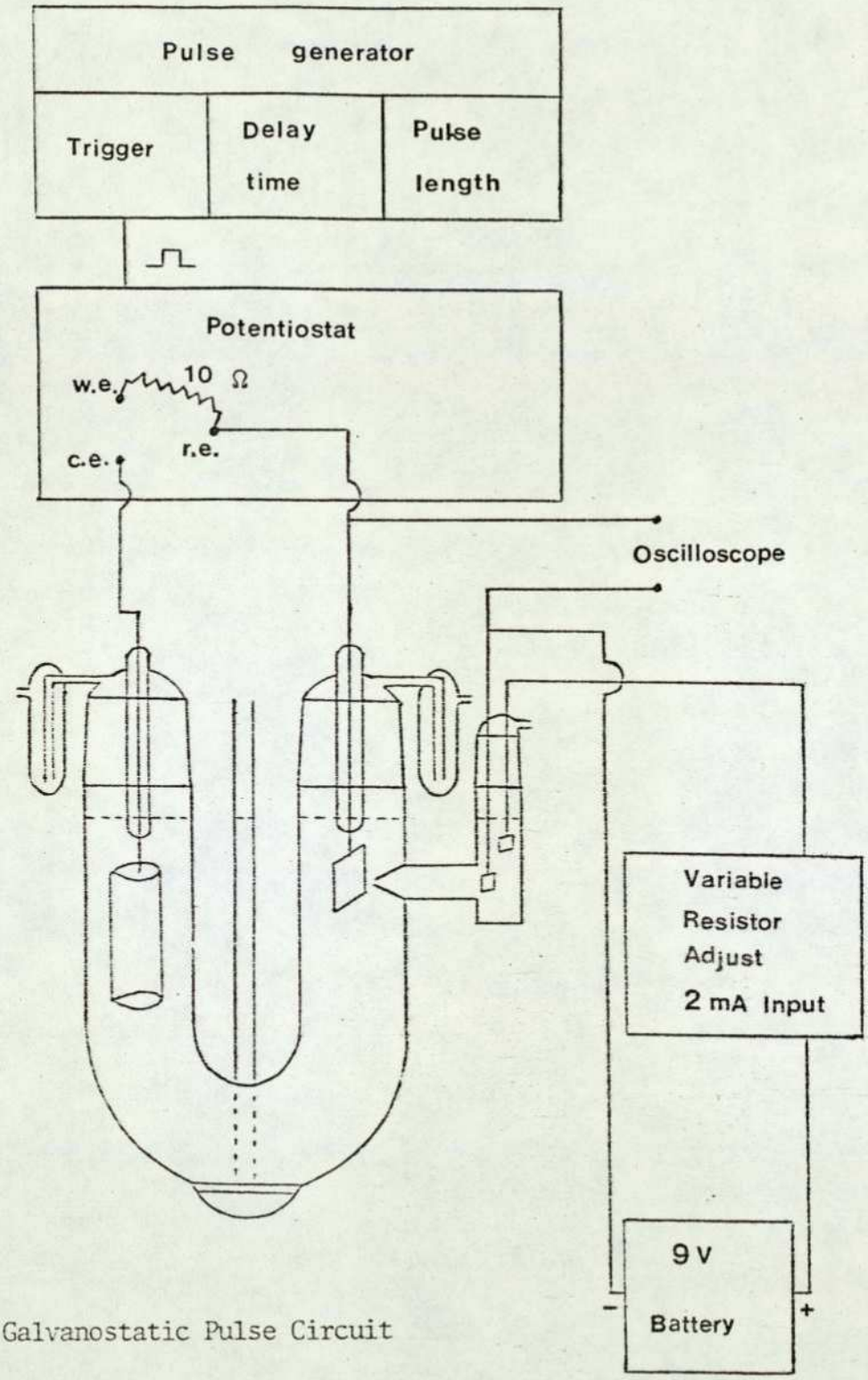

Figure 5.2. Galvanostatic Pulse Circuit

3.3. Double Layer Charging

In order to carry out the potentiostatic pulse experiment for the measurement of current/time transient, it is essential to find out how long it takes to charge the double layer. Usually, the rest potential or the open circuit voltage (O.C.V.) of the tested electrode, in nitrogen saturated electrolyte is a good indication that no electrochemical reaction is occurring at or on the tested electrode. A deviation of maximum ± 100 mV from this O.C.V. value is the working range where the double layer charging time can be determined. This voltage range is termed the non-faradaic region or the double layer region. A more precise method to determine the non-faradaic region is to use the cyclic voltammetry technique[98].

3.3.1. Experimental : Double Layer Charging Technique

The circuit diagram used is essentially the same as the potentiostatic pulse technique. The rest potential of the tested electrode in nitrogen saturated electrolyte is first set on the potentiostat. A potential jump of maximum ± 100 mV of the O.C.V. value is applied to the test electrode and the current/time response is displayed on a storage scope similar to the procedure in the potentiostatic pulse technique mentioned earlier. A typical double layer charging curve is shown in Figure 5.3. The time to charge the double layer is finite, i.e. does not depend on the magnitude of the applied potential and the surface area of the electrode. However, the peak charging current is proportional to the applied

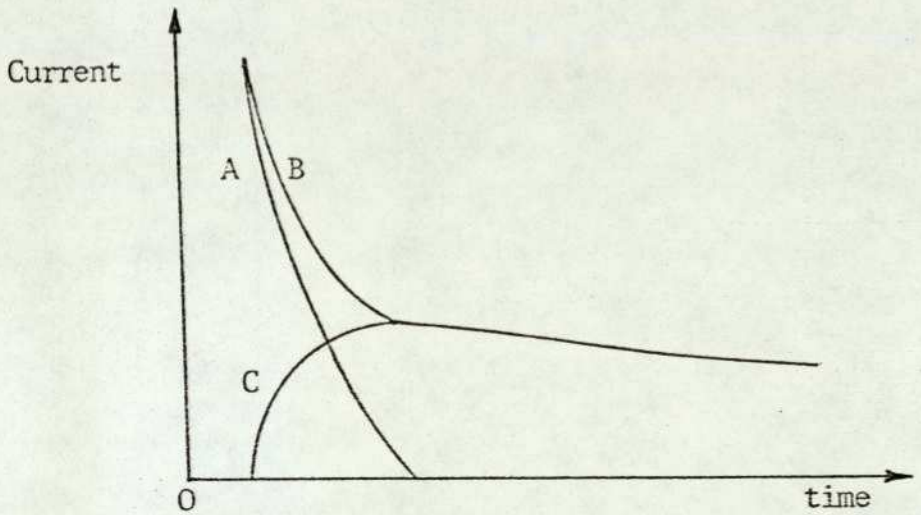

A - charging current

B - total current i.e. charging and faradaic currents

C - faradaic current

Figure 5.3. The effect of double layer charging

potential and the surface area of the electrode. The area of the curve from t = 0 to t = t_c is the double layer charge and can be approximated as 0.5 i_p t_c, where i_p = peak charging current. Since the double layer capacity is proportional to the surface area of the electrode, (i.e. $t_c = C_D R$, where C_D = double layer capacity and R = electrolyte, resistance between the luggin tip and the working electrode), it follows that doubling the surface area should result in a doubling of the double layer charge as observed. The doubling is achieved by increasing i_p, i_t remains constant.

4. ELECTROCATALYST CHARACTERISATION

4.1. X-ray Powder Diffraction

Cobalt-nickel sulphide powder, prepared from Section 2.2., together with the mixed oxides and spinel cobalt-nickel oxide were subjected to x-ray analysis.

X-ray diffraction was also carried out on the cobalt-nickel sulphide powder, which had been removed from a freshly prepared dipping porous electrode.

Two samples of cobalt-nickel sulphide were also examined by x-ray diffraction. They were removed from two different dipping porous electrodes, which had been previously subjected to electrochemical galvanostatic polarisation at constant cathodic currents of 400 mA and 500 mA for 5 hours in 5N KOH at 25°C.

5. RESULTS

5.1. X-ray Analysis

All samples were exposed to molybdenum k_α radiation for

3 hours.

X-ray powder data for the cobalt-nickel sulphide which had been removed from a freshly prepared dipping porous electrode, and cobalt-nickel sulphide prepared from Section 2.2., are listed in Table 5.1. They both show very similar patterns, but the lines become broader and less well defined for the latter sample. Their calculated lattice parameters are 9.39Å and 9.40Å respectively, which are in very close agreement with the literature[99].

Even after being used in the hydrogen evolution reaction at various current densities, all cobalt-nickel sulphide samples remain unchanged structurally. The x-ray data for these cobalt-nickel sulphide samples are listed in Table 5.2. Their calculated lattice parameters are also included.

X-ray data for the spinel cobalt-nickel oxide, which was removed from a freshly prepared dipping porous electrode and spinel cobalt-nickel oxide prepared from Section 2.2. are also tabulated in Table 5.3.

5.2. Half-Cell Electrochemical Testing Results

Potentiodynamic polarisation was performed on both types of porous electrode structures with at least four different catalyst loadings. All experimental procedures are the same as before. (See Chapter 2, Section 4.3 and Chapter 5, Section 3). The double layer charging time for the dipping porous electrode was found to be 300-400 μs which was slightly longer than that of the teflon-bonded porous electrode (i.e. 200-300 μs). Figure 5.4

TABLE 5.1. X-ray Powder Data for Cobalt-Nickel Sulphide Prepared from Thermal Decomposed Cobalt-Nickel Oxide and Cobalt-Nickel Sulphide Removed from a Freshly Prepared Dipping Porous Electrode.

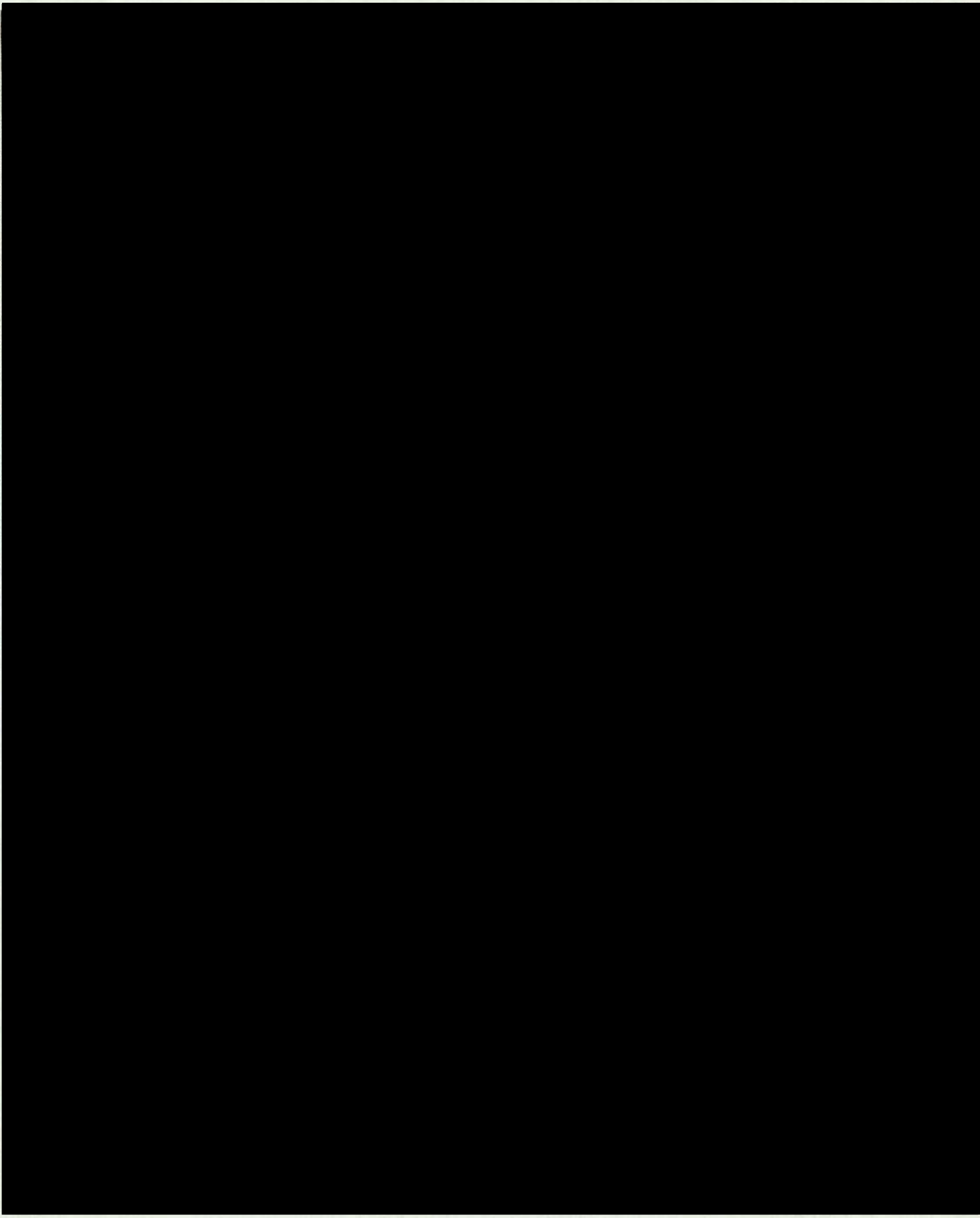

TABLE 5.2. X-ray Powder Data for Cobalt-Nickel Sulphides Removed from Dipping Porous Electrodes, Which Have Been Used in h.e.r. at 400 mA and 500 mA for 5 hrs in 5N KOH at 25°C

[redacted]

TABLE 5.3. X-ray Powder Data for Cobalt-Nickel Oxide Removed from a Freshly Prepared Dipping Porous Electrode and Thermal Decomposed Cobalt-Nickel Oxide

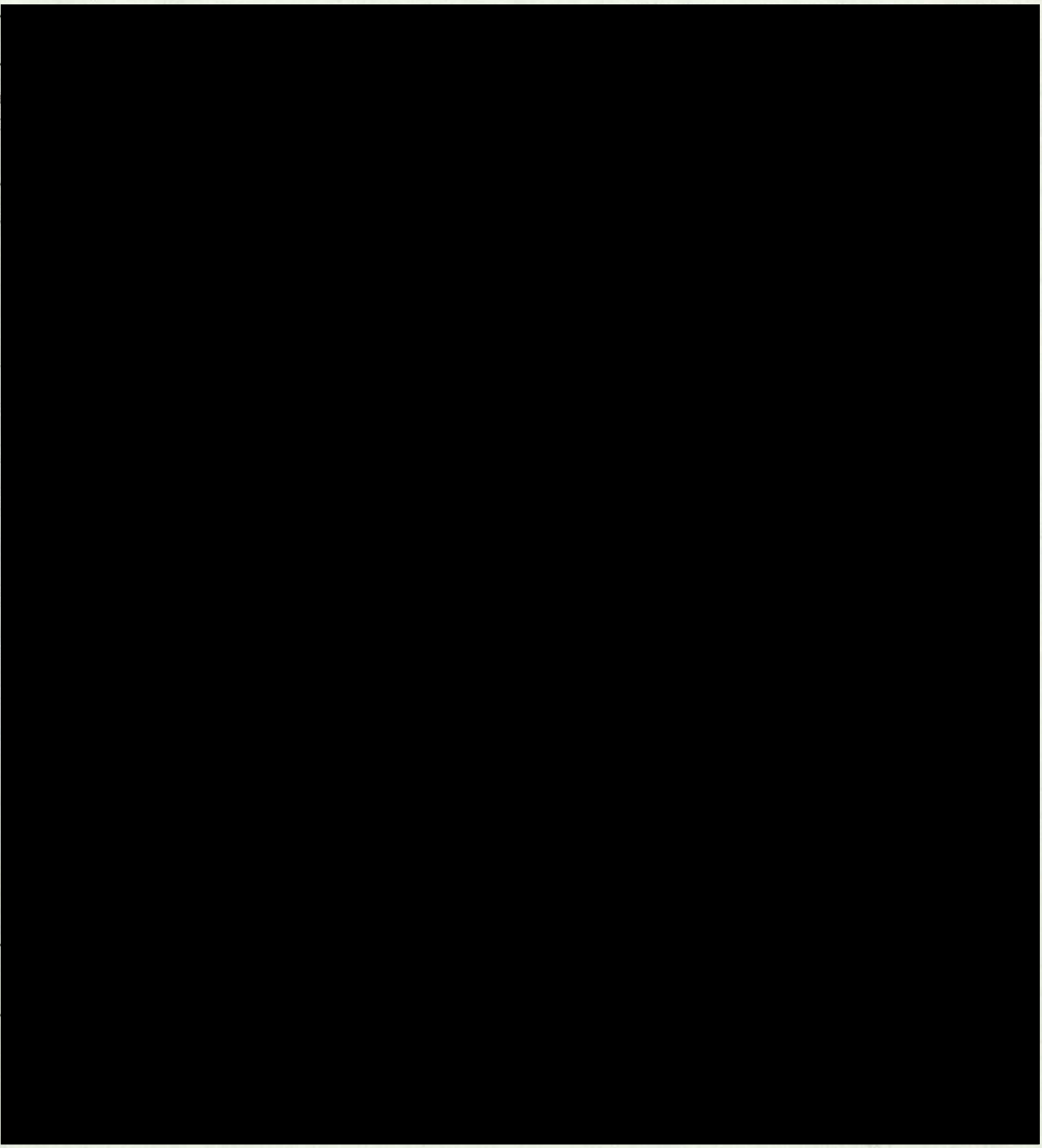

Figure 5.4 Voltage/current curves for cobalt-nickel sulphide in different porous electrode structures at 70°C.

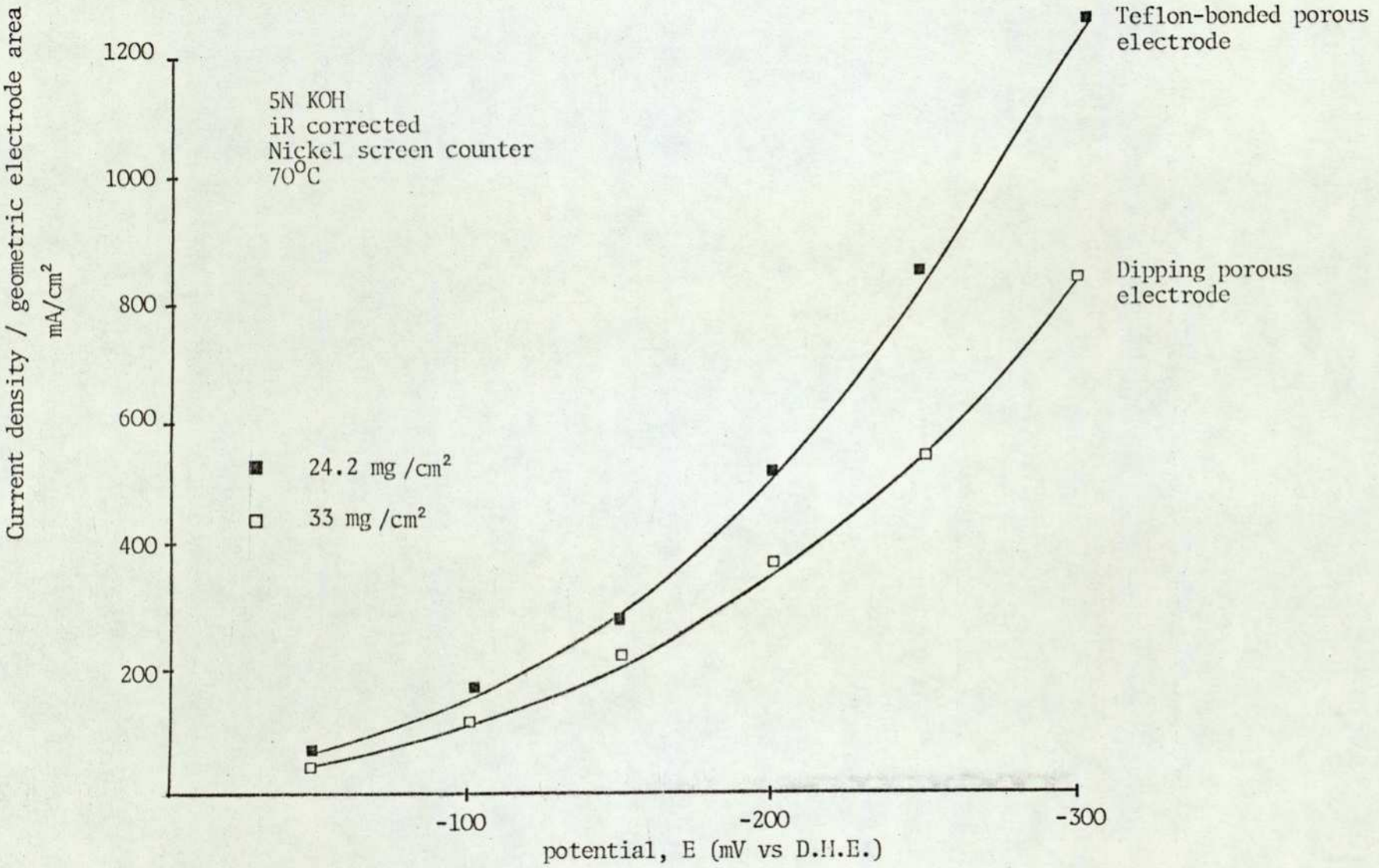

shows the potentiodynamic voltage/current relationship of the dipping porous electrode and the teflon-bonded porous electrode. Figure 5.5 shows the activity vs catalyst loading plot for both types of porous electrode structures. Figure 5.6 shows the activity vs teflon loading plot for the teflon-bonded porous electrode structure.

Potentiodynamic and potentiostatic transient measurements at different temperatures for both types of porous electrode structures are shown in Figures 5.7, 5.8, 5.9, 5.10, and Figure 5.11. The effectiveness factors for both types of porous electrode structures at different potentials and temperatures are listed in Table 5.4.

6. DISCUSSION

Figure 5.4 shows that the steady state performance of the dipping porous electrode is slightly lower than that of the teflon-bonded porous electrode. Since the catalyst loading of these porous electrodes are not the same, it is not a fair comparison.

Figure 5.5 shows the effect of performance on both types of porous electrode structures with respect to catalyst loading at a constant cathodic potential of -300 mV (vs D.H.E.). A volcano-type relationship was found for the dipping porous electrode structures, and the maximum activity achieved at a catalyst loading of approximately 14.3 mg/cm^2. The first part of the curve (i.e. at catalyst loading of 4 mg/cm^2 to 10 mg/cm^2) clearly indicates

Figure 5.5 Performance of cobalt-nickel sulphide in various porous electrode structures as a function of catalyst loading.

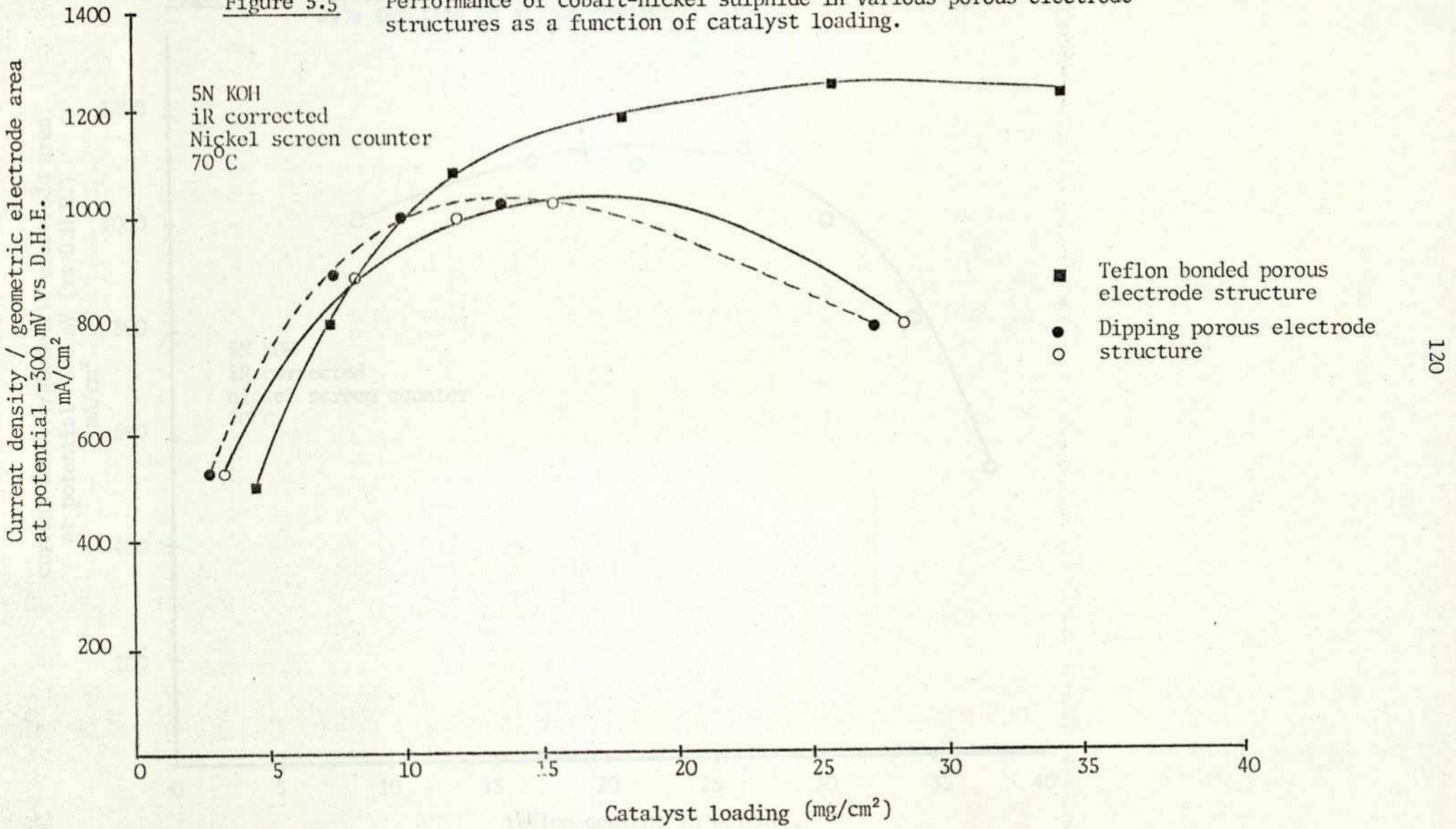

Figure 5.6. Performance of cobalt-nickel sulphide in teflon-bonded porous electrode structure as a function of teflon content.

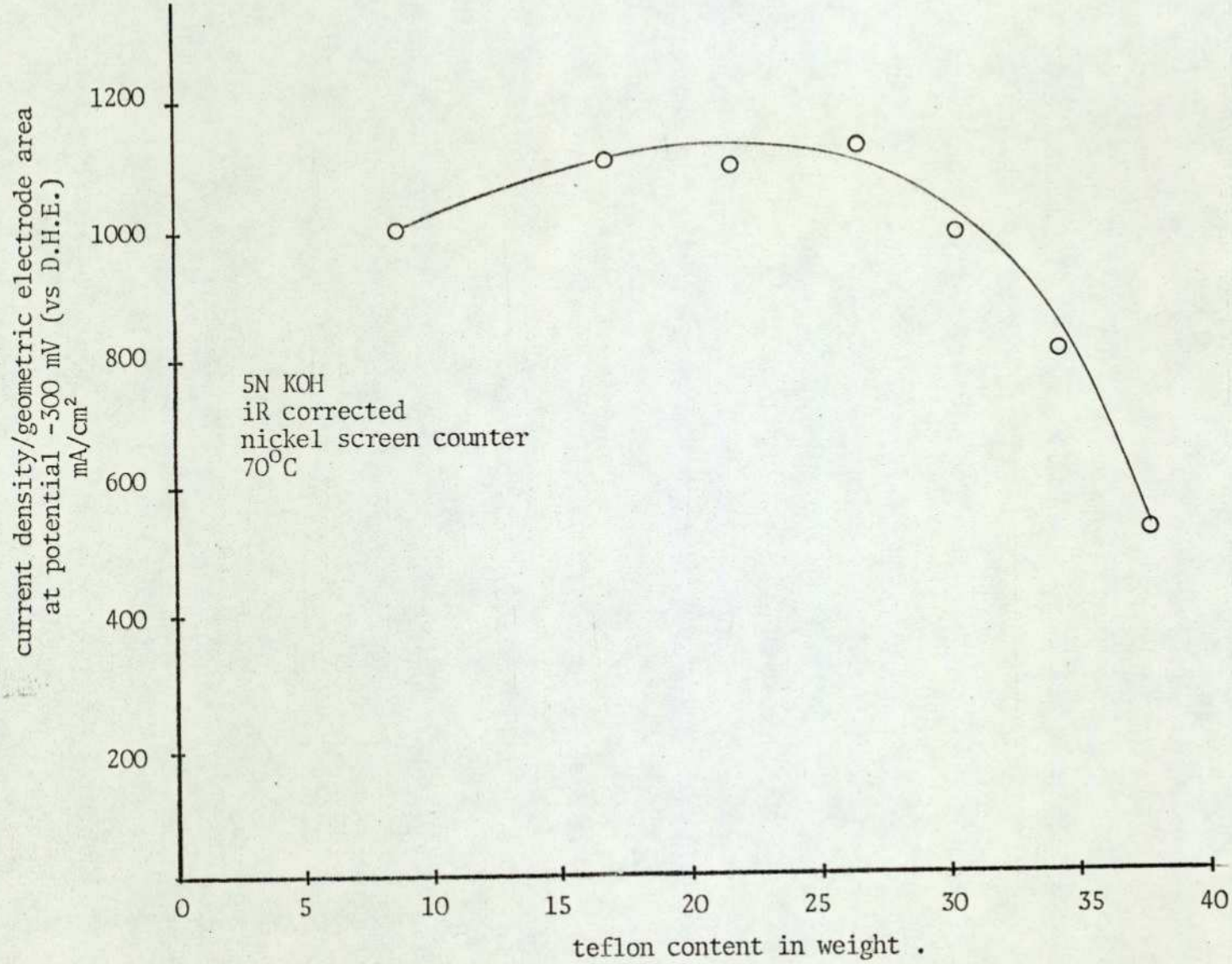

Figure 5.7. Potentiodynamic and potentiostatic transient measurements for cobalt-nickel sulphide in dipping porous electrode structure at 25°C.

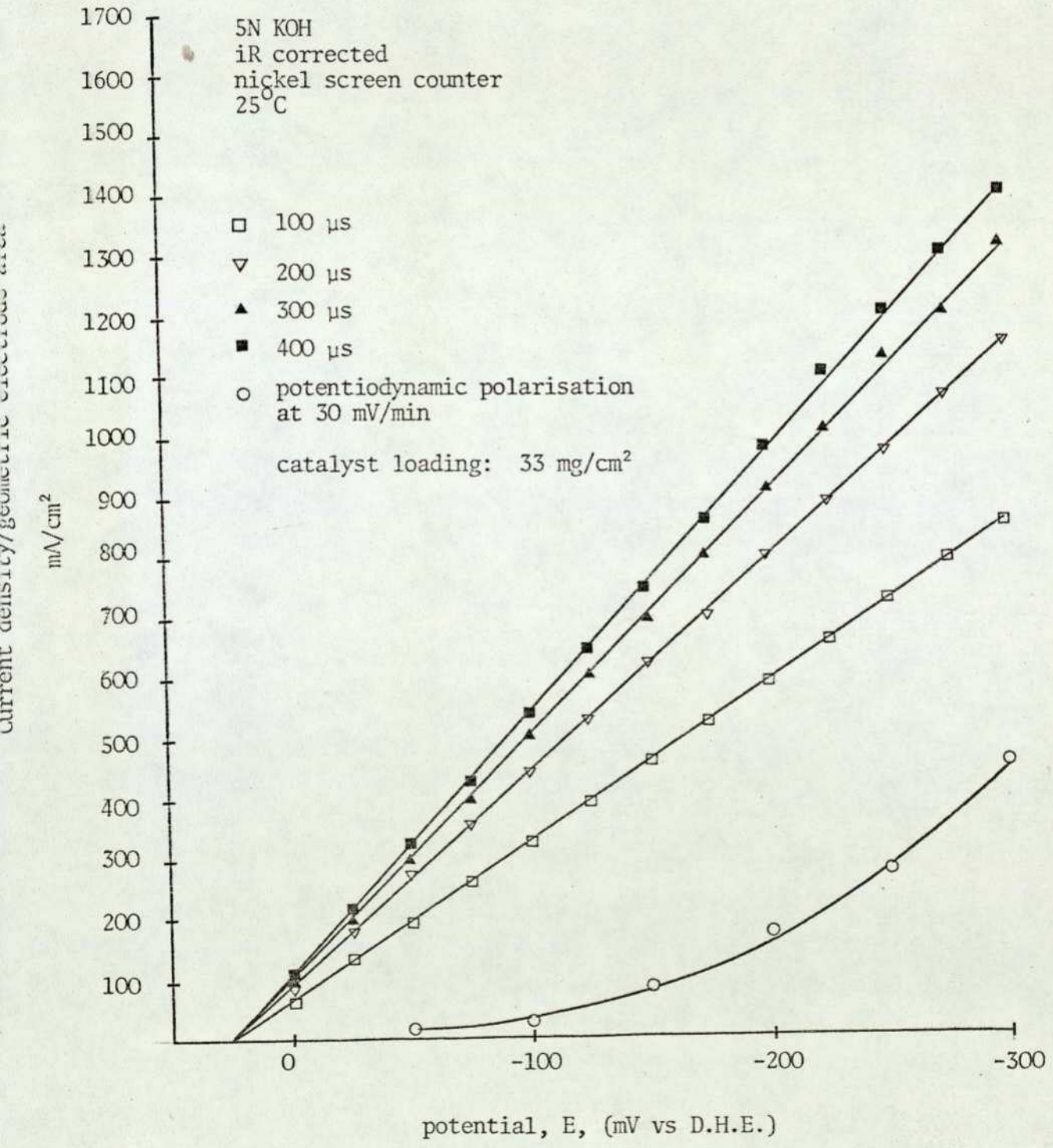

Figure 5.8. Potentiodynamic and potentiostatic transient measurements for cobalt-nickel sulphide in dipping porous electrode structure at 40°C.

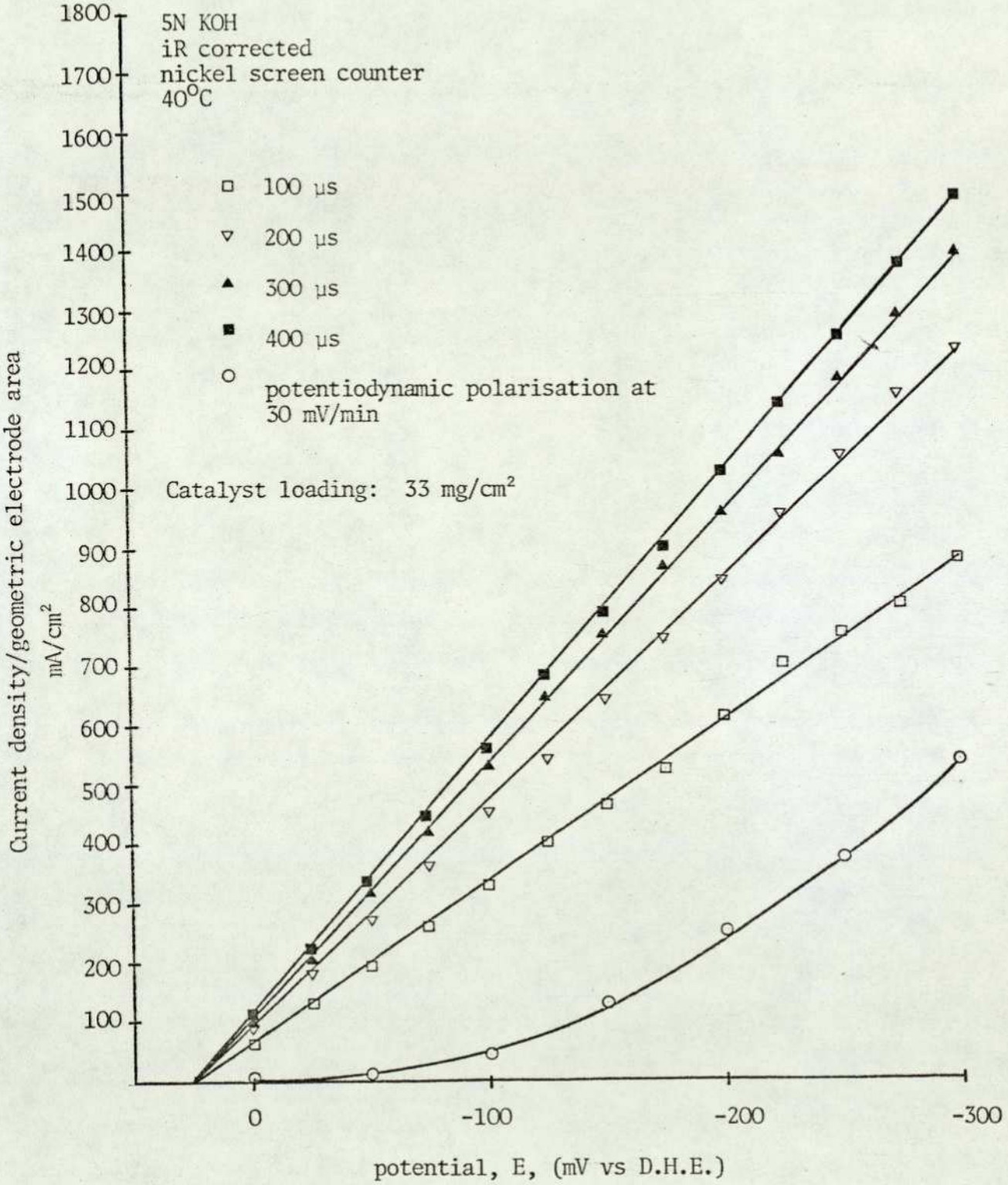

Figure 5.9. Potentiodynamic and potentiostatic transient measurements for cobalt-nickel sulphide in dipping porous electrode structure at 70°C

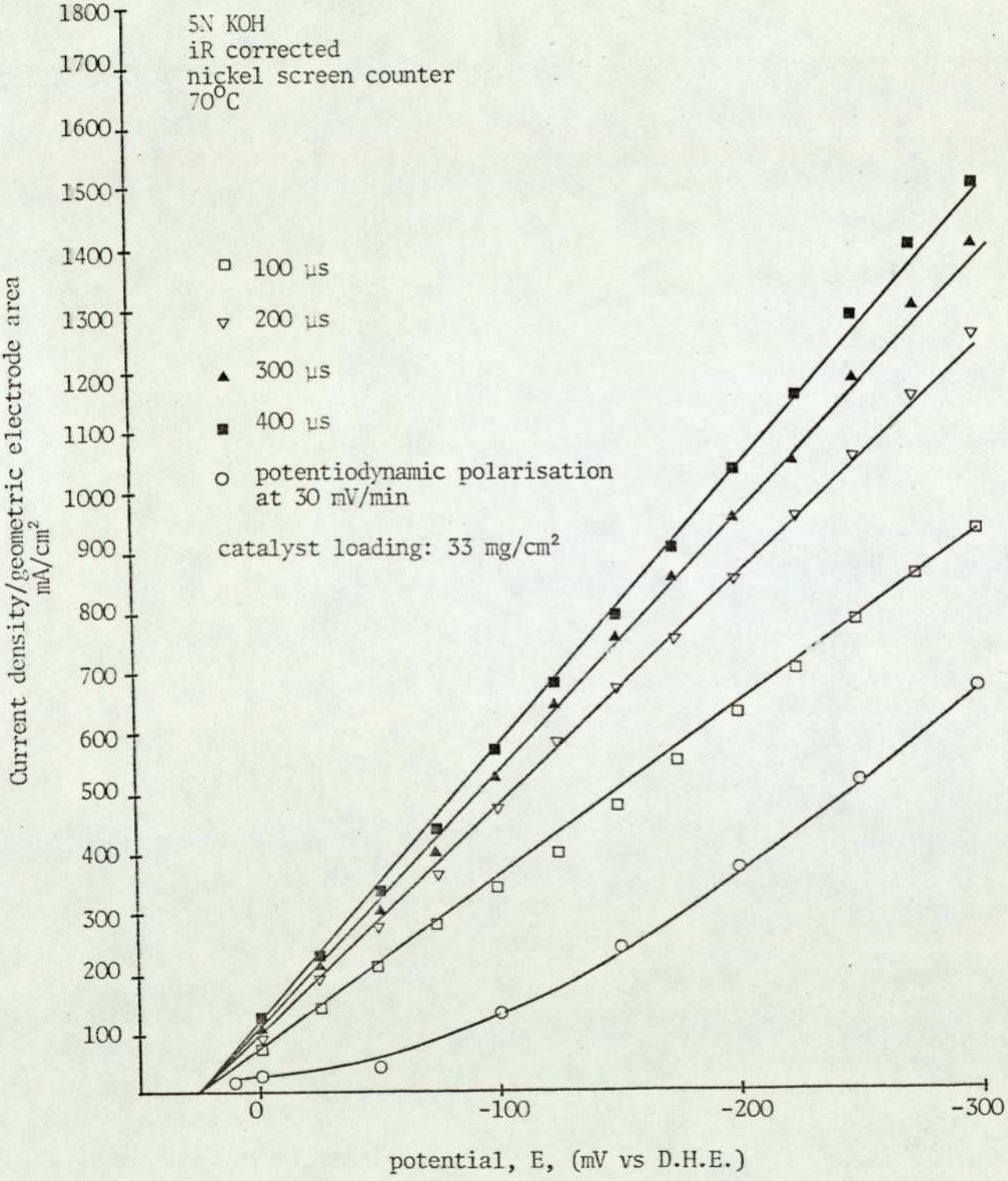

Figure 5.10. Potentiodynamic and potentiostatic transient measurements for cobalt-nickel sulphide in teflon-bonded porous electrode structure at 25°C.

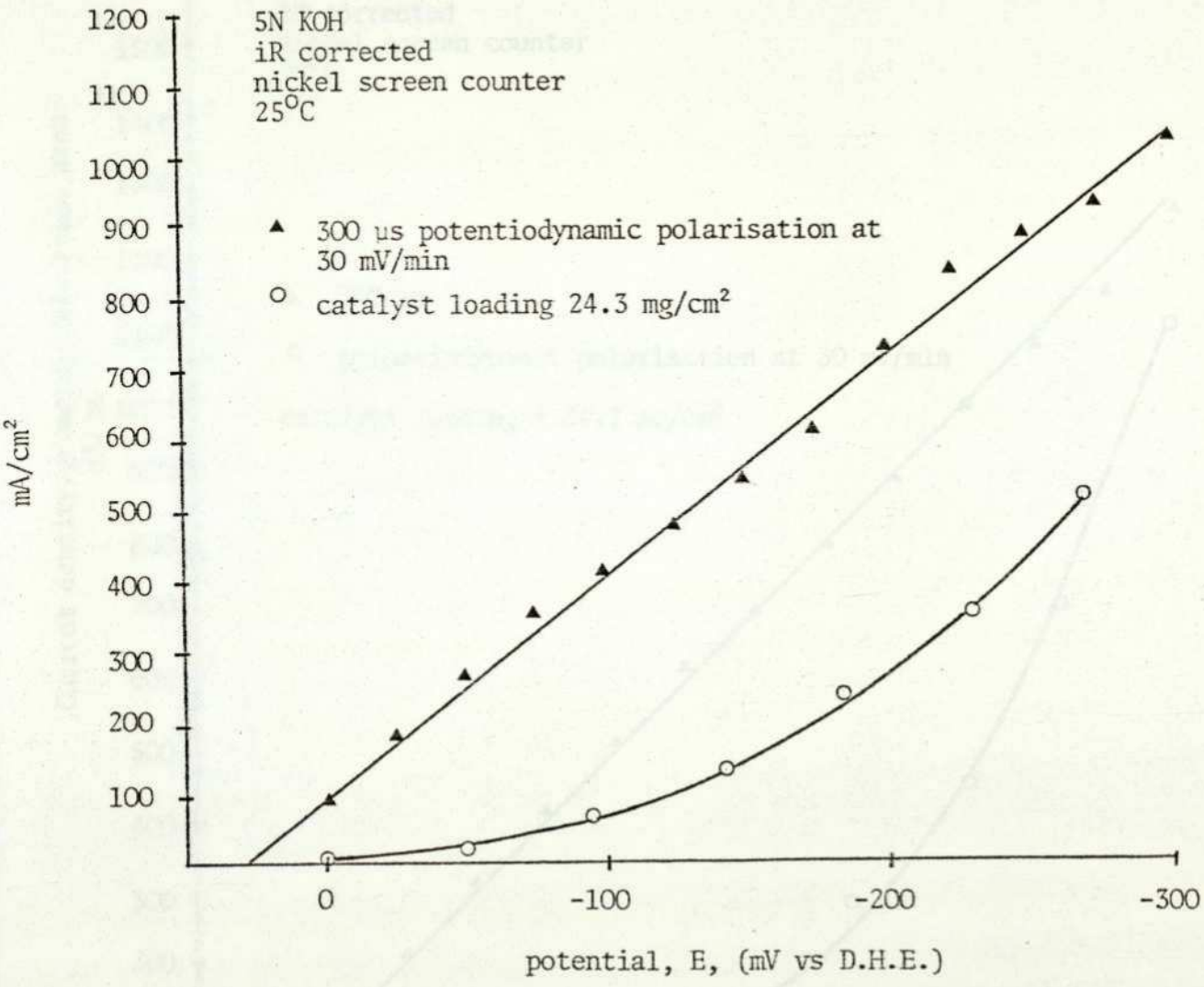

Figure 5.11. Potentiodynamic and potentiostatic transient measurements for cobalt-nickel sulphide in teflon-bonded porous electrode structure at 70°C.

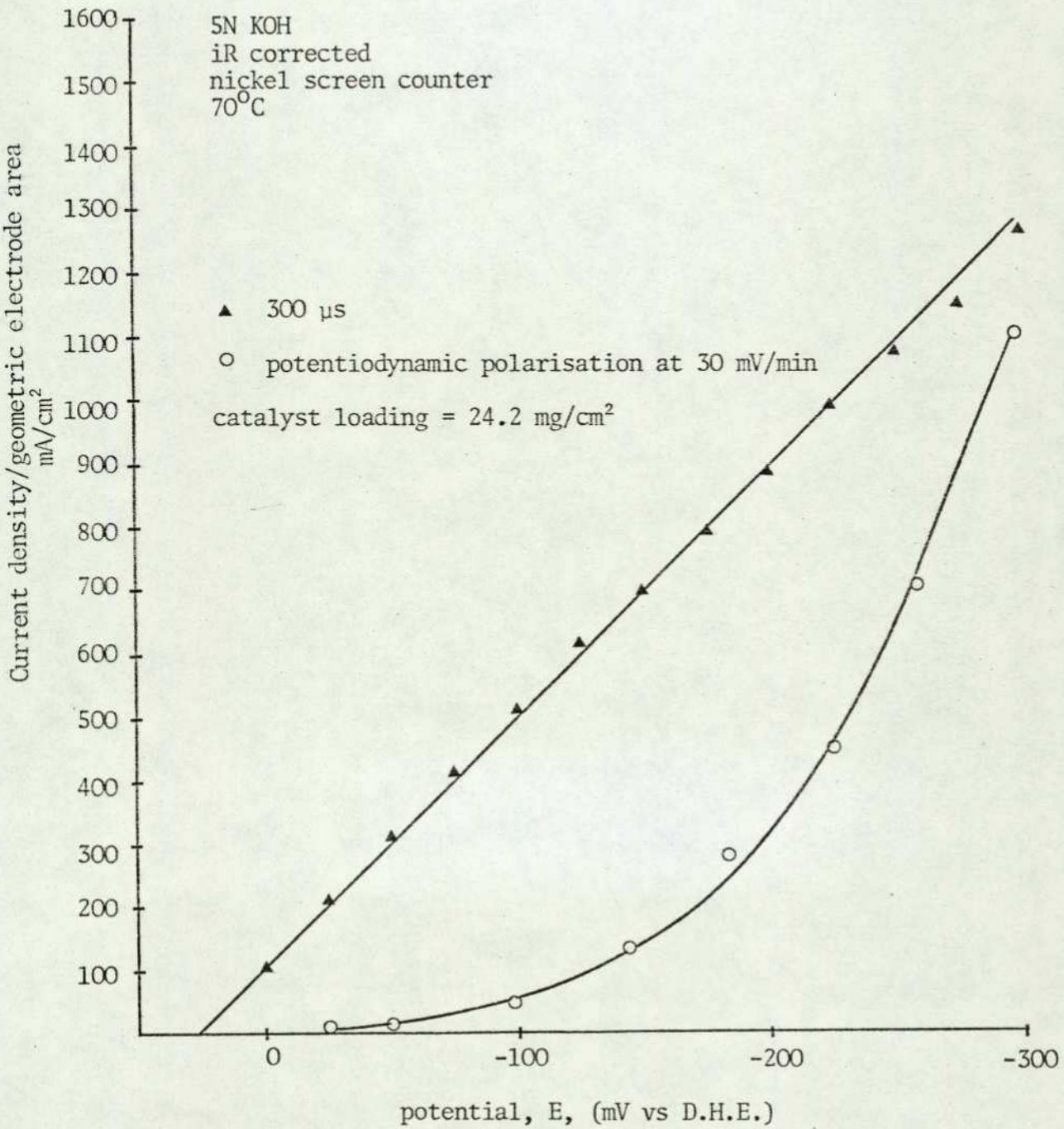

TABLE 5.4. The Effectiveness Factors for Dipping Porous Electrode Structure and Teflon-bonded Porous Electrode Structure at Different Potentials and Temperatures

Temperature (^{o}C)	potential (mV vs D.H.E.)	Current (mA)		Effectiveness factor
		i_{ss}	$i_{300\mu s}$	$i_{ss}/i_{300\ \mu s}$
Porous dipping electrode ($33\ mg/cm^2$)				
25	- 100	30	500	0.06
25	- 200	150	920	0.16
25	- 300	460	1300	0.35
40	- 100	50	540	0.09
40	- 200	250	950	0.26
40	- 300	525	1380	0.38
70	- 100	130	525	0.25
70	- 200	360	970	0.37
70	- 300	780	1400	0.56
Teflon-bonded porous electrode ($24.2\ mg/cm^2$)				
25	- 100	75	400	0.19
25	- 200	275	750	0.37
25	- 300	750	1025	0.73
70	- 100	70	500	0.14
70	- 200	325	900	0.36
70	- 300	1100	1280	0.86

i_{ss} = steady state current

$i_{300\mu s}$ = transient current at 300 μs

that the dipping porous electrode structures are more active than the teflon-bonded porous electrode structure at the same catalyst loading. However, at a catalyst loading of over 14 mg/cm^2, activity decreases drastically for the dipping porous electrode structures.

A completely different trend was found for the teflon-bonded porous electrode structures. Initially, electrocatalytic activity increases sharply with an increased catalyst loading until a catalyst loading of approximately 18 mg/cm^2 is reached. Further increases in the catalyst loading only shows a slight increase in activity. i.e. the rate of increase in electrocatalytic activity is minimal.

The dotted lines in Figure 5.5 show the effect of the performance of the dipping porous electrode structures at a constant cathodic potential of -300 mV (vs D.H.E.) w.r.t. the actual catalyst loading. For all the tested dipping porous electrodes, it was observed that the catalyst powders fall off from the porous electrodes during the initial stage of the polarisation process. This is most serious, especially at a higher current density. However, this phenomena dies down after the hydrogen evolution reaction proceeds for a certain period of time (i.e. no more catalyst powders fall off.) The dipping porous electrodes are vacuum dried and then re-weighed to give the actual catalyst loading.

When comparing activity between two types of porous electrodes, it is quite clear that the teflon-bonded porous electrode structures are more active than the dipping porous

electrode structures, especially at a high catalyst loading. Further evidence shows that the binding mechanism of the catalyst powders onto the catalyst supports in the dipping porous electrode structures are much weaker than compared to the teflon-bonded electrode structures, which shows that the catalyst powders are firmly bound onto the catalyst supports. (i.e. no catalyst powders fall off even at a current density of as high as $1.2A/cm^2$).

It is further observed that during the h.e.r., a very fine mist of hydrogen bubbles evolve from the dipping porous electrodes, while the hydrogen bubbles were much larger in the case of the teflon-bonded porous electrodes. These large hydrogen bubbles grow from small hydrogen bubbles, which are attached to the electrode surface. At this stage, it was not possible to measure the dimensions of the large and small hydrogen bubbles. However, the relatively long time the hydrogen bubbles sit on the electrode surface may be due to surface tension resulting from the hydrophobicity of the teflon binder. Therefore, a large proportion of the electrode surface cannot be used most of the time; i.e. as it is covered with hydrogen bubbles.

Figure 5.6 shows the effect of teflon-content in the teflon-bonded porous electrode structures with respect to electrocatalytic activity at a constant cathodic potential of -300 mV (vs D.H.E.). At a very low teflon loading (i.e. 10% by weight), catalyst powders fall off from the porous electrodes during the h.e.r., similar to the observation made with all dipping porous electrodes. The maximum electrocatalytic activity was achieved with a teflon loading of 28% by weight. Further increases in the

teflon loading would ubstantially reduce the electrocatalytic activity which is attributed to the formation of very large hydrogen bubbles. At a high teflon loading, a freshly prepared teflon-bonded porous electrode appears whitish in colour. During the h.e.r., small hydrogen bubbles appear all over the surface of the porous electrode, these join and grow bigger to form a single hydrogen bubble covering the entire surface of the porous electrode. This hydrogen bubble finally detaches from the electrode surface. This suggests that teflon as an electrocatalyst binder can be harmful as well as beneficial to the porous electrode structure for the h.e.r. The inclusion of teflon in the porous electrode structure can provide more dry gas 'channels' for the gas to escape more easily and also function as a binder to give a better mechanical strength than the dipping porous electrode structure. Excessive presence of teflon would damage performance drastically due to the loss of electrode surface in the formation of hydrogen bubbles. From Figure 5.4, in the low potential or overpotential region, voltage-current plots for both types of porous electrodes were linear showing that very little of the surface area of the electrodes were not in electrolyte contact. It is probable that in this potential region, the hydrogen formed inside the pores escapes by dissolving in the electrolyte under pressure and then diffusing away through the electrolyte. Therefore, hydrogen bubbles tend to build up within the electrodes and effectively block off a lot of active surface area during this process. As the current increases, the hydrogen bubbles form within the electrodes, attaining high pressures before they escape. These

bubbles can break away from the electrode surface more easily and thus explose more surface area to be utilised again. Since no limiting currents were observed in both types of the porous electrode structures, it is reasonable to suggest that mass transfer is not the rate determining factor. However, if the electrode is too hydrophobic, especially on the electrode surface, performance would definitely be impaired owing to the loss of surface area in the formation of hydrogen bubbles. Nevertheless, for the hydrogen evolution reaction and most other gas evolution reactions, the constant utilisation of 100% of the active surface area is most improbable. Because at any instance, there would be some hydrogen bubbles sitting on the electrode surface, and therefore there would always be some loss of surface area. However, if the residence time of these hydrogen bubbles is very short, the lost surface area can be recovered and used again. The effect of high teflon-loading in the teflon-bonded electrode structure with respect to the potentiostatic activity in Figure 5.6, can be most effectively explained by this argument.

The potentiostatic current/time transients for both types of porous electrodes are shown in Figure 5.7, to Figure 5.11. The effectiveness factors ($i_{s.s.}/i_{300\mu s}$ at constant potential or overpotential) are tabulated in Table 5.5. The effectiveness factor for both types of porous electrode structures at different temperatures have similar patterns, in that they increase with increase in potential or overvoltage. At a high overpotential, the effectiveness factor is about 0.7-0.8 for the teflon-bonded porous electrode and only about 0.5-0.6 for the dipping porous electrode.

A teflon-bonded porous electrode with a high teflon loading at the same potential has the effectiveness factor of about 0.4. Furthermore, effectiveness factors are temperature dependent.

At a low overpotential, the effectiveness factors are much smaller and approximately constant over the potential range in which steady-state current-voltage curves are linear. The difference of effectiveness factors at high and low overpotential being entirely due to the degree of blocking of the porous electrode structures by hydrogen bubbles.

Finally, x-ray analysis and transmission electron microscope probe have indicated that the bulk composition of the cobalt-nickel sulphide powder samples are unchanged even after being used in h.e.r. The results also show that the spinel structure of the cobalt-nickel sulphide sample are also unchanged throughout.

CHAPTER SIX

KINETIC PARAMETERS FOR HYDROGEN EVOLUTION REACTION OF COBALT-NICKEL SULPHIDE IN THE DIPPING POROUS ELECTRODE STRUCTURE

1. INTRODUCTION

Chapter 5 showed that the electrocatalytic activity of cobalt-nickel sulphide in the teflon-bonded porous electrode structure is more stable and far superior than that of the dipping porous electrode structure, which is mainly due to higher utilisation of available surface area and stronger mechanical strength of the electrode structure. In order to elucidate the mechanism of h.e.r. on cobalt-nickel sulphide electrocatalyst, the present study is to obtain fundamental kinetic parameters for the h.e.r. on cobalt-nickel sulphide in potassium hydroxide solutions at temperatures of 25°C, 40°C and 70°C.

2. POSSIBLE MECHANISMS

It is well known[100,101], that the source of protons in the h.e.r. in acidic solution is the hydrogen ions, whereas in alkaline solutions it is predominantely the water molecules. Three main mechanisms are considered:

I. The Volmer-Heyrovsky mechanism (Charge transfer-electrochemical desorption path)

$$(a) \quad H_2O + e \longrightarrow H_{ad} + OH^- \qquad \text{Volmer}$$

where a hydrogen atom adsorbed on the electrode surface (H_{ad}) and a hydroxide ion is formed from a water molecule.

$$(b) \quad H_2O + H_{ad} + e \longrightarrow H_2 + OH^- \qquad \text{Heyrovsky}$$

where a molecule of water reacts with a hydrogen atom previously adsorbed on the electrode surface to form a molecule of hydrogen and a hydroxide ion. It can be seen immediately by comparison of this reaction with the corresponding process in acidic solutions, in which the solvated hydrogen atom is discharged close to the adsorbed hydrogen atoms, that the coverage of the surface with atomic hydrogen is less critical for alkaline solutions, owing to the great abundance of water molecules available close to the electrode surface.

II. The Volmer-Tafel Mechanism (Charge transfer-recombination path)

(a) $H_2O + e \longrightarrow H_{ad} + OH^-$ Volmer

(b) $H_{ad} + H_{ad} \longrightarrow H_2$ Tafel

After the charge transfer reaction, adsorbed hydrogen atoms diffuse across the surface and meet each other so that they may combine to form hydrogen molecules.

III. The Horiuti-Okamoto Mechanism

(c) $2H_2O + e \longrightarrow H_2^+ + 2OH^-$

(d) $H_2^+ + e \longrightarrow H_2$

According to Horiuti and Okamoto [102], in some cases (e.g. on mercury and platinum electrodes) the primary product of electron transfer may be an H_2^+ ion, which is followed by the discharge of hydrogen molecule.

Any one of the steps in the three mechanisms can be rate determining. The available body of experimental information indicates that none of the alternatives is of universal validity. The reaction mechanism and the rate determining step changes depending on the nature of the material, the condition of the surface and various other factors. Besides the above possible mechanism, the case with mercury, the reaction mechanism involves the charge transfer reaction, which is the deposition of the alkali metal ion on the mercury to form an amalgam, which is followed by its irreversible reaction with water molecules to produce hydrogen. The reactions are represented as follows:

$$Na^+ + e + xHg \longrightarrow NaHg_x$$

$$2NaHg_x + 2H_2O \longrightarrow 2NaOH + 2HgH + (2x-2)Hg$$

$$2HgH \longrightarrow 2Hg + H_2$$

In general, other possible steps that might follow are:

(e) $H_{ad} \longrightarrow H_{ab}$ diffusion into metal or catalyst

(f) $H_{2\,ad} \longrightarrow H_{2\,sol}$ desorption

(g) $H_{2\,ad} \longrightarrow H_{2\,g}$ gassing

(h) $H_{2\,sol} \longrightarrow H_{2\,g}$ gassing

(i) $OH_{ad} + e \longrightarrow OH^-$ reduction of the surface

3. BASIC ELECTRODE KINETICS

For simplicity, the electrode reaction is represented

as:

$$O + e \longrightarrow R$$

where O and R represent the oxidised and reduced species respectively. The forward current density (cathodic current) and the reverse current density (anodic current) may be expressed by:

$$\vec{i} = F\vec{K}C_O\exp^{(-\alpha VF/RT)}$$

$$\overleftarrow{i} = F\overleftarrow{K}C_R\exp^{((1-\alpha)VF/RT)}$$

where $\vec{K}$ and $\overleftarrow{K}$ are the rate constant of the forward and reverse reaction, α is the transfer coefficient, V is the electrode potential, C_O and C_R are the concentration of the oxidised and reduced species. The net forward current density may be expressed as:

$$i = \vec{i} - \overleftarrow{i} = F(\vec{K}C_O\exp^{(-\alpha VF/RT)} - \overleftarrow{K}C_R\exp^{((1-\alpha)VF/RT)}) \qquad (1)$$

The overall rate is zero at equilibrium potential, i.e. $\vec{i} = \overleftarrow{i} = i_o$

$$i_o = F\vec{K}C_O\exp^{(-\alpha V_r F/RT)}$$

$$= F\overleftarrow{K}C_R\exp^{((1-\alpha)V_r F/RT)} \qquad (2)$$

where V_r is the equilibrium potential, using the equations (1) and (2), this gives:

$$i = i_o(\exp^{(-\alpha\eta F/RT)} - \exp^{((1-\alpha)\eta F/RT)} \qquad (3)$$

where η is the overpotential and is equal to the difference of $(V - V_r)$.

At highly negative overpotential (cathodic), the second exponential term on the right hand side of equation (3) is negligible

compared with the first, and the equation reduces to:

$$\eta = \frac{RT}{\alpha F} \log i_o - \frac{RT}{\alpha F} \log i$$

$$= a + b \log i$$

This equation is referred to as the Tafel equation, where $a = \frac{RT}{\alpha F} \log i_o$ and $b = -\frac{RT}{\alpha F}$ (Tafel slope).

At low negative overpotential ($|\eta| < RT/F$), equation reduces to:

$$= \frac{RTi}{Fi_o}$$

A knowledge of the Tafel parameters, exchange current density, stoichiometric numbers and variation of coverage of hydrogen with potential, is very useful in mechanism determinations. In general, the elucidation of the reaction mechanism can be performed mainly by studying the following correlations:

(1) The relationship between overvoltage and current, determination and interpretation of Tafel constant b.

(2) Determination of the concentration dependence of current density and overvoltage i.e. determination of $(\frac{\partial \eta}{\partial \ln(H^+)})_i$ and $(\frac{\partial \ln i}{\partial \ln(H^+)})_\eta$ as well as the related $(\frac{\partial \ln i}{\partial \ln(H^+)})_\psi$ or $(\frac{\partial \ln i}{\partial \ln(H^+)})_{\eta\psi}$, partial derivatives, the latter two permitting conclusions about the reaction order.

(3) Study of the electrode area covered by adsorbed species, measurement of adsorption capacity.

(4) Determination of the apparent activation energy by polarisation at constant current density, or from the temperature dependence of the current density at constant potential.

(5) Study of isotope effects, i.e. that of the variations of (H) : (P) and (H) : (T) ratio between solution and gas.

(6) The effect of added foreign substances.

The theoretical forecast mechanism indicating criteria for the discharge recombination and discharge-electrochemical desorption paths are shown in Table 6.1. The detailed methods of deriving these predicted kinetic parameters have been treated in the literature.

4. HALF-CELL ELECTROCHEMICAL TESTING

Cobalt-nickel sulphide in dipping porous electrode structures are prepared as before (see Chapter 5, Section 2.1.), and are used exclusively for mechanism determination. Due to the lack of time and irreversible nature of the cobalt-nickel sulphide electrocatalyst (i.e. no reversible hydrogen electrode potential is established when the electrode is equilibriated in hydrogen saturated electrolyte). The galvanostatic stripping[103] and double charging method[104] cannot be used for the measurement of hydrogen coverage on the electrode. Moreover, also it is not desirable to obtain the absolute value of the exchange current density from the current potential line at low overpotential

TABLE 6.1. Theoretical Forecast Kinetic Parameters for the most Probable Mechanisms of the Hydrogen Evolution Reaction

	CONDITION $\Theta \to 0$				CONDITION $\Theta \to 1$					
	$\frac{\partial \eta}{\partial \ln i}$	$\frac{\partial \eta}{\partial \ln a_{H_3O^+}}$	$\frac{\partial \eta}{\partial \ln p_{i_2}}$	$\frac{\partial \eta}{\partial \ln \Theta}$	$\frac{\partial \eta}{\partial \ln i}$	$\frac{\partial \eta}{\partial \ln a_{H_3O^+}}$	$\frac{\partial \eta}{\partial \ln p_{H_2}}$	$\frac{\partial \eta}{\partial \ln \Theta}$	ν	
Slow discharge-fast recombination	$-\frac{RT}{\beta F}$	$\frac{RT}{F}$	$\frac{RT}{2F}$	0	$-\frac{RT}{\beta F}$	$\frac{RT}{F}$	$-\frac{RT}{2F}\frac{(1-\beta)}{\beta}$	0	2	
Fast discharge-slow recombination	$-\frac{RT}{2F}$	0	$\frac{RT}{2F}$	$-\frac{RT}{F}$	∞	0		0	1	
Coupled discharge-recombination	$-\frac{RT}{\beta F}$	$\frac{RT}{F}$	$\frac{RT}{2F}$	$\frac{2RT}{F}$	$-\frac{RT}{\beta F}$	$\frac{RT}{F}$	$-\frac{RT}{2F}\frac{(1-\beta)}{\beta}$	$-\infty$		
Slow discharge-fast electrochemical desorption	$-\frac{RT}{\beta F}$	$\frac{RT}{F}$	$\frac{RT}{2F}$	$+\frac{RT}{F}$	$-\frac{RT}{(1+\beta)F}$	$\frac{(1-\beta)RT}{(1+\beta)F}$	$-\frac{RT}{2F}\frac{(1-\beta)}{(1+\beta)}$	0	1	
Fast discharge-slow electrochemical desorption	$-\frac{RT}{(1+\beta)F}$	$\frac{(1-\beta)RT}{(1+\beta)F}$	$\frac{RT}{2F}$	$-\frac{RT}{F}$	$-\frac{RT}{\beta F}$	$\frac{RT}{F}$	$\frac{RT}{2F}$	0	1	
Coupled discharge-electrochemical desorption	$-\frac{RT}{\beta F}$	$\frac{RT}{F}$	$\frac{RT}{2F}$	0	$-\frac{RT}{\beta F}$	$\frac{RT}{F}$	$\frac{RT}{2F}$	0		
Slow molecular hydrogen ion discharge	$-\frac{RT}{(1+\beta)F}$	$\frac{(1-\beta)RT}{(1+\beta)F}$	$\frac{RT}{2F}$	$-\frac{RT}{F}$	$-\frac{RT}{\beta F}$	$\frac{RT}{F}$	$\frac{RT}{2F}$	0	1	
Slow molecular hydrogen diffusion	$-\frac{RT}{2F}$	0		$-\frac{RT}{F}$	∞	0		0	1	

by using the equation $i = i_o(\frac{nF\eta}{vRT})$, where v is the stoichiometric number and n is the total number of electrons transferred in the overall reaction. This is partly due to difficulty in determining the surface area of the cobalt-nickel sulphide catalyst. The usual B.E.T. method for the determination of surface area for powder sample is not applicable in this case, since cobalt-nickel sulphide decomposes during the initial degassing process at 300°C. It is found that red mercuric sulphide is formed at the mercury meniscus of the manometer arm. In addition, the active area in porous electrodes is more difficult to determine and usually only a small fraction of the total B.E.T. surface area covered. Therefore, for determination of Tafel parameters, potentiodynamic polarisation and potentiostatic current transient methods are used, taking measurements in the low overpotential region ($|\eta| < RT/F$) in order to avoid or minimise contribution due to activation, ohmic and concentration polarisation at higher overpotentials.

4.1. Experimental

Immersed electrodes are cathodically polarised at constant potential of -300 mV vs D.H.E. for twenty minutes before potentiodynamic measurements are taken in the direction of high current to low current. A scan rate of 30 mV / minute is used (near steady state). The tested half-cell is continuously purged with nitrogen when the electrodes are at open circuit. Potentiostatic current transients are also taken immediately after each potentiodynamic run at each temperature. The correction of iR drop is finally made using the interrupter technique. The electrodes are periodically

tested for the duration of a week before changing the electrolyte to KOH solutions of different pH.

5. RESULTS

Figure 6.1 shows the plots of log i vs potential in 5N potassium hydroxide solution at 25°C. In the same graph, potentiostatic current transients are also plotted. Good reproducibility is observed when comparing the first and second day potentiodynamic results. This is most important as this implies that the change in afel slope is minimal which in turn suggests that the change of surface area of the electrode during the hydrogen evolution reaction is negligible.

Figures 6.2 and 6.3 show similar plots of log i vs potential, but at temperatures of 40°C and 70°C respectively. Since distinct dual tafel slopes are observed, the heat of activation at high and low overpotentials is obtained from a plot of log i vs the reciprocal of the absolute temperature. The results are shown in Figure 6.4. The numerical value of the heat of activation may yield information on reaction mechanism (e.g. the heat of activation is expected to be high for the slow discharge mechanism, which involves breaking of a strong O-H^+ bond and formation of a relatively weak M-H bond and low for the slow recombination mechanism, which involves breaking of two relatively weak M-H bonds to form a strong H-H bond).

Similarly, Figures 6.5, 6.6 and 6.7 show the plots of log i vs potential in potassium hydroxide solutions of pH = 14.32, 14.0, 13.06 at temperatures of 25°C, 40°C and 70°C respectively.

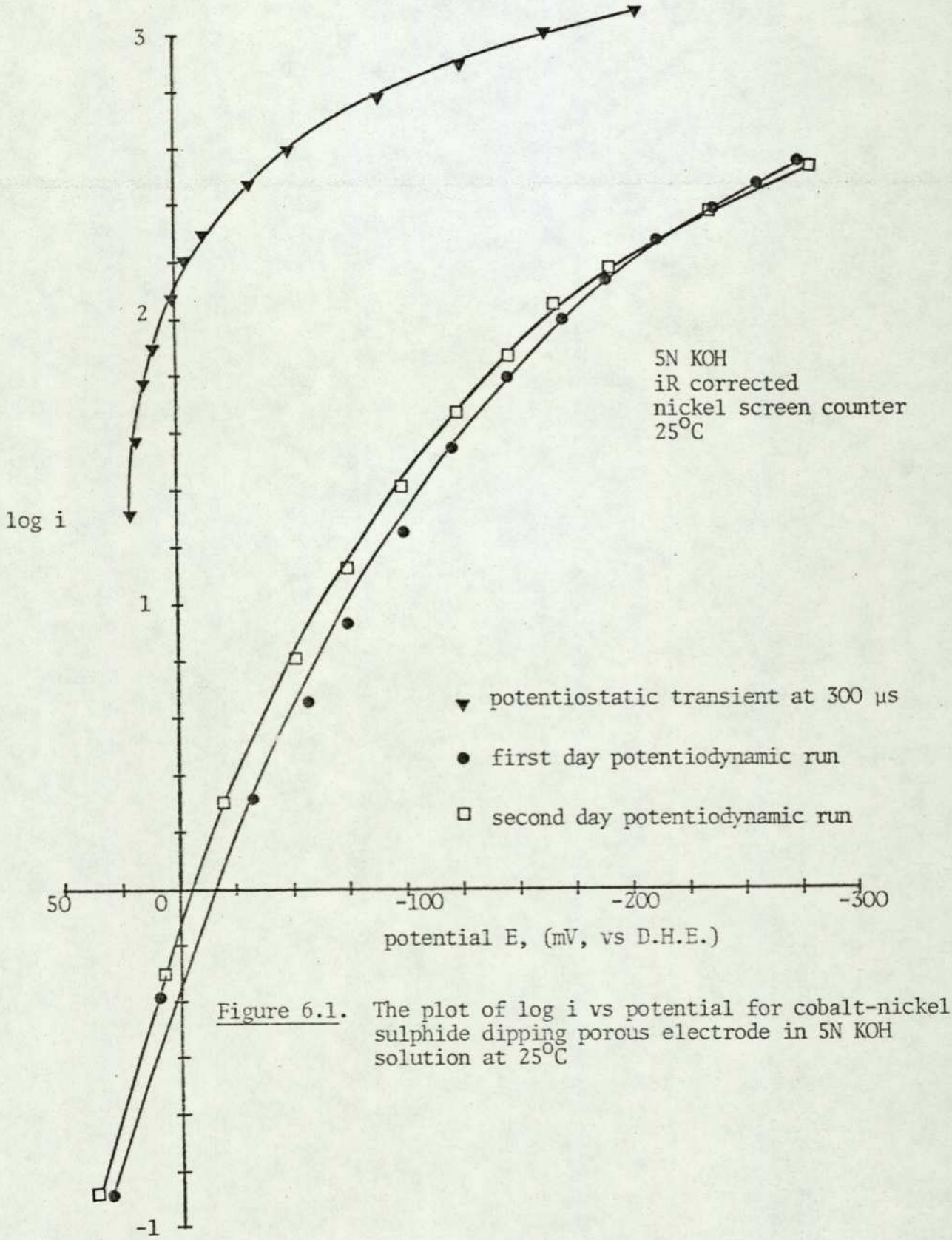

Figure 6.1. The plot of log i vs potential for cobalt-nickel sulphide dipping porous electrode in 5N KOH solution at 25°C

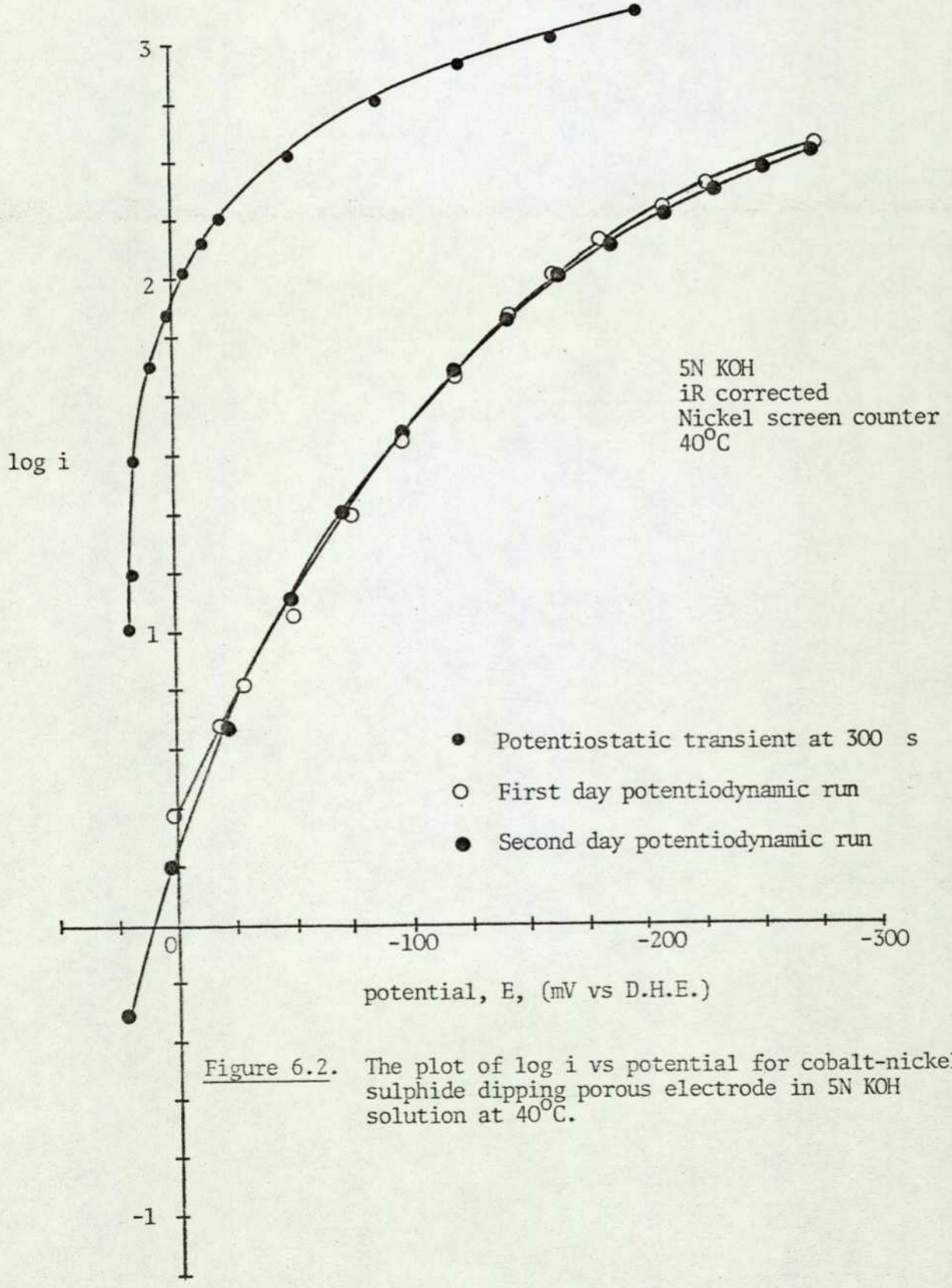

Figure 6.2. The plot of log i vs potential for cobalt-nickel sulphide dipping porous electrode in 5N KOH solution at 40°C.

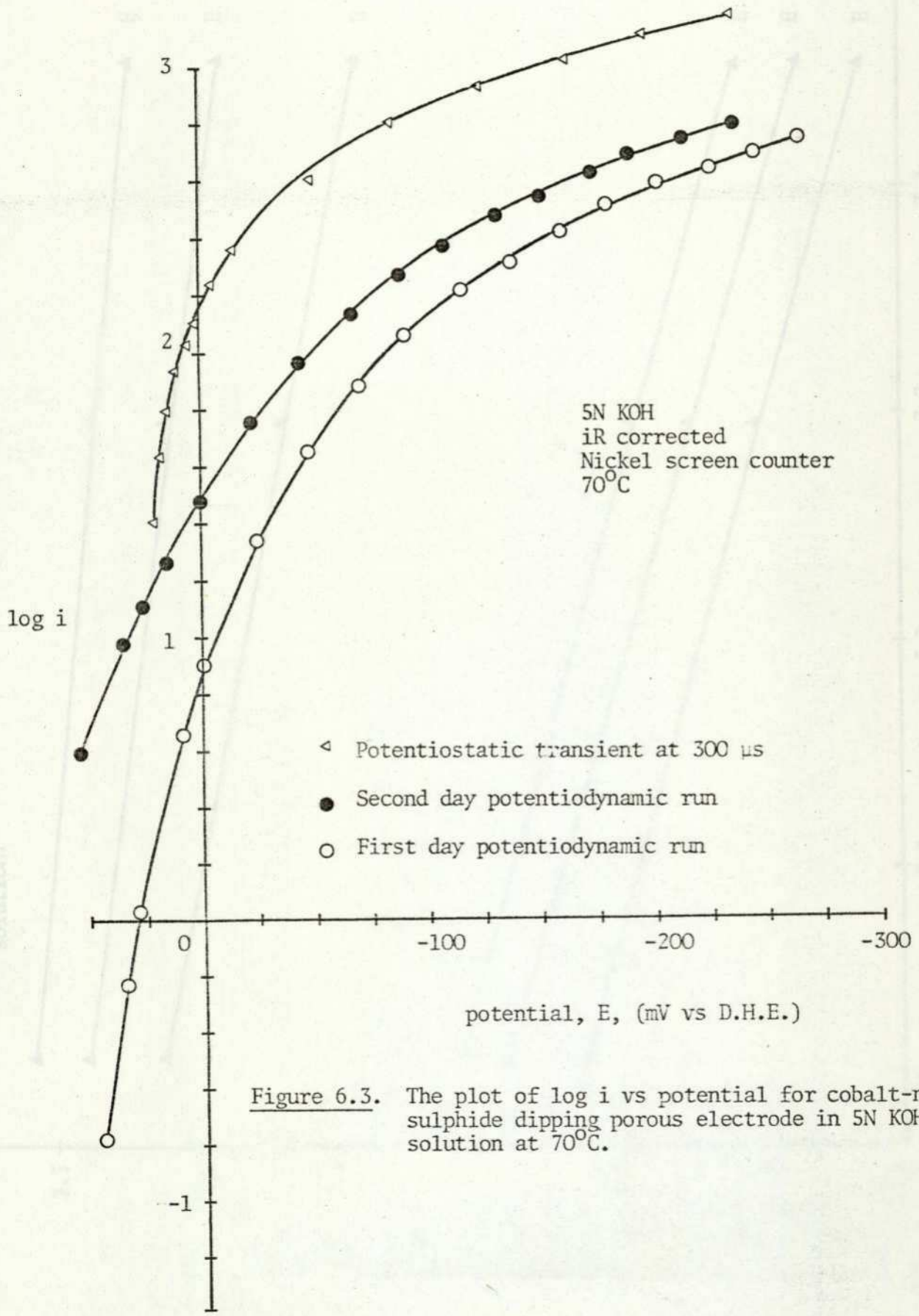

Figure 6.3. The plot of log i vs potential for cobalt-nickel sulphide dipping porous electrode in 5N KOH solution at 70°C.

Figure 6.4. The plot of log i vs 1/T, for cobalt-nickel sulphide dipping porous electrode in 5N KOH solution.

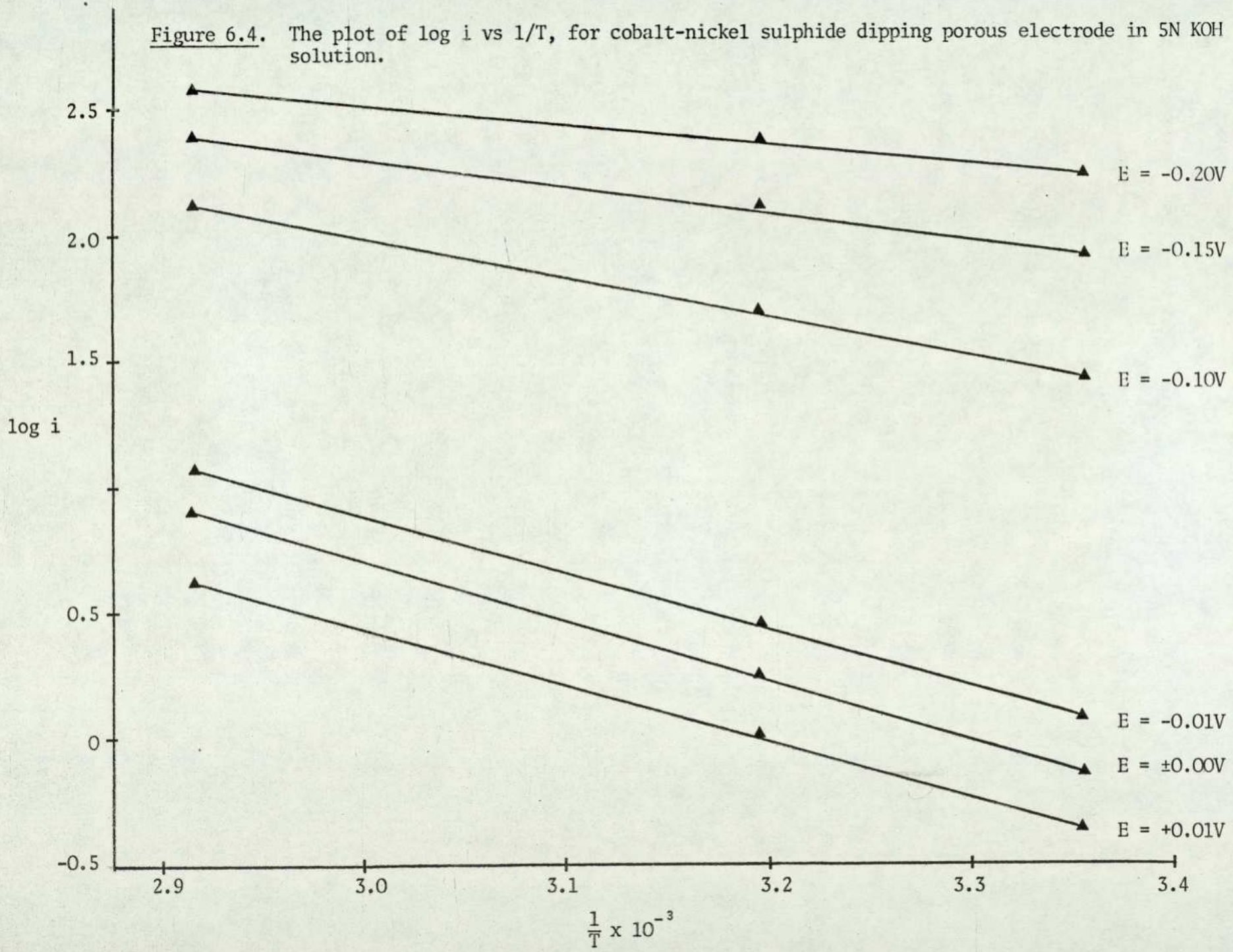

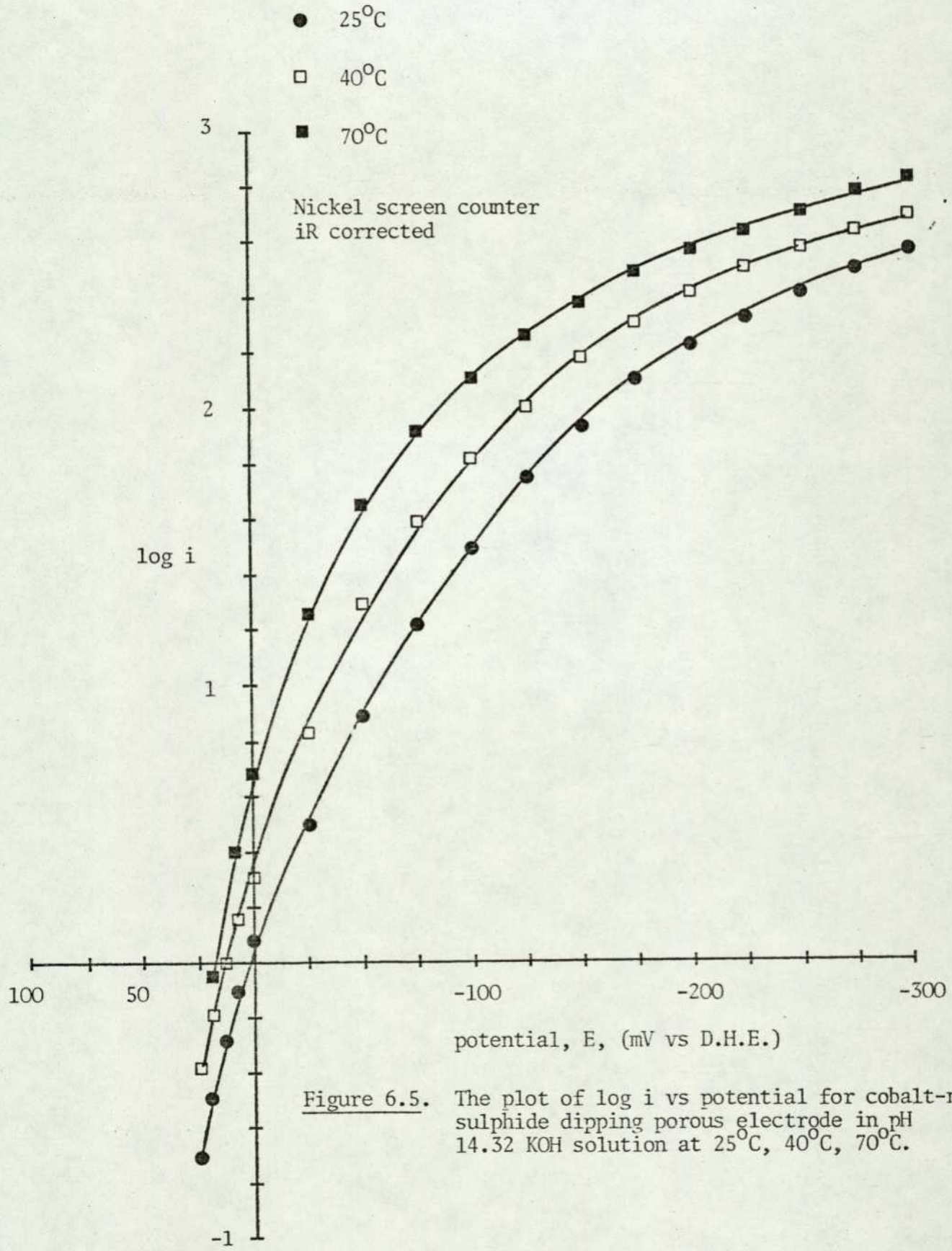

Figure 6.5. The plot of log i vs potential for cobalt-nickel sulphide dipping porous electrode in pH 14.32 KOH solution at 25°C, 40°C, 70°C.

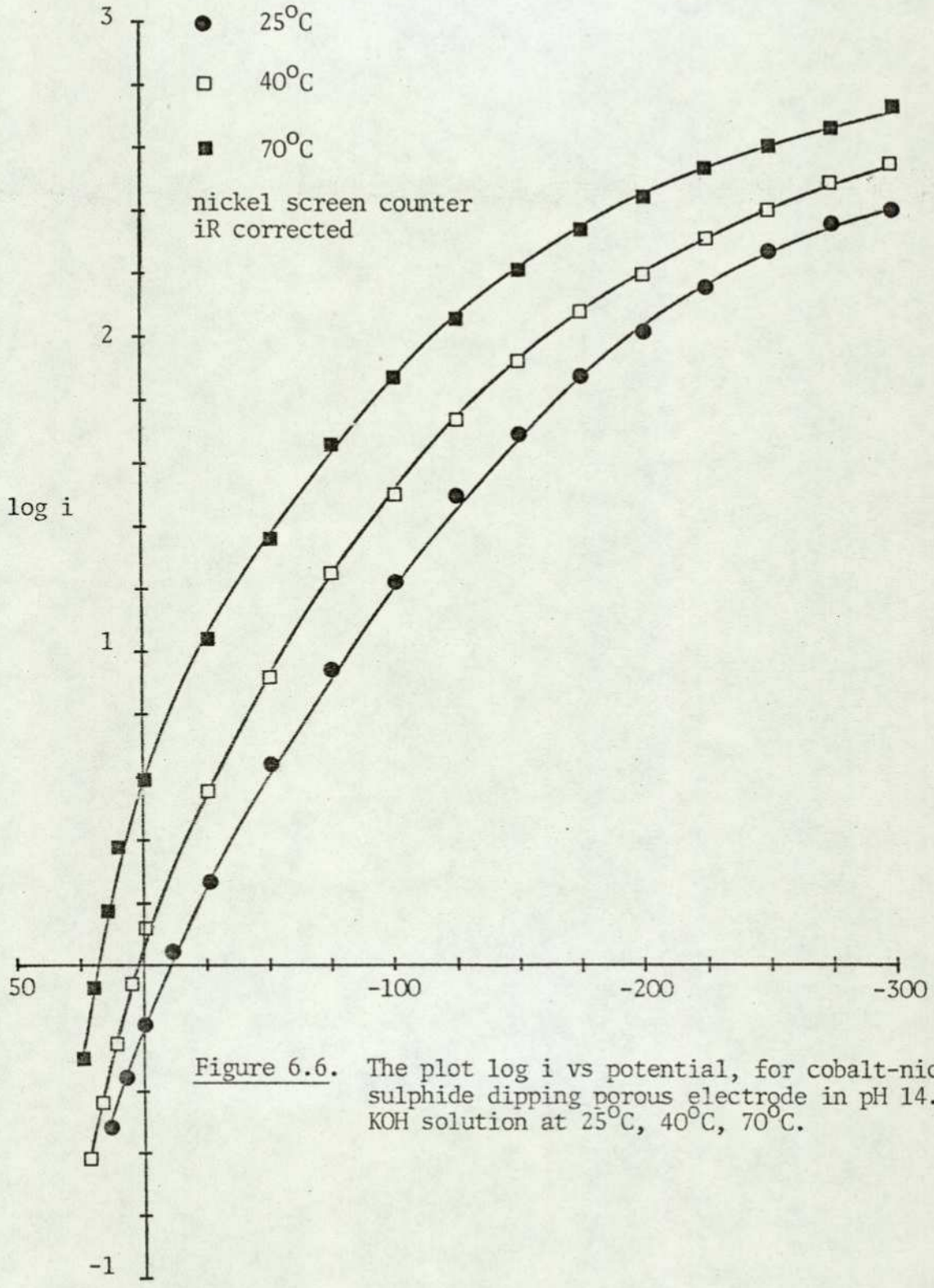

Figure 6.6. The plot log i vs potential, for cobalt-nickel sulphide dipping porous electrode in pH 14.0, KOH solution at 25°C, 40°C, 70°C.

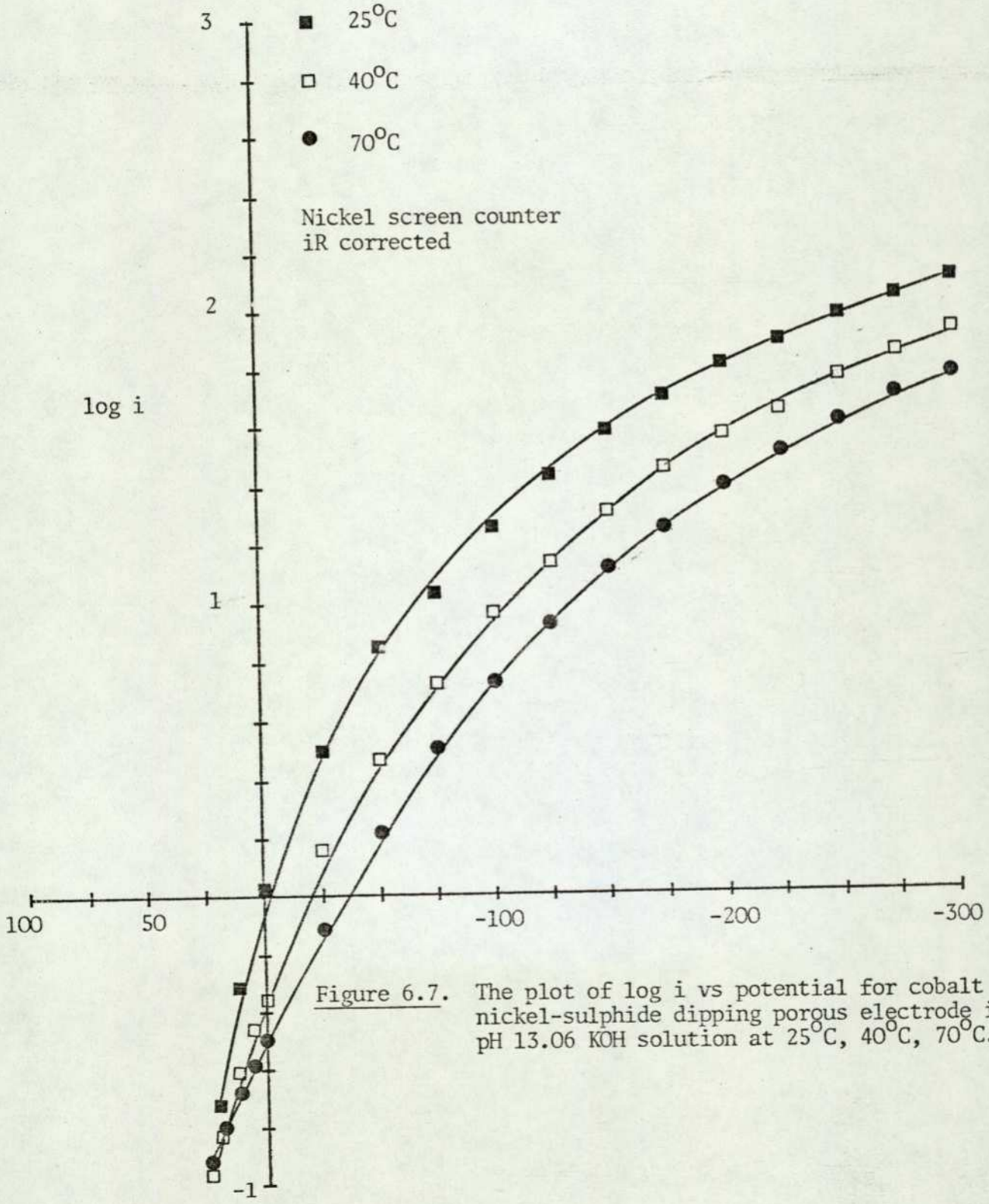

Figure 6.7. The plot of log i vs potential for cobalt nickel-sulphide dipping porous electrode in pH 13.06 KOH solution at 25°C, 40°C, 70°C.

6. DISCUSSION

Due to the diversity of reaction mechanism for the hydrogen electrode and limited kinetic results, only the charge-transfer-recombination and charge transfer-electrochemical desorption paths are seriously considered, both cases depend on the coverage of the surface with atomic hydrogen. The values of the kinetic parameters, and particularly the Tafel slope and the electrochemical reaction order with respect to the hydrogen ions, depend on this value. When the coverage is very high or very low, the Langmuir[106] adsorption isotherm should be valid, whereas the Temkin[107] isotherm should be valid in intermediate cases. A phenomenological interpretation of the experimental results should be given by assuming that the hydrogen evolution process takes place according to the mechanisms mentioned earlier, and each step may be the rate determining step.

For the pH range from 13.06 to 14.32, electrocatalytic activity increases at a constant potential as the electrolyte becomes more alkaline. The Tafel slopes at low overpotential are relatively constant throughout this pH range. This strongly suggests that the reaction mechanism remains the same. The Tafel slopes, transfer coefficients at temperatures of 25°C, 40°C and 70°C from different pH are presented in Table 6.2. The two Tafel slopes resulted from the low overpotential and high overpotential suggested that there is a change in reaction mechanism.

The experimental Tafel slope of 2RT/3F, i.e. $\alpha = 1.5$ observed at low overpotential at temperatures of 25°C, 40°C and 70°C in pH range of 13.06 to 14.32 suggests that either a fast

TABLE 6.2

Kinetic Parameters for the Hydrogen Evolution Reaction on Cobalt Nickel Sulphide Dipping Porous Electrode in KOH Solutions.

pH	T(°C)	Tafel slope (v)		Transfer coefficient (α)	
		low η	high η	low η	high η
14.32	25°C	0.041	0.140	1.4	0.4
	40°C	0.036	0.152	1.7	0.4
	70°C	0.033	0.172	2.1	0.4
14.00	25°C	0.050	0.104	1.2	0.6
	40°C	0.041	0.152	1.5	0.4
	70°C	0.041	0.135	1.7	0.5
13.06	25°C	0.056	0.116	1.1	0.5
	40°C	0.040	0.128	1.6	0.5
	70°C	0.039	0.143	1.8	0.5

$$\alpha = \frac{2.303 \times RT}{b\ F}$$

b = Tafel slope

charge transfer - slow electrochemical desorption mechanism under conditions of low hydrogen coverage ($\theta \sim 0$) or a slow charge-transfer-fast electrochemical desorption mechanism under conditions of high hydrogen coverage ($\theta \sim 1$)[108]. It is further observed that the Tafel slope changes from 2RT/3F to 2RT/F, i.e. $\alpha = 0.5$ at high overpotential. This indicates a rate determining step involving an electron transfer step or the electrochemical desorption step. Since Lechatelier's principle predicts a decreasing equilibrium coverage of adsorbed hydrogen atoms with increasing temperature, the condition of low coverage at low overpotential seem even more probable at higher temperatures, hence a slow electrochemical desorption step is suggested.

The plots of log i vs 1/T in KOH solutions of pH 14.32, 14.0 and 13.06 are shown in Figures 6.8, 6.9 and 6.10. The Arrhenius activation energies obtained from the slopes of these plots are tabulated in Table 6.3. Although the change of log i with 1/T is different at different pH, it is possible to estimate the heat of activation at low overpotentials to be about 30 kcal-mole^{-1} and about 14 kcal-mole^{-1} at high overpotentials.

Reaction orders are determined in the absence of excess foreign electrolyte, though the experimental investigation of the pH dependence of the overpotential is simpler if ψ remains constant while the pH is varied (i.e. $\left(\frac{\partial \ln i}{\partial \ln(H^+)}\right)_{\eta,\psi}$, where ψ is the potential on the site of the helmhotz double-layer corresponding to the centre of the ionic changes, with respect to the bulk of the solution where the potential is regarded as zero). Normally, this can be accomplished by adding a foreign electrolyte in high enough

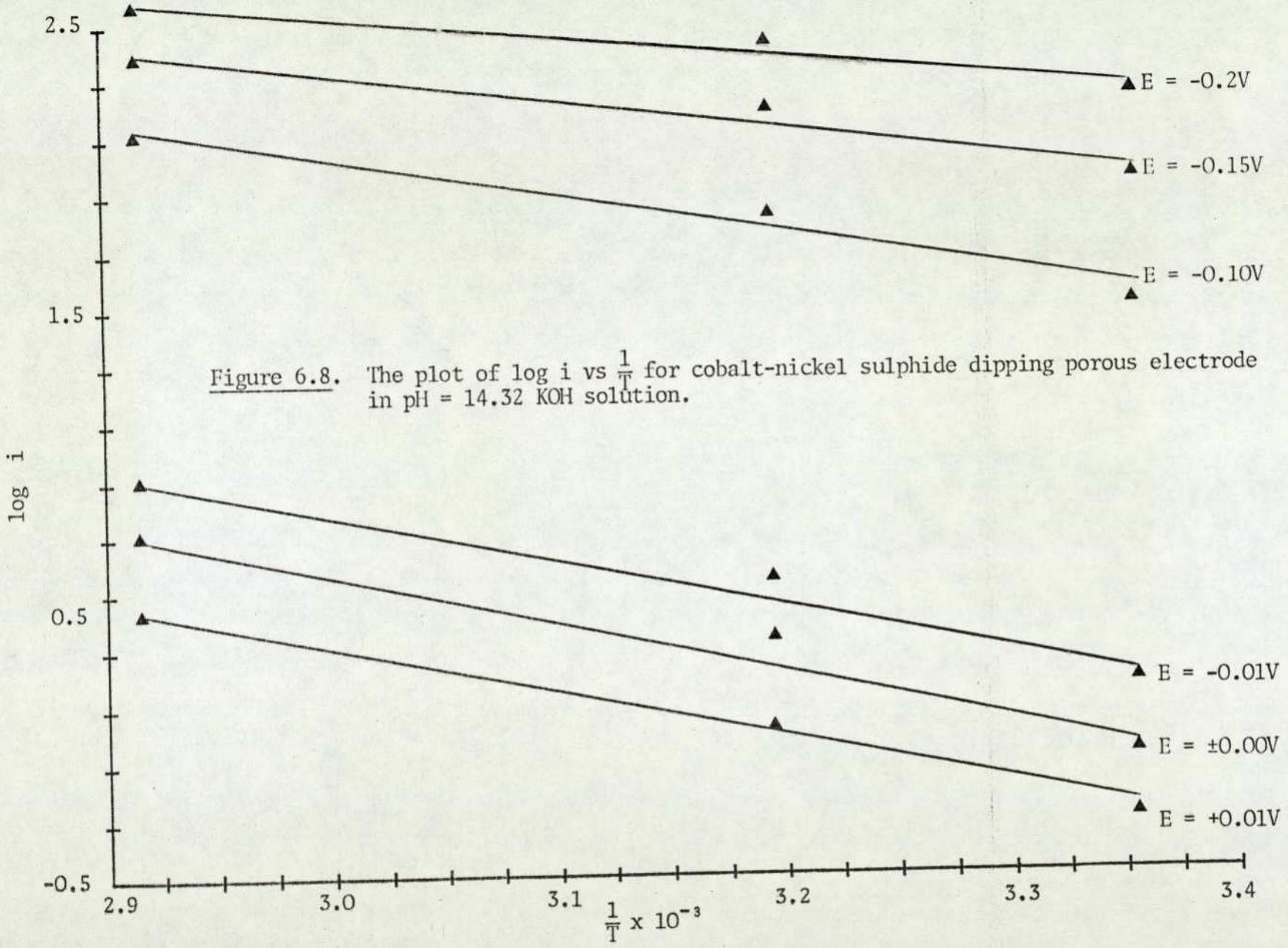

Figure 6.8. The plot of log i vs $\frac{1}{T}$ for cobalt-nickel sulphide dipping porous electrode in pH = 14.32 KOH solution.

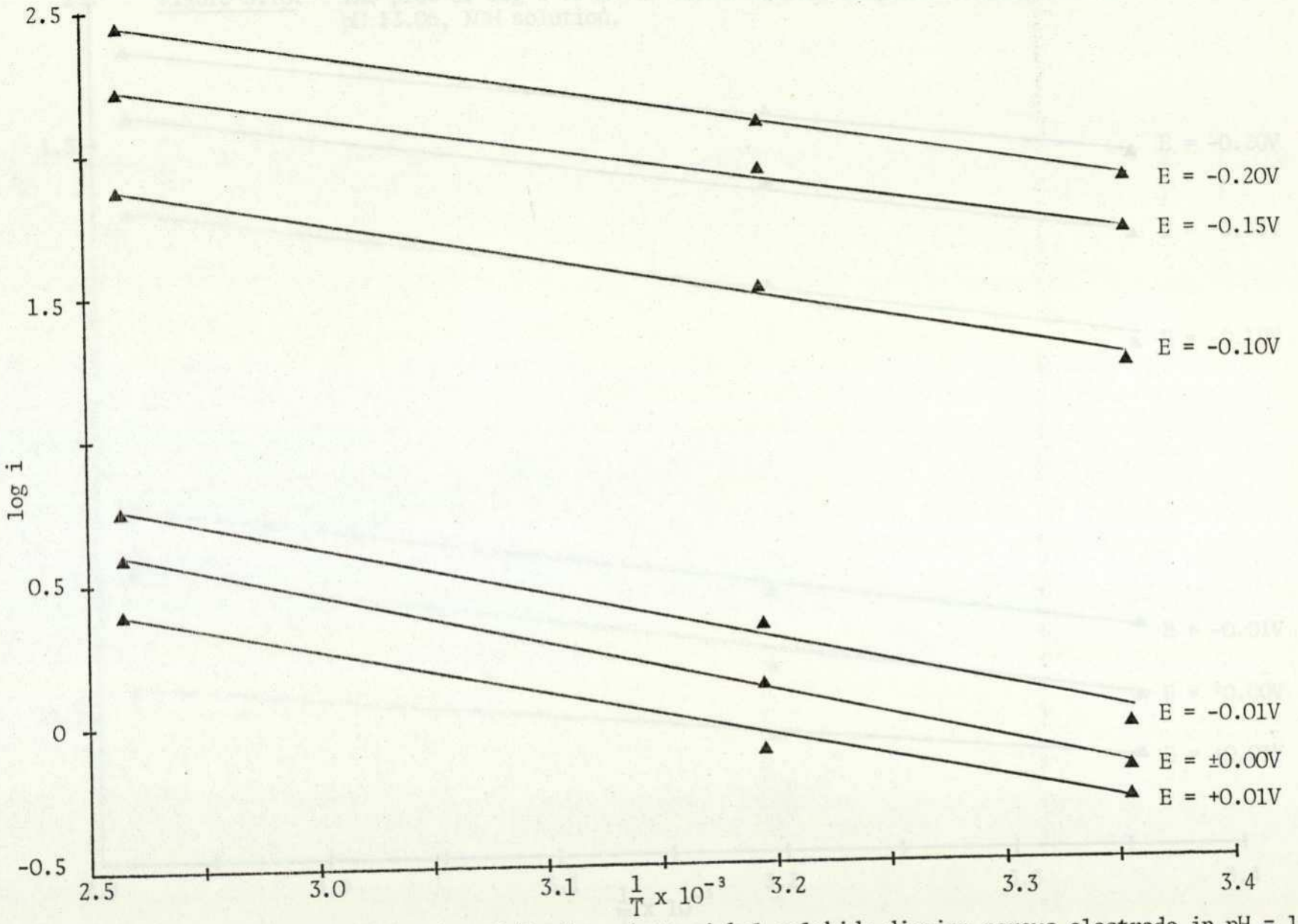

Figure 6.9. The plot of log i vs 1/T, for cobalt-nickel sulphide dipping porous electrode in pH = 14.0 kOH solution.

Figure 6.10. The plot of log i vs $\frac{1}{T}$ for cobalt-nickel sulphide dipping porous electrode in pH 13.06, KOH solution.

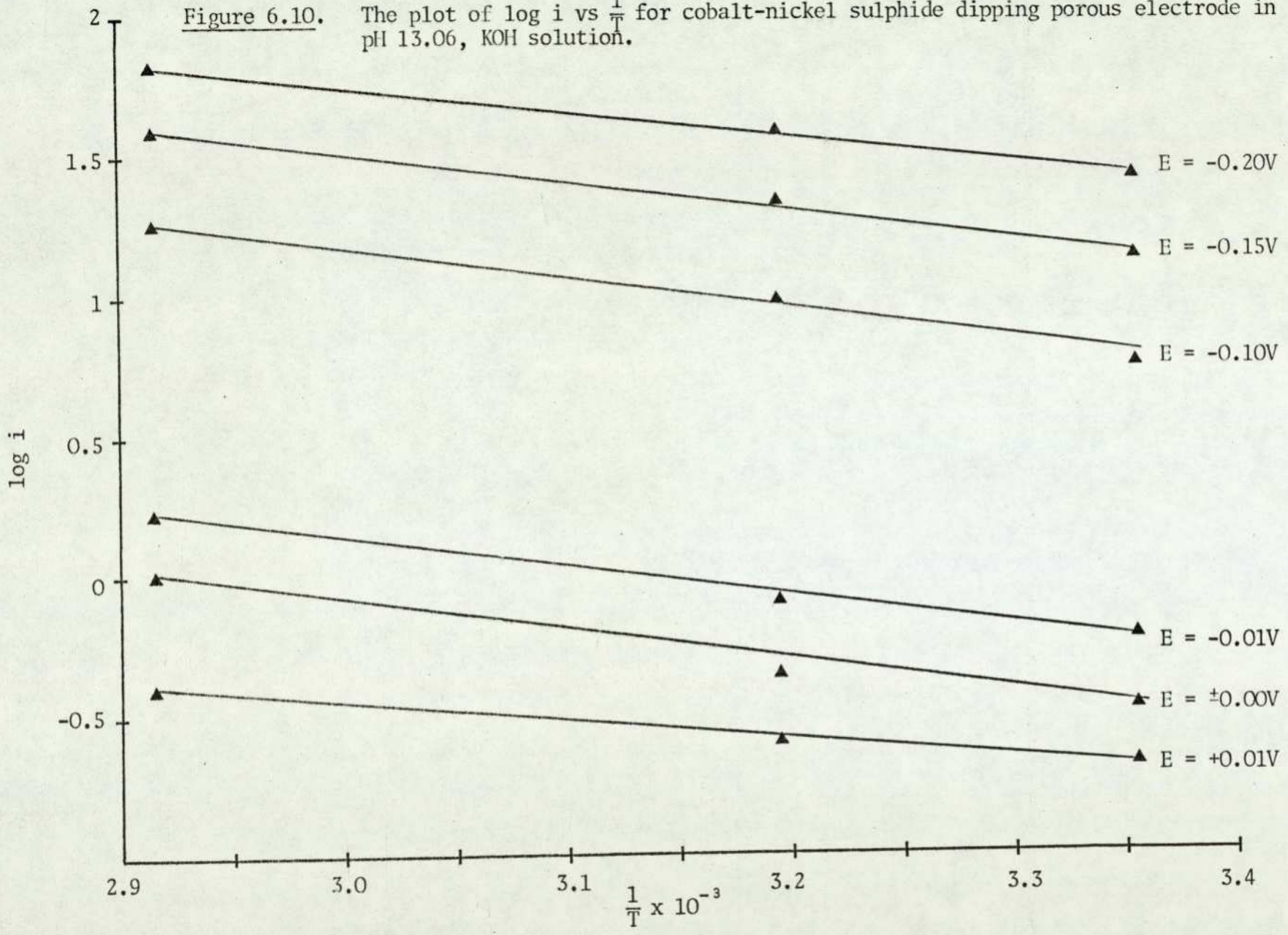

TABLE 6.3. Arrhenius Activation Energies at Different Overpotentials in KOH Solutions of pH 14.32, 14.0 and 13.06.

pH	Potential E, (mV vs D.H.E.)	Arrhenius activation energy, ΔH (kcal/mole)
14.32	10	30
14.32	0	32
14.32	- 10	30
14.32	-100	25
14.32	-150	17
14.32	-200	14
14.0	10	32
14.0	0	30
14.0	- 10	32
14.0	-100	27
14.0	-150	21
14.0	-200	17
13.06	10	27
13.06	0	19
13.06	- 10	23
13.06	-100	21
13.06	-150	19
13.06	-200	17

concentration so that the variation of the hydrogen ion concentration does not appreciably change the ionic strength. However, in the present study, due to the complexity of the electrode material, it was not possible to select an appropriate inert supporting electrolyte, and the variation of pH was done simply by dilution. Therefore, the relationship $(\frac{\partial \log i}{\partial pH})_E$ was studied and the results at different temperatures tabulated in Table 6.4. The plots of log i vs pH at temperatures of 25°C, 40°C and 70°C are shown in Figures 6.11, 6.12 and 6.13, since the pH effect for the slow electrochemical desorption mechanism are similar to those for the slow charge transfer mechanism, and there are no pH effects for the slow recombination mechanism. The electrochemical orders are calculated as 0.55 at low overpotentials and 0.68 at high overpotentials. This eliminates the validity of the Tafel reaction as the rate-determining step of the process. It is therefore possible to conclude that the hydrogen evolution mechanism on cobalt-nickel sulphide does not change in potassium hydroxide solutions of pH range from 13.06 to 14.32 and the dual Tafel slopes observed for the hydrogen evolution reaction suggests a slow electrochemical desorption step. Further experimental investigations are required to deduce the kinetic mechanism in more detail.

TABLE 6.4. Reaction Orders at Different Temperatures and Potentials

T°C	$(\frac{\partial \log i}{\partial pH})_E$	potential E, (mV vs D.H.E.)
25°C	0.56	10
25°C	0.44	0
25°C	0.40	- 10
25°C	0.58	- 100
25°C	0.66	- 150
25°C	0.67	- 200
40°C	0.51	10
40°C	0.56	0
40°C	0.51	- 10
40°C	0.68	- 100
40°C	0.68	- 150
40°C	0.68	- 200
70°C	0.58	10
70°C	0.56	0
70°C	0.54	- 10
70°C	0.68	- 100
70°C	0.62	- 150
70°C	0.62	- 200

Figure 6.11. The plot of log i vs the pH at different potentials for cobalt-nickel sulphide dipping porous electrode at 25°C.

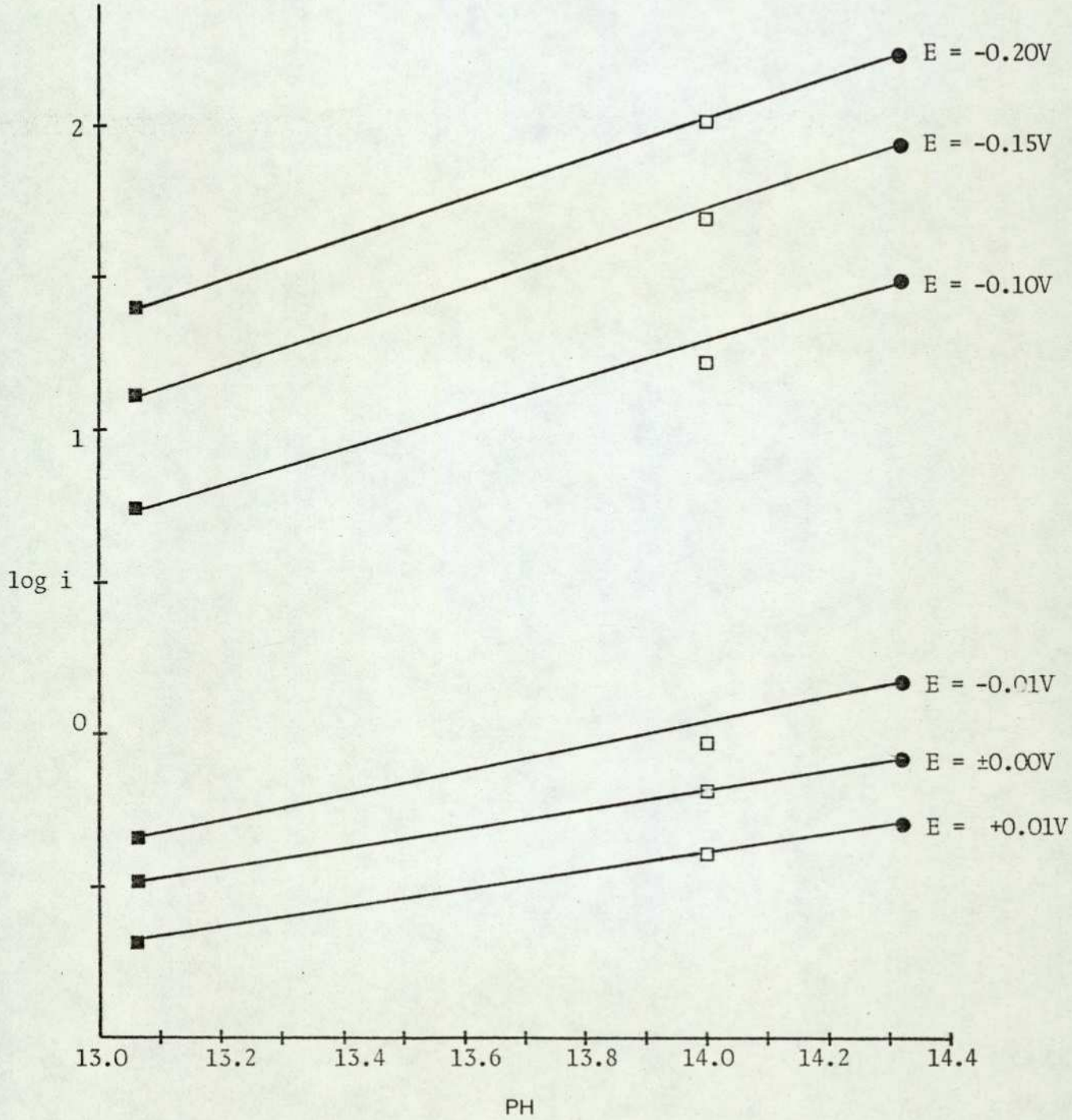

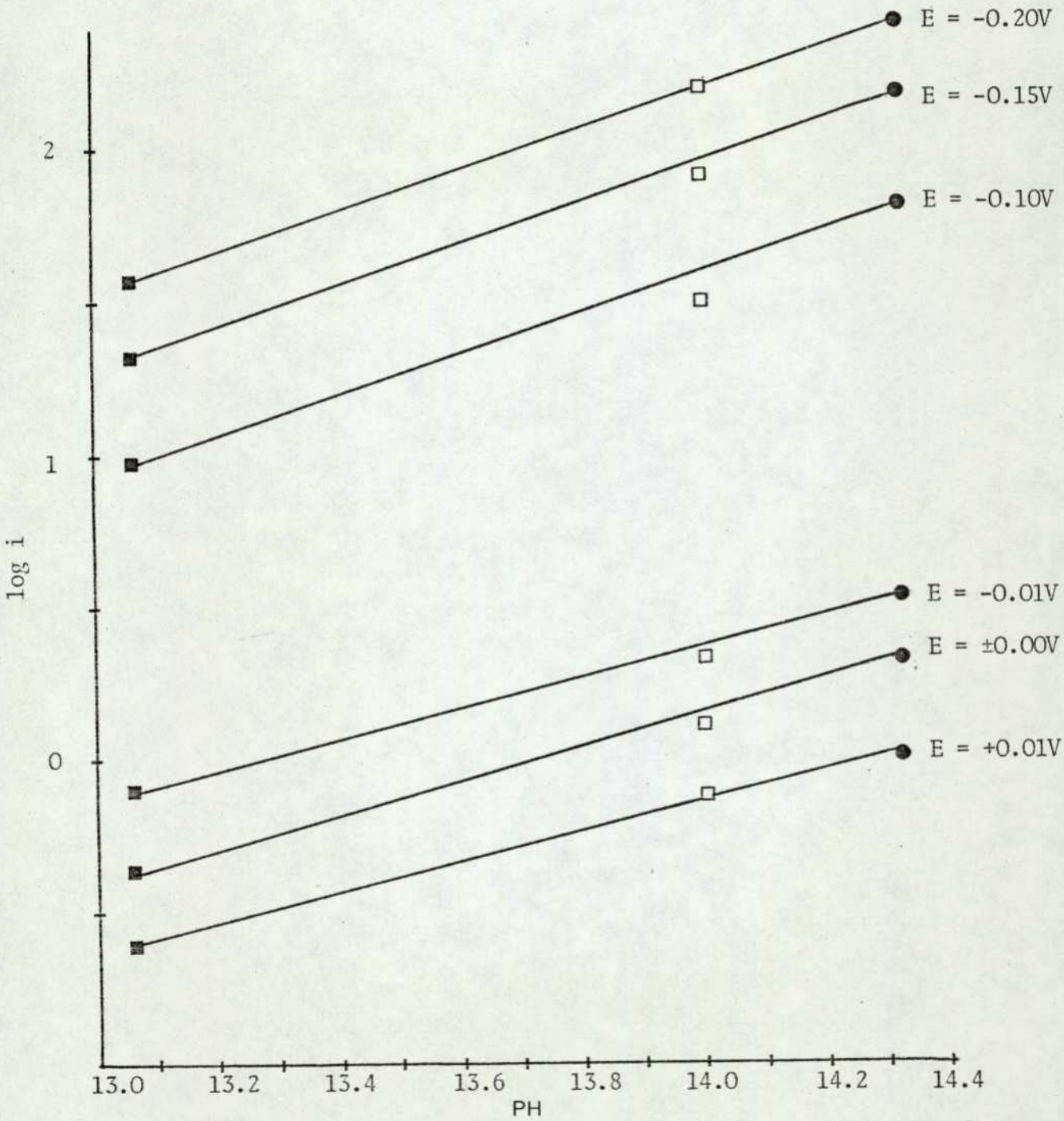

Figure 6.12. The plot of log i vs the pH at different potentials, for cobalt-nickel sulphide dipping porous electrode at 40°C.

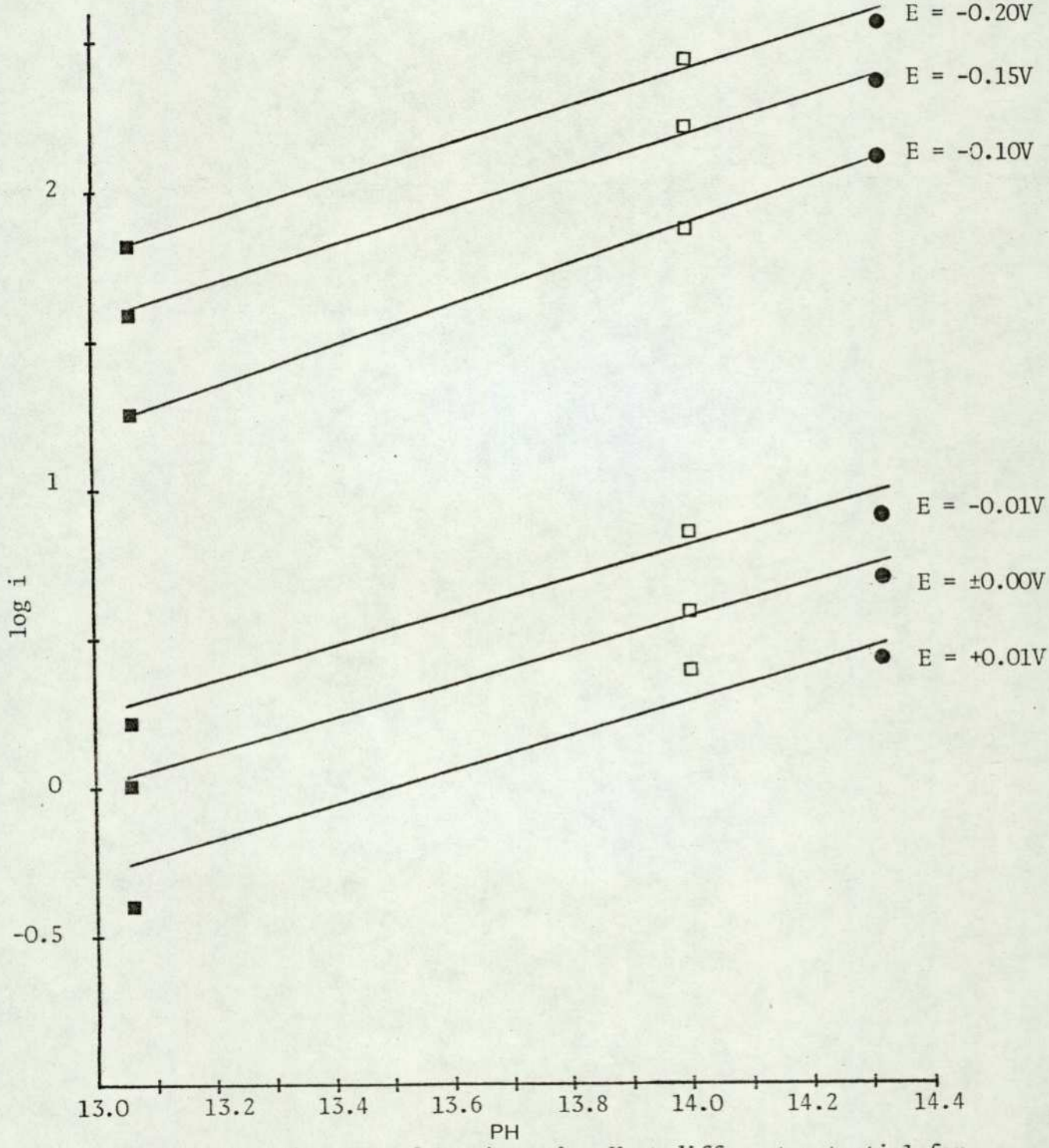

Figure 6.13. The plot of log i vs the pH at different potential for cobalt-nickel sulphide dipping porous electrode at 70°C.

CHAPTER SEVEN

CONCLUSIONS AND RECOMMENDATIONS FOR FURTHER WORK

1. CONCLUSIONS AND SUMMARY

Based on certain important criteria, such as corrosion resistance in strongly alkaline electrolyte; adequate electrical conductivity to minimise resistive losses; relatively easy to prepare in a high surface area form, nickel sulphides of different compositions and origins are initially evaluated as possible potential materials for hydrogen cathode electrocatalysts in alkaline media. Logical and scientific deductions of the experimental results obtained for these nickel sulphides lead to the preparation and investigation of cobalt-nickel-sulphur compounds, which show very promising electrochemical activity towards the h.e.r. in potassium hydroxide solutions, as compared to the conventional more expensive electrocatalyst such as platinum black. More importantly, the hydrogen evolution activity of these cobalt-nickel-sulphur compounds is not affected even if they are periodically exposed to air oxidation in the strong alkaline electrolyte.

By choosing the preparation parameters carefully, the kinetics of the sulphiding process are investigated and the validity of sulphiding from freeze dried cobalt-nickel oxide of composition $NiCo_2O_4$ at relatively low temperatures is also confirmed, although it is found that ultra-pure cobalt-nickel sulphides are not easy to obtain in this way. The presence of mixed phases, such as NiO, Co_3O_4, S and the degree of contamination depends on the sulphiding conditions. For complete transformation of $NiCo_2O_4$ to $NiCo_2S_4$, freeze dried cobalt-nickel oxide is sulphided in hydrogen sulphide at a constant flow rate of 60-65 mls/min., for 5-6 hours at 550°C.

Powder crystallographic measurements show a similar spinel-type structure for all cobalt-nickel-sulphur compounds; the calculated lattice parameters for these compounds are in very close agreement with that of $NiCo_2S_4$, which can be represented as:

$$Ni^{2+}_{tet}\ (Co^{3+}_{oct}\ Co^{3+}_{oct})S_4$$

From the reported Curie constant, $C_{at} \sim 0.3$, and lattice parameter, a = 9.392Å, $NiCo_2S_4$ shows deviations from ionic structure. (Based on ionic S^{2-} close packing, the cell edge of $NiCo_2S_4$ should be $\sim$ 9.85Å). It is plausible that a covalent structure is formed where a cobalt atom is octahedrally co-ordinated with six sulphur atoms, and six hybrid bond orbitals d^2sp^3 are used to form Co-S bonds. A nickel atom is tetrahedrally co-ordinated by four sulphur atoms and Ni-S bonds are formed by using the hybrid bond orbitals sp^3. A sulphur atom is surrounded by one nickel atom and three cobalt atoms and can form one Ni-S and three Co-S bonds using the s and the three p orbitals. $NiCo_2S_4$ is synthesized from the high temperature method of direct combination of metals and sulphur, this is essentially an n-type metallic conductor. The mechanism for metallic conductivity may be due to partially filled band states and are formed as a result of cation-anion covalence, which can occur with both octahedral and tetrahedral ions. Since the sulphide ions have four near neighbour cations, σ bonding is much stronger than π bonding, and the partially filled band is composed of antibonding σ^* states.

Chemical analysis and DTA analysis have shown that all cobalt-nickel-sulphur compounds prepared in this work are best

represented by the general formula of $NiCo_2O_xS_y + S_z$, where $x + y \lesssim 4$, and $y >> z \geq 0$. A series of cobalt-nickel-sulphur compounds with different percentages of sulphur content are evaluated for hydrogen evolution activity and it was found that the highest electrochemical activity was achieved by the sample with a sulphur content of about 27% (w/w). Electrochemical activity gradually decreases as the sulphur content increases to a maximum of approximately 45-47% (w/w). It is unlikely that the electrochemical activity is due mainly to the presence of free sulphur, which is found to be minimal in cobalt-nickel-sulphur compounds with low sulphur content. It is probable that the purity of the cobalt-nickel-sulphur compounds have some effect on the electrochemical activity. It was also established that cobalt-nickel-sulphur electrodes behave as irreversible hydrogen electrodes. The open circuit voltages (O.C.V.) of these electrodes in a hydrogen saturated electrolyte at temperatures of 25°C, 40°C and 70°C fluctuate between 600 mV to 300 mV (vs D.H.E.), depending on the pre-treatment of the electrodes.

However, if these electrodes are cathodically polarised for sometime below the equilibrium reversible hydrogen potential, the O.C.V. when immediately measured is valued at about 40 mV to 80 mV (vs D.H.E.), but rises slowly with respect to time even if the electrolyte is continuously purged with hydrogen. From these observations alone, it is possible to suggest that freshly prepared cobalt-nickel sulphide electrodes have either weak, or no affinity for hydrogen (i.e. do not chemisorb hydrogen). Slow potentiodynamic runs found that prior to the h.e.r., some other

cathodic electro-reductions take place at about 100 mV to 200 mV (vs D.H.E.). Although the precise nature of this reduction region has not been resolved in the present study, it is suggested that this is due to the electroreduction of oxide films on the surface of the electrode. These oxide films may be formed either chemically with the strongly alkaline electrolyte or formed during the curing process, in the fabrication of the teflon-bonded porous electrode. However, for electrodes which are prepared differently by the dipping method and with careful exclusion of the curing procedure, the same phenomena is observed. Thermodynamically, at a potential immediately below the equilibrium reversible hydrogen potential, it is plausible that electrochemical reduction on the electrode material with electrochemical discharge of either hydrogen sulphide, S^{2-} or SH^{-} ions, is accompanied with the evolution of hydrogen. The reduction of the cobalt-nickel sulphide is presented according to the following equation:

(1) $$NiCo_2S_4 + 4H_2O + 8e \longrightarrow 4HS^{-} + NiCo_2 + 4OH^{-}$$

It is well known that cobalt-nickel alloy has a relatively low hydrogen overpotential and therefore it is quite probable that the very good performance achieved by the cobalt-nickel sulphide electrode may be due to the result of the above reaction. However, the gases evolved at various potentials from 25 mV to -300 mV (vs D.H.E.) are analysed and no traces of hydrogen sulphide are detected. Chemical analysis of the electrodes which have been used in the hydrogen evolution mode for a long period show that sulphur is still bound in the cobalt-nickel sulphide electrode as sulphide state.

Although quantitative results are not available, due to the extremely small quantities of samples to work with, it is quite plausible that sulphur in the surface region of the cobalt-nickel sulphide electrode is removed according to the following equation:

(2) $NiCo_2S_4 + xH_2O + 2xe \rightarrow xHS^- + NiCo_2S_{4-x} + xOH^-$

where $4 > x > 0$

The degree of sulphur removal depends on various factors such as the stability of different cobalt-nickel sulphide stoichiometries at potential in which the reduction occurs. Therefore, at different potentials, surface layers of various cobalt-nickel sulphide stoichiometries may be formed. In all cases, the surface layer of the cobalt-nickel sulphide electrode would be covered with a metal rich sulphide, which according to solid state theory, would enhance the h.e.r. by the creation of more n-type characteristics at the electrode surface. It has also been suggested that since the sulphur atom is generally considered to have low mobility in the sulphide lattices, it cannot diffuse out to the surface. The evidence indicates that reduction of cobalt-nickel sulphide can occur only at, or very close to, the interface between cobalt-nickel sulphide and the electrolyte. It has been proved in this work that the structure in the bulk of the cobalt-nickel sulphide catalyst, which has been removed from a cobalt-nickel sulphide electrode after being used in the hydrogen evolution mode for a prolonged period, is unchanged when compared to the freshly prepared cobalt-nickel sulphide catalyst. This evidence alone eliminates conclusively the possibility of the

reduction of the electrode material to cobalt-nickel alloy as parallel reduction reaction during the hydrogen evolution process in the potential range of 25 mV to -300 mV (vs D.H.E.). When a working cobalt-nickel sulphide electrode is periodically exposed to air oxidation in the electrolyte, layers of oxide films are thought to have formed on top of the $NiCo_2S_{4-x}$ surface, which is formed during the earlier hydrogen evolution runs. It is also thought that these oxide films can be easily reduced electrochemically owing to the more conducting nature of these oxide layers. (The electrical resistivity of $NiCo_2O_4$ is about 10 ohm cm^{-1} as compared to NiO, which is non-conducting). The formation of these oxide layers may either be due to the chemical corrosion of the metal sulphide, or the charge compensation on the metal rich sulphide surface.

In terms of practical application, electrochemical activity is closely related to the type of porous electrode structure used, and the higher performance and better stability sustained by a teflon-bonded porous electrode as compared to a porous electrode without binding agent (i.e. dipping porous electrode) is mainly due to the properties of the teflon. The hydrophobic character of the teflon can provide (a) dry gas 'channels' in the porous electrode structure for gas to escape more easily; (b) a strong binding ability of holding the catalyst and the catalyst support together (c) elastic property to withstand the high gas pressure inside the pores, developed during the h.e.r., and (d) higher utilisation of the available surface areas of the electrode. However, excessive teflon or uneven distribution of teflon would reduce the activity drastically

due mainly to the formation of exceptionally large hydrogen bubbles, which contribute to high ohmic losses.

In the absence of foreign electrolyte, the dual Tafel slopes observed for the hydrogen evolution reaction suggest a slow electrochemical desorption step in aqueous solution of potassium hydroxide with pH values of between 13.06 and 14.32.

2. RECOMMENDATIONS FOR FURTHER WORK

The interesting and encouraging results in the present study shows that there is a break of the monopoly of precious metals and metal alloys being used exclusively for h.e.r. catalysts in alkaline media. A lot more work has to be generated before the complicated cobalt-nickel-sulphur tertiary system can be fully resolved and understood. By then, it is hoped that certain critical correlations will emerge and serve as indicators for the future selection of even better electrocatalysts for h.e.r. As far as the present work is concerned, the recommendations for further work are concentrated in four areas, each of which is closely inter-related and should be investigated concurrently:

(1) Electrochemical activity and physical parameters (such as surface area, crystal structure, electrical conductivity, average particle size and magnetic property etc.) on the effect of:

(a) The change in atomic ratio of Ni/Co from 0.5 to 2, while keeping the sulphur composition constant;

(b) The doping or substitution of either cobalt or nickel atoms, completely or partially by other

transition metals, such as Mn, Fe, Cr etc.

(c) The substitution of sulphur atoms, either completely or partially by elements in the same group of the periodic table. i.e. Se and Te.

(2) The studies of the surface state in the fresh and used electrodes would yield valuable information concerning active sites and different oxidation states for different surface atoms. This is most conveniently achieved by using fast improving techniques, such as X-ray Photoelectron Spectroscopy (XPS or ESCA), Auger Electron Spectroscopy (AES) and Secondary Ions Mass Spectroscopy (SIMS). In addition, these techniques would also be suitable for surface analysis and the study of surface reactivity as well as adsorption phenomena.

(3) Further refinement in the preparation method is required in order to obtain an ultra-pure sample. The contribution due to the presence of impurities can then be eliminated.

(4) Further improvements to the teflon-bonded porous electrode structure is directed towards the reduction of the hydrogen bubble size, and shortening the time that the hydrogen bubbles reside on the electrode surface before they are finally liberated.

REFERENCES

1. D. P. Gregory, D. Y. C. Ng, and G. M. Long in J. O'M. Bockris (ed.), The Electrochemistry of Cleaner Environments (New York: Plenum), (1972).

2. M. A. Elliot and N. C. Turner, paper presented at the ACS Meeting, Fuel Chemistry Symposium, April 9-14, (1972).

3. P. R. Vassie, A. C. C. Tseung, Electrochim. Acta, 20, (1975), 763.

4. A. C. C. Tseung and P. R. Vassie, Electrochimica Acta, 21, (1976), 315-318.

5. G. Singh, M. H. Miles and S. Srinivasan, National Bureau of Standards Special Publication 455, (1976), 289-296.

6. J. O'M: Chapter 4, in J.O'M. Bockris and B. E. Conway (eds.), 'Modern Aspects of Electrochemistry', Vol. 1, Butterworth & Co. (Publishers) Ltd., London, (1954).

7. A. N. Frumkin: Chapter 2, Vol. 1, and Chapter 5, Vol. 3, in P. Delahay and C. W. Tobias (eds.), "Advances in Electrochemistry and Electrochemical Engineering", Interscience Publishers, Inc., New York, (1961) and (1963).

8. J. O'M Bockris, Trans. Faraday Soc., 43 (1947) 417.

9. B. E. Conway and J. O'M. Bockris, J. Chem. Phys., 26 (1957) 532.

10. J. O'M Bockris and H. Wroblowa, J. Electroanal. Chem., 7 (1964), 428.

11. J. O'M Bockris and S. Srinivasan, Proc. Ann. Power Sources Conf., 9 (1965) 1.

12. R. Parsons, Discuss. Faraday Soc., 45 (1968) 40.

13. M. W. Breiter and R. Clamroth, Z. Elektrochem., 58 (1954) 493.

14. S. Trasatti, J. Electroanal. Chem., 39, (1972) 163.

15. H. Kita, "Electrochemistry - The Past Thirty and the Next Thirty Years", ed. H. Bloon and F. Gutmann, Plenum Press, London, New York, (1977) p. 117.

16. H. Kita and T. Kurisu, J. Res. Inst. Catal., 21, (1973), 200.

17. A. T. Kuhn, C. J. Mortimer, G. C. Bond and J. Lindley, J. Electroanal. Chem., 34, (1972), 1.

18. M. H. Miles and M. A. Thomason, J. Electrochem. Soc. 123, (1976), 1459.

19. V. S. Bagotsky, L. S. Kanevsky and V. Sh. Palanker, Electrochim. Acta, 18, (1973), 473.

20. M. Grenness, M. W. Thompson and R. W. Cahn, J. Appl. Electrochem., 4, (1974), 211.

21. J. Vondrak and J. Balej, Electrochim. Acta, 20, (1975), 283.

22. J. P. Randin and A. K. Vijh, Electrochim. Acta, 20, (1975), 37.

23. N. V. Kerovin, A. G. Kicheev and I. G. Shmachkova, Proc. Symp. Electrocatalysis, ed. M. W. Breiter, (1974), p. 156, Electrochem. Soc.

24. M. H. Miles, J. Electroanal. Chem., 60, (1975), 89.

25. E. W. Brooman and A. T. Kuhn, J. Electroanal. Chem., 49, (1974) 325.

26. J. O.'M. Bockris, A. Damjanovic and R. Mannan, J. Electroanal. Interfacial Electrochem., 18 (1968), 349.

27. P. R. Vassie, A. C. C. Tseung, Electrochimica Acta, 20, (1975), 762.

28. G. Benozur-Ürmössy, paper presented on the 'Symposium on Novel Electrode Materials', 25-26 September (1975), Brighton.

29. G. Kullerud and R. A. Yund, J. Petrology., 3 (1962), 126.

30. D. Lundqvist, Arkiv. Kemi, Miner. Geol., 24A; (1947), no. 21.

31. T. Rosenquist, J. Iron Steel Inst., 176, 37.

32. E. Donges, Z. Anorg. Chem., 253 (1947), 337, 345, 254 (1947), 133, 267.

33. R. de Medicis, Dissertation, Louvain (1967).

34. N. Elliot, J. Chem. Phys., 33 (1960), 903.

35. R. Benoit, J. Chim. Phys., 52 (1955), 119.

36. T. A. Bither, Second Intern. Conf. Solid Comp. Trans. Elem., Enschede (1967), 26, T. A. Bither, R. J. Bouchard, W. H. Cloud, P. C. Donohue and W. J. Siemons, Inorg. Chem., 7 (1968), 2208.

37. G. Kullerud, Carnegie Inst. Wash., Yearbook 67, (1969), 179.

38. J. Drowart and R. Goldfinger, Quant.rev., 20 (1966), 545.

39. F. Gronvold, R. Mollerud and E. Rost, Acta Chem. Scand. 20 (1966), 1997.

40. V. G. Kuznetsov, A. A. Eliseev, Z. G. Shpak, K. K. Palkina, M. A. Sokolova, and Dmitriev (1961), Vopr. Met. i. Fiz. Poluprov., 159 (Moscow).

41. K. Hangsten, E. Rost, Acta. Chem. Scand., 23 (1969), 3599.

42. F. Jellinek, Inorganic Sulphur Chemistry (1968), 669.

43. F. Hulliger, J. Phys. Chem. Solids 26 (1965) 639.

44. J. T. Sparks and T. Komoto, Phys. Lett., 25A (1967), 398.

45. J. T. Sparks and T. Komoto, Rev. Mod. Phys., 40 (1968), 752.

46. J. Trhan, R. G. Goodrich and S. F. Watkins, Phys. Rev., B2 (1970), 2859.

47. J. L. Horwood, L. G. Ripley and M. G. Townsend, J. Appl. Phys., 42 (1971), 1476.

48. T. Kato and T. Oki, Nippon Kinzoku Gakkaishi 38, (1974), 663.

49. T. Kato and T. Oki, Kinzoku Gakkaishi, 37, (1973), 1338, (The Bulletin of the Scientific Metallurgical Society).

50. J. Gerlach, H. Hähne and F. Pawlek, Enzmetall., 18 (1965), 73.

51. C. De Ranter and R. Breckpot, Bull. Soc. Chim. Belges, 78, (1969), 503-522.

52. E. Peters, "The Electrochemistry of Sulphide Minerals", 4th Conf., on Trends in Electrochemistry (Australia), (1976), p. 267-290.

53. D. A. J. Rand, J. Electroanal. Chem. and Interfacial Electrochem. 83, (1977), 190.

54. A. K. M. Shamsul Huq and Arthur J. Rosenberg, J. Electrochem. Soc., 111, (1964), 270-277.

55. R. Jasinski, J. Electrochem. Soc., 116, (1969), 452-453.

56. J. Giner, M. Perry, S. Smith and M. Turchan, J. Electrochem. Soc., 116 (1969), 1692.

57. P. R. Vassie, Ph.D. Thesis, The City University, (1972).

58. B. S. Hobbs, Ph.D. Thesis, The City University, (1970).

59. J. Giner and S. Smith, J. Electrochem. Technol., 5 (1967), 59.

60. J. Giner, J. Electrochem. Soc., 111, (1964), 376.

61. M. C. M. Man, M.Sc. Dissertation, The City University, (1973).

62. P. Delahay, "New Inst. Methods in Electrochem.", Chapter 6, p. 115 Interscience Publishers, (1966).

63. K. R. Williams, "An Introduction to Fuel Cells", Elsevier, (1966).

64. W. J. Moore, "Physical Chemistry", Longmans Press, Chapter 9, (1965), p. 326.

65. J. O'M. Bockris and A. M. Azzan, Trans. Farad. Soc., 48 (1952), 145.

66. H. E. Kubirschek, 'Research' 13, (1960), 178.

67. N. F. M. Henry, H. Lipson and W. A. Wooster, "The Interpretation of X-ray Diffraction Photographs".

68. H. A. Barnett, P. B. Adams, "Atomic Adsorption Spectroscopy", ASTM special technical publication 443, A symposium presented at the seventy-first annual meeting of the American Society for testing and materials, San Fransisco, Calif., 23-28 June, (1968).

69. A.S.T.M. Data File, 2-1349, 11-99.

70. Nat. Bur. Standards (US) Mono. 25, Sec. (1961).

71. A. C. C. Tseung and H. L. Bevan, J. Mat. Sci. 5, (1970), 604.

72. P. R. Vassie, A. C. C. Tseung, Electrochim. Acta, 20 (1975), 759.

73. F. K. Lotgering, Phillips Res. Rept., 11, (1956), 337.

74. H. Hahn, C. De Lorent, and B. Harder, Z. Anorg. Allgem. Chem., 283, (1956), 138.

75. H. Hahn and B. Harder, Z. Anorg. Allgem. Chem., 288 (1956), 257.

76. R. J. Bouchard, P. A. Russo, and A. Wold., Inorganic Chemistry, Vol. 4, No. 5, (1965), 685.

77. J. B. Goodenough, Int. Collaq. du C.N.R.S., Bordeaux, France, Sept., (1963).

78. H. Behret, H. Binder and G. Sandstede, Electrochimica Acta, 20, (1975), 111.

79. E. Whipple and A. Wold., J. Inorg. Nucl. Chem., 24 (1962), 23.

80. W. J. King, Ph.D. Thesis, The City University, (1972).

81. H. L. Bevan, Ph.D. Thesis, The City University, (1970).

82. J. R. Goldstein, Ph.D. Thesis, The City University, (1970).

83. H. Tributsch and H. Gerischer, J. Appl. Chem. Biotechnol, 26, (1976), 747.

84. X-ray Powder Data File 2-1074.

85. V. A. Kal'mutskaya and S. S. Lisnyak., Ukrainskii Khimicheskii Zhurnal 39 (1973), 1089.

86. M. Heimbrecht, W. Biltz and K. Meisel, Z. Anorg. Chem. 242 (1939), 229.

87. O. Knop, K. I. G. Reid, Sutarno and Yasuaki NaKagawa, Canadian J. of Chemistry, 46, (1968), 3463.

88. P. Dumas, J. C. Colson and A. Fauvre, J. Chem. Research (S), (1977), 192-193.

89. B. I. Boltkas, Diffusion in Semiconductors, Fm. Moscow, (1961).

90. J.O'M Bockris and S. Srinivasan ed., "Fuel Cells : Their Electrochemistry". Ch.3, Ch.8 and Ch.9.

91. C. N. Satterfield, "Mass Transfer in Heterogeneous Catalysis", M.I.T. Press, London, (1970).

92. D. P. Gregory and A. C. Riddiford, J. Chem. Soc., (1956), 3756.

93. P. Delahay, "New Instrumental Methods in Electrochemistry", Pub. Interscience (1966), Ch.9, p. 217.

94. P. Delahay, "New Instrumental Methods in Electrochemistry", Pub. Interscience (1966), Ch.9, p. 233.

95. Tibor Erdey-Gruz, "Kinetics of Electrode Processes", p. 428.

96. P. Delahay, "New Instrumental Methods in Electrochemistry", Pub. Interscience (1966), Ch.3, p. 47.

97. P. Delahay, "Advances in Electrochemistry and Electrochemical Engineering", Vol. 1, Pub. Interscience (1961), Ch.5, p. 247.

98. P. Delahay, "New Instrumental Methods in Electrochemistry", Pub. Interscience (1966), Ch. 6, p. 115.

99. A.S.T.M. X-ray Powder Data file.

100. K. J. Vetter, "Electrochemical Kinetics", Academic Press, New York, 1967.

101. J. O'M Bockris, A. K. N. Reddy: "Modern Electrochemistry", Plenum Press, New York, (1970).

102. J. O'M Bockris, D. F. A. Koch, J. Phys. Chem. 65 (1961), 1941.

103. M. A. V. Devanthan and M. Selvaratham, Trans. Faraday Soc., 56, (1960), 1820.

104. M. A. V. Devanathan, J. O'M Bockris and W. Mehl, J. Electro-analytical Chem., 1, (1959/60), 143.

105. S. Braunauer, P. H. Emmett and E. Teller, J. Am. Chem. Soc., 60, 309-19.

106. B. E. Conway, "Theory and Principles of Electrode Processes", New York, (1965).

107. M. Temkin, Zhur. Fiz. Khim. 15 (194), 296; 21 (1947), 517.

108. S. Srinivasan, Thesis, University of Pennsylvania, Philadelphia, Pa. (1964).